# COMPOSITE COMPLIANT COATINGS FOR DRAG REDUCTION UTILIZING LOW MODULUS HIGH DAMPING SILICONE RUBBER

by

Kyu-Ha Chung

B.S.E., Seoul National University
(1974)

S.M., Massachusetts Institute of Technology
(1980)

Submitted to the Department of
Materials Science and Engineering
in Partial Fulfillment of the
Requirements for the
Degree of

DOCTOR OF PHILOSOPHY

at the

MASSACHUSETTS INSTITUTE OF TECHNOLOGY

February 1985



Signature of Author _____
Department of Materials Science and Engineering
January 11, 1985

Certified by _____
Edward W. Merrill
Thesis Supervisor

Accepted by _____
Bernhardt J. Wuensch, Chairman
Departmental Committee on Graduate Students

TO HEKYUNG

# COMPOSITE COMPLIANT COATINGS FOR DRAG REDUCTION UTILIZING LOW MODULUS HIGH DAMPING SILICONE RUBBER

by

Kyu-Ha Chung

Submitted to the Department of Materials Science and Engineering on January 11, 1985 in partial fulfilment of the requirements for the Degree of Doctor of Philosophy in Polymerics

## ABSTRACT

The drag coefficients on discs rotating in a cylindrical tank was studied in relation to the nature of a composite compliant coating attached to the underside of the disc, and direct comparisons were made with reference discs of identical geometry which were completely rigid. The composite coating was formed by the sequence of processing steps: (1) bonding of velvet fabric to the metal disc with velour face outward, (2) casting a premixed silicone composition over the velvet fabric to an exactly controlled depth, (3) covering the silicone layer with a thin, stiff polymer film, and (4) causing the silicone composition to form a network. Principle components of the silicone composition were: difunctional chain molecules, difunctional extender molecules, tetrafunctional junction molecules, non-functional diluent, and Platinum catalyst. Except the catalyst all species were methyl or dimethyl siloxanes. End-linking of chains occurred through vinyl groups to silane hydrogens on the extender and junction molecules. As a result of the tests on rotating discs described herein, wherein in certain cases the apparent drag coefficient was reduced by 20% or more as compared to reference rigid discs, three conclusions are possible; (1) true reduction of energy exchange in the turbulent boundary layer was achieved, perhaps by damping of the turbulent bursting process; (2) a significant increase in the laminar region at the center of the disc was obtained (transition of laminar to turbulent delayed); or (3) possible geometrical change of the coating surface occurred during rotation which provided a favorable effect on the boundary layer. Because of the levels of Reynolds numbers employed, and because by stroboscopic illumination no significant deformation of the coating could be seen, the first conclusion appears most plausible.

The stiffness of the top film influenced the performance of the coating profoundly: teflon film 0.005 inch thick led to the best results in the Reynolds number range of $8.92 \times 10^5$ to $1.94 \times 10^6$. A possible role of the top film in reducing skin-friction is by resonating at high frequency, one of the necessary conditions for a compliant coating to achieve drag reduction, according to Ash

and Bushnell. The degree of change of drag coefficient of the discs with compliant coatings as compared to rigid discs was found to be strongly influenced by the dynamic mechanical properties of the silicone elastomer network (storage modulus and the loss tangent). Coatings having high loss tangent and low storage modulus network showed higher drag reduction than those with low loss tangent and low storage modulus network.

Thesis Supervisor: Dr. Edward W. Merrill
Title: Carbon P. Dubbs Professor of Chemical Engineering

TABLE OF CONTENTS

## LIST OF FIGURES

## LIST OF TABLES

## ACKNOWLEDGEMENT

Very special thanks are due to Prof. E. W. Merrill for his pacience, constant encouragement, and over-all guidance. Without his stimulation and helpful ideas, the successful completion of this work would have been impossible.

Professors Armstrong and Wnek deserve special credit for the guidance of my thesis work. I am also indebted to Prof. Leehey who helped me carry out this work.

My warmest appreciation goes to Drs. Hansen and Hunston who helped us design the rotating disc system.

Special thanks to Seh-Way and Kathy for making our laboratory warm and friendly place to work. Many thanks to my fellow students in Materials Science and Engineering, Chan-Eun and Anoop and Drs. Han-Ill Yoo and Injoo Chin for their valuable criticisms and discussions along with this work.

I express my deepest gratitude to my friend, Dr. Yang-Hann Kim who has provided encouragement and support when it was most needed.

I would like to thank my parents and the whole family for their many sacrifices and stimulating encouragements for me.

Finally, I would like to dedicate this dissertation to my wife, Hekyung. Without her effort, help and encouragements, this dissertation would not have been possible. Credit also goes to my son, Woojin.

This work was funded under contract CCDR Program with the Oiffice of Naval Research. Their support is gratefully acknowledged.

## Introduction

Recently, interest in reducing skin-friction has reintensified. This resurgence of emphasis is mainly due to the pressing need to conserve fuel resources. And it is partially due to the level of sophistication reached in reducing form drag (thus further significant drag reductions in that area are limited) and also to the magnitude of skin-friction drag contribution to the total drag. For instance[1], full form (large volume) vessels have approximately an equal amount of form drag and skin-friction drag. Naval vessels (fine form) such as aircraft carriers, destroyers and so forth have a large percentage of skin-friction drag which is 75-80% of the total drag. Submarines operating at depth and high speed have about 90% skin-friction drag.

After Kramer's original publications[2,3] in which compliant coating reduced skin-friction drag upto 59 percent, viscous drag reduction via compliant coatings has been a popular topic of research. Kramer[3,4] attributed his measured drag reduction on bodies of revolution to delay of the laminar to turbulent transition to higher Reynold's number, although later research has indicated that transition region lengthening and drag reduction in fully developed turbulent boundary layers are also possible. However, the problem is that to-date there

has been no consistent widely repeatable series of experiments of viscous drag reduction in water. And also there has been no reliable theory in this field. The reason for that may be the complexity of the interaction between fluid flow and compliant wall.

Since there was no theoretical guide how to design coating material, it was required that the properties of coating material could be widely varied, such as, dynamic modulus and loss tangent (damping factor) to find a correlation between the material properties and the drag reduction phenomenon. Because of more encouraging experimental results [11-19] in the fully developed turbulent flow, the present work has been done in the fully developed turbulent boundary layer. Many theoretical investigators[10,16,20-23] suggest that the compliant wall should give a motion of small amplitude, short wavelength and high frequency interacting with turbulent fluctuations to achieve drag reduction by compliant coating. To fulfil these requirements a composite coating was suggested.

Reduction of skin-friction was studied with a rotating disc in a cylindrical tank, following the design of Hansen and Hunston.[5] An apparatus of rotating disc was built to measure viscous drag on compliant coatings in the turbulent water flow. The drag force was measured by the torque required to rotate the disc at the testing speeds. The torque on the compliant disc was compared with that on smooth rigid reference

disc which was geometrically identical to the compliant disc. The whole measurements were carried out in the turbulent boundary layer.

For this this test, one of the disc surfaces carried a compliant coating, the other surface being smooth metal. The composite compliant coating was formed by the sequence of processing steps:

1. Bonding of velvet fabric to the metal disc with velour facing outward

2. Casting on silicone composition over the velvet fabric to an exactly controlled depth

3. Covering the silicone layer with a thin, stiff polymer film.

The purpose of the velvet fibers was, by embedment in the silicone network, to prevent wave formation: The fiber being capable of buckling when the coating was compressed, but incapable of stretching when the coating was placed in local tension. Special attention was devoted to the formation of the silicone networks, and in prelimary studies networks were prepared from α,ω-divinyl polydimethylsiloxane (chain material, Mn=7,000 and 28,600), 1,3,5,7-tetramethylcyclotetrasiloxane (junction material), catalysed by platinum(II), to which was admitted prior to crosslinking non-reactive PDMS which served

as diluent. The viscosity of the diluent (molecular weight) is the major variable controlling loss/storage modulus; and the compliance (as measured by storage modulus) was governed both by diluent content and the chain length of the α,ω-divinyl PDMS.

The silicone networks in the final compliant coatings as tested on the rotating disc were composed of four major components, ie, α,ω-divinyl polydimethylsiloxane (mainly Mn= 26,400) as chain molecule, dihydrogen terminated PDMS(M.W.=400) as chain extender, tetrakis(dimethylsiloxy) silane as junction molecule and nonfunctional PDMS(M.W.=1,200 - 17,250) as diluent. The networks were formed by reacting vinyl groups on chain molecules to SiH groups on junction molecule and chain extender in the presencce of the diluent. To avoid trapping air bubbles in the networks due to the high viscosity of the precursor it was essential to use the chain extender in the reaction.

The compliant coating was constructed with three major components which were preswollen network, rayon velvet fabric and thin stiff film on the top of it. The original reason for using the velvet was to prevent the type of drag increases due to surface roughness recorded by many investigators.[5,6] As the network was cured in between the fiber piles, the surface motions of the coating would be restricted. It was discovered that, while the velvet was not completely successful by itself

in preventing standing wave formation, it was essential in securing the silicone composition to the disc surface, because of the very low compliance of the composition. A number of coatings were made to measure the skin-friction drag in the fully turbulent boundary layer. The dynamic properties of coatings were varied from hard to soft,and low and high damping factors. The drag forces of the compliant wall was very strongly related to the dynamic properties of the coatings. The effect of the top film of the coating on the drag forces was carefully examined. It was found that the thin top film played an essential role in the drag reduction. The dynamic storage modului and loss tangents of all tested coatings were measured at 1 % strain of compression mode from Ø.1 to 1ØØ Hz.

As a result of the tests on rotating discs described herein, wherein in certain cases the apparent drag coefficient was reduced by 2Ø% or more as compared to equivalent metal discs in three conclusions are possible:

1. true reduction of energy exchange in the turbulent boundary layer is achieved, perhaps by damping of the turbulent bursting process, or

2. a <u>significant</u> increase in the laminar region at the center of the disc was obtained (transition to turbulence delayed), or

3. possible geometrical change of the coating surface would

have occurred during rotating which provided a favorable effect on the boundary layer.

Because of the levels of Reynolds numbers employed, the first conclusion appears more plausible.

## Literature Survey

### 1. Viscous Drag Reduction Via Compliant Coatings

M.O. Kramer[2,3,4] has been credited with the original idea of drag reduction by flexible or compliant surface. His early experiments with submerged flexible rubber cylinders indicated drag reduction of upto 59 percent. One of the best coatings consisted of thin natural rubber diaphragm (Top layer) that was supported by a multitude of tiny rubber stubs. A thin rubber inner layer was bonded to the base of the stubs. After mounting of the coating on the rigid structure, the space between tiny stubs was filled with a damping fluid of appropriate viscosity. The coating composed of medium hardness diaphragm (E = 100 psi) showed best performance in the Reynolds number range of $6 \times 10^6$ to $15 \times 10^6$. And there was an optimum viscosity of damping fluid silicone oil of 300 ctsk.

Kramer interpreted the drag reduction by compliant coating as an artificial boundary layer stabilization which he termed "stabilization by Distributed Damping". As his preliminary experiment[2] indicated, by the compliant coating the transition of laminar-turbulent boundary layer delayed to higher Reynolds number significantly compared to that on rigid wall (140 percent higher Reynolds number). Kramer proposed the mechanism of the drag reduction via compliant coating was stabilization of boundary layer due to delay of transition of

laminar to turbulent boundary layer.

Because of the very promising results of Kramer, investigations and development projects have started in various places, but most investigators have reported fail to demonstrate drag reduction by their coatings. Many investigations[24,25] were made to duplicate Kramer's coating and his results. None of them reproduced the exciting result including Kramer himself.

Theoretical models proposed by many investigators[10,26,27] have indicated that it was possible to stabilize a laminar boundary layer with appropriate flexible wall materials. However, numerous experiments with compliant wall models in water and air flows have produced no conclusive data showing a drag reduction due to transition delay. Aside from the transition delay, Kaplan[28] and Gyogyfalvy[27] have indicated that it is theoretically possible to produce some drag reduction by expanding the region of the transition boundary layer. That is, even though a compliant wall may in fact cause a laminar boundary layer to become unstable sooner (farther upstream), the rate of amplification of local fluctuations may be lower, causing the fully turbulent boundary layer to develop more slowly. Experiments by Karplus[29] have shown that simultaneous early instability and arrested turbulent development can occur on some compliant surface. At the present time, serious questions exist concerning whether

any real material can be employed to either delay transition or retard the development of fully turbulence in a manner which can significantly reduce the skin friction drag.

On the other hand, experiments with fully turbulent boundary layer have been more encouraging.[11-19] In late 1960's Blick and his students[15] reported the drag reduction of upto 60% via their compliant coatings in the fully turbulent air boundary layer. In the studies[15] they also showed substantial reductions in Reynolds stress, turbulent intensity, and production of turbulent energy. However, there were some contradictions in their experiment, too. A more modest drag reduction of 10 percent has been reported by Lissaman and Harris[30] when they tried to duplicate Blick and co-workers' work. There were another unsuccessful attempts at the Langley Research Center[31] to experimentally verify the works of Blick et al. at the University of Oklahoma. An explanation for these contradictory results, in terms of an apparatus related experimental bias in the University of Oklahoma experiments with water-backed membranes has been offered by Hefner and Weinstein[32]. No such explanation, however, has been found for the 25% Reynold stress reduction reported by Blick et al.[15] More recently, McMichael et al.[33] reported no significant change of friction drag on their compliant wall which is similar to that of the Blick et al. To-date, it is not very clear why the contradictory results have occurred. It

may be, however, due to the complexity of the phenomenon of drag reduction by compliant wall.

## A. Some Theories of Drag Reduction Compliant Coating in Fully Turbulent Boundary Layer

Several theoretical works[20-23,34-36,38] have been done to find out the mechanism of compliant coating drag reduction in fully turbulent boundary layer. All of them indicate that it is possible to reduce skin-friction drag in fully turbulent boundary layer with appropriate coatings. Ffowcs Williams[35] used the assumption of two-dimensional disturbances and linearized equations to derive an expression for shear stress near a compliant wall. From this examination he concluded that moving waves in a surface with low wave speed can produce a region of "negative Reynolds stress" which could "starve the turbulent eddies" and "may lead to a reduction in the turbulent level." Therefore, this approach suggests that the use of surfaces designed to generate low speed waves (less than about eighty percent of the free stream velocity) gives low shear stress, ie., drag reduction in the turbulent boundary layer. Zimmermann[36] considered the surface motion as a small disturbance to the basic turbulent flow, which is assumed known in detail. Further assumptions include low damping in the surface and small thickness. This approach is similar to that used in the conventional stability theory of compliant

walls.[10] He used measured pressure-velocity correlation data from rigid walls to estimate the change in shear stress due to the flexible surface. His results showed only a small reduction for air but a measurable (ca. 5%) reduction for water where the interaction is greater between the water and compliant wall.

Among the thoretical works there is an approach[20] which seems to be the most attractive idea, therefore, become a guideline for the present study. The idea[20,38] is that the wall influences the turbulent burst phenomenon by providing a pressure field that tends to inhibit bursts when they normally occur. This idea leads to significant qualitative understanding of the effect of compliant walls. There has been accumulated a wealth of experimental evidence that the a "quasi-ordered" or "coherent" series of fluid dynamic events in the turbulent boundary layer flows (turbulent bursting). These events occur randomly in time and space and originate above the surface in the near wall ($y^+ < 100$) region.[20,21] A plausible coherent sequence of events for formation and regeneration of bursts is as follows:

1. 'old' bursts produce a large adverse pressure pulse that moves at a speed of roughly 0.8 $U_\infty$ and has an amplitude of roughly 3 $P'_{rms}$, where $U_\infty$ and $P'_{rms}$ are the free stream velocity and the rms wall pressure fluctuation intensity, respectively.[21]

2. This adverse gredient retards the flow near the wall and produces a low-speed streak.

3. A new burst is created when the low-speed streak creates highly inflectional velocity profiles in the wall region (Inflection point at $y^+ = 25$).

4. The favorable part of the large-scale pressure pulse due to previous bursts tends to assist the new burst in 'sweeping' out away from the wall. Most of Reynolds stress and turbulence production occurs during the burst and sweep process, with relatively low turbulence activity between bursts.

5. The 'new' bursts set up conditions similar to that discussed in process 1. above and the whole sequence of events is repeated.

Many authors suggest that the (retardation-influenced) pre-burst profile undergoes the instability growth/amplification in a fashion similar to the burst formation in transitional flows. The burst initiation seems to involve the lower frequency portion of the wall pressure fluctuation spectra. In other words, only the large amplitude, long lasting pulses can cause sufficient retardation to produce the necessary pre-burst condition. The scheme of the bursting process is shown in Figure 1.

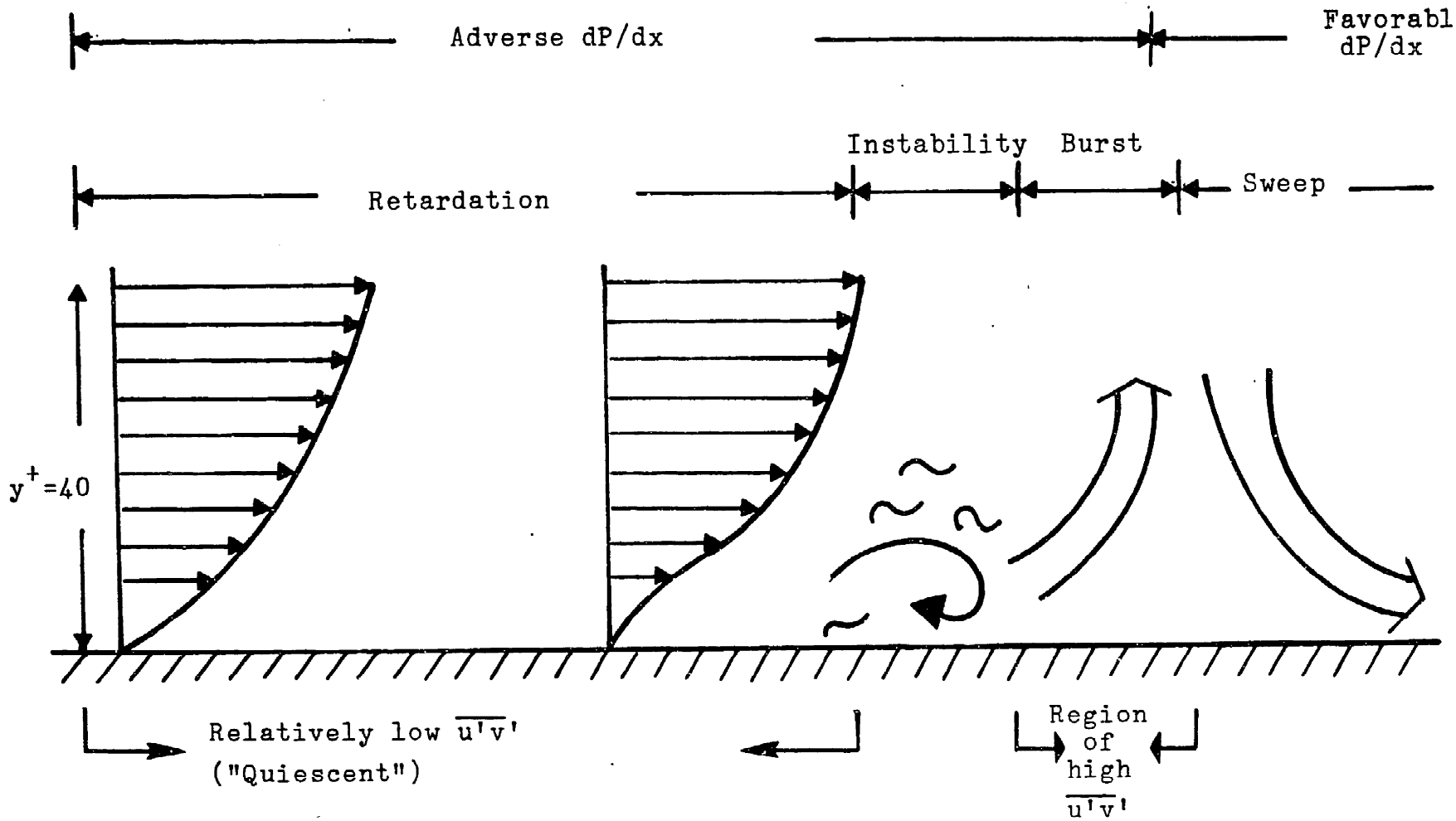


Figure 1. Sketch of Possible Turbulent Event Cycle.[38]

Ash et al[38] have proposed that the above sequence of event can be used to formulate a quantitative flow model for the prediction of properties of turbulent boundary layers. The idea is to impose the experimentally measured pressure pulse due to 'old' bursts, to model the background turbulence between bursts using a crude turbulence model and then to calculate the inflectional mean-velocity profiles produced by the pressure pulse using a two-dimensional Naviastokes equation computer code. Finally, the occurence of new bursts can be investigated in this flow model by calculating the growth of Tollmien-Schlicting waves and using amplitude-growth criterion[37] to predict the onset of new bursts. Furthermore, the model also suggests a mechanism for drag reduction by compliant walls. If the wavelength of wall motions is small (at most the wavelength of the imposed pressure pulse), the wall motion can interrupt the feedback loop outlined above somewhere between step 2 and 4. If the short wavelength wall motions can delay burst formation through the adverse part of the imposed pressure pulse then the favorable part of the imposed pressure pulse may inhibit bursting. In this case, turbulence production and turbulent boundary layer drag are decreased. In addition to the wavelength, amplitude and wave speed of the wall motions are also important to reduce skin-friction. The amplitude of the wall motion should be the order of the sublayer thickness, whereas in most of the "wavy wall" experiments the wall motion amplitude is large enough to

possibly create an effective roughness, which could alter the magnitude of the wall induced pressure. They have mentioned the wave speed of wall motion and a phase shift occurred between the wall motion and the induced pressure field are also important factors to get drag reduction by the compliant wall, although these factors were not considered for their calculation. There is important concept of the compliant wall motions. In the stability theories[10,26] of compliant coating, the following compliant wall characteristics were suggested[10] as necessary for stabilization of oscillations in the early stages of transitional flow: (1) wall density is the order of the fluid density; (2) shear modulus is the order of the fluid dynamic pressure; (3) small wall dissipation; (4) impervious wall. This motion is directly related to the local instantaneous disturbance field ("conventional compliant" wall). However, as Kramer's original coatings[2,3] indicated, the relatively large damping coating showed very high drag reduction, which could not be explained by the stability theory. In other words, the wall motion could not be a "conventional compliant" wall motion. Ash et al. again suggested that a "resonance motion" of compliant wall, where a certain dominant wavelength, wave speed, and amplitude occur by the external disturbance. This motion is not instantaneous response of pressure fluctuations, but a modulation between compliant wall and the disturbances. Since Ash et al. employed resonance type wall motion to interpret the compliant

wall drag reduction, the damping of the coatings is not necessarily very low to achieve drag reduction. They have re-examined the previous successful experiments to verify the proposed mechanism. And it turned out that it was very consistent with their idea, ie., there was some evidence which suggests such small wavelength motion ( $\lambda^+$ = 20 - 200) could have occurred.[38] Finally, three types of potential compliant surface designs have been suggested. (1) Membrane with small air gap: It appeared to allow both small wavelength and amplitude motion.

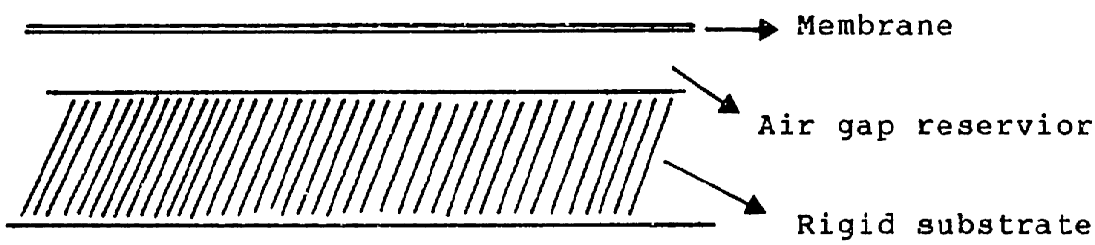


Figure 2. Scheme of a Structure of Membrane with small air gap.

(2) Laminated structure: It was indicated less motion control (based on eigen value calculations). Some experimental data exists which indicates modest reductions in skin friction over laminated surface, but the high substrate damping appears to retard effective amplification of desired wall motions.

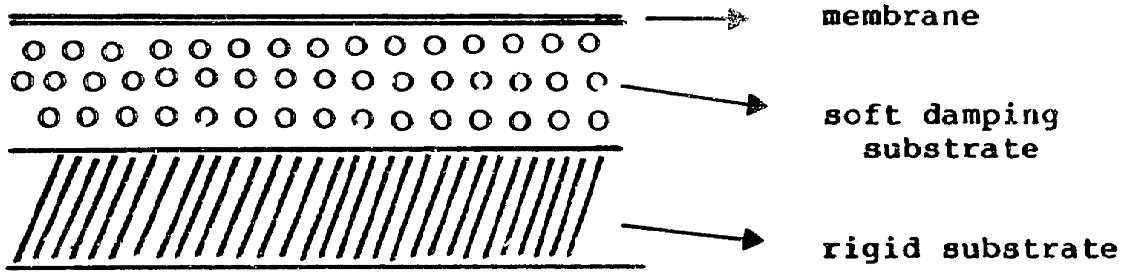


Figure 3. Scheme of Laminated structure.

(3) Periodic anisotropic structure: It appears to combine durability with wavelength and frequency control (the present design).

Orszag[20,21] examined the above model for drag reduction by computer simulation. He was able to achieve reasonable agreement with experimental measurement of mean velocity profiles during the burst process on a flat plate. And stability calculations of the resulting mean velocity profiles showed compliant walls with relatively short wavelengths might have an appreciable effect in stabilizing the boundary layer to further bursts. On the other hand, long wavelength wall motions did not seem to limit the burst process, and therefore, do not appear good candidates for drag reduction.

Grosskreutz[39] who proposed different mechanism of drag reduction indicated anisotropic periodic coating could reduce skin-friction. As shown in Figure 4(a), the imbedded blades

restricts the surface motion of wall. The restricted motions may reveal small wavelength and amplitude (spacing of blade could be the wavelength and blades restrict large amplitude of surface motion). His concept of wall motion was one of the "conventional compliant" wall ones. The small favorable wall motion may interact with the pressure fluctuation of fluid and lead the sign of the fluctuation velocities ($\overline{uv}$) to be positive. Therefore, the contribution of turbulent stress to the total friction would be negative, ie., reducing friction drag (Refer Figure 4(b)). The early model of Ash[23] for compliant drag reduction was very similar to this idea. Later, he proposed the mechanism of delaying bursting process mentioned above in some detail. Regardless of the proposed mechanism, the anisotropic periodic structure must be one of good candidates for drag reduction.

## B. Review of Current Experimental Works of Compliant Coating Drag Reduction

After Kramer's original publications,[2,3] there have been numerous experiments to develop favorable coatings and understand the phenomenon of drag reduction via compliant walls. As mentioned above, the pheonomenon is not fully understood and only a few works indicate positive results, while rest of them are inconclusive or negative. Table A-1 in the Appendix A shows the scope of the current experimental

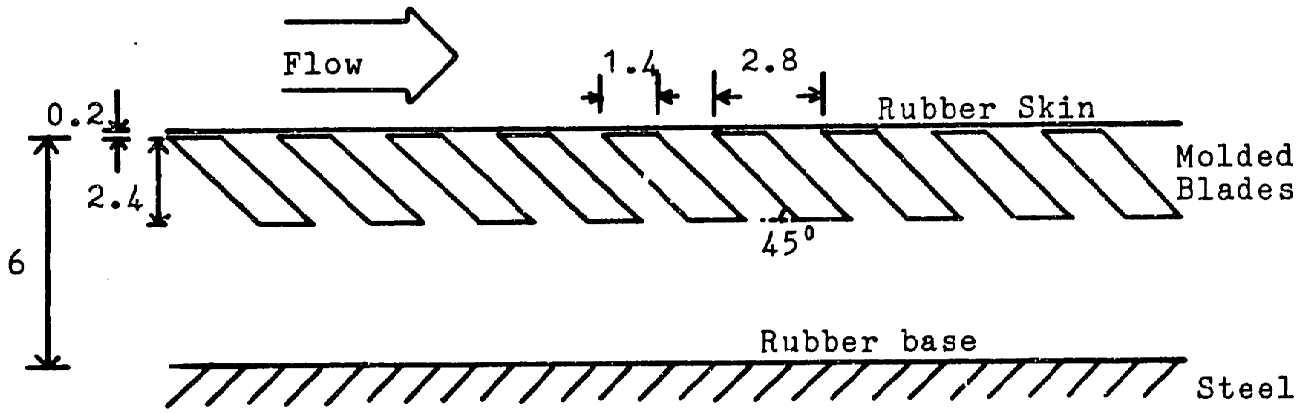


Figure 4(a). Cross-section of Grosskreutz's Periodic Coating.[39]

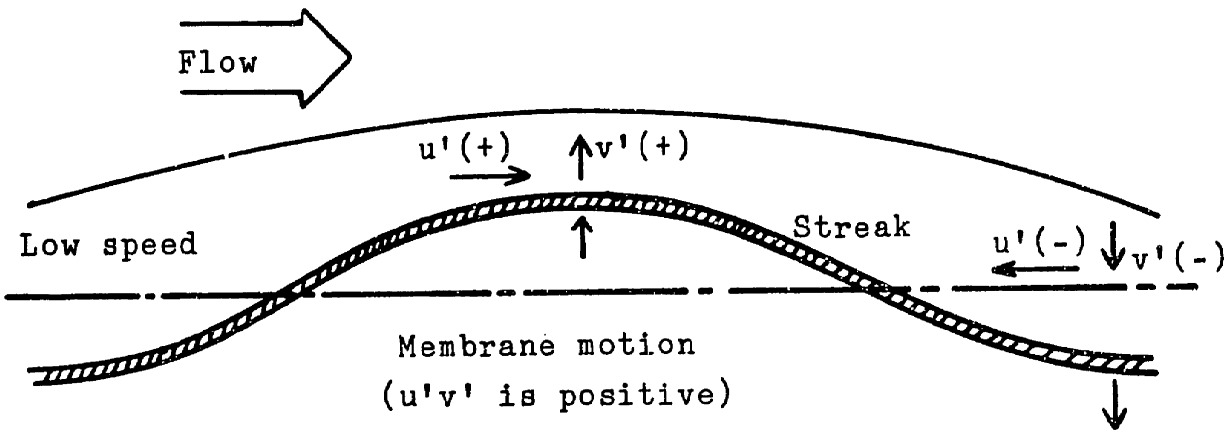


Figure 4(b). Interaction between a Low Speed Streak and a Vibrating Membrane (R. Ash[23]).

investigations of compliant wall for drag reduction, which lists the compliant materials used, their material properties, type of coating (porous substrate covered with thin film was classified as anisotropic coating) and apparent results of the studies. There are hundreds of unsuccessful results which are not listed in the table.

Among the listed works, Kramer,[2,3,4,7,40] Teslo and Filipchuk[17] and recently Kozlov et al[19] reported compliant coating drag reduction in the water fluid. Klinzing et al[42] revealed the possibility to reduce drag in the coated pipe. And in late 1960's Blick and his students[12-15,41] showed drag reduction upto 60 percent by mainly laminated-structured coatings in the air fluid turbulent boundary layer. Other positive results[1,18,30,38,43] were shown in the air fluid. As mentioned earlier, there were lots of unsuccessful attempts[24,31,25] to duplicate the positive results[3,12-15] in air and water fluid flow. The design factors of the compliant coating are not well understood, yet. In the later part of this section, several successful and unsuccessful coatings are introduced in some detail.

(1) Unsuccessful Coatings (drag increase or no change)

Four large constant pressure bodies were covered with various types of soft rubbers and were tested at the David Tayor Model Basin Carderock, Maryland in 1961.[44] The coatings

were composed of 1,000 centistoke solution of polyethyleneoxide in water as damping fluid and natural rubber membrane (E = 10.5 x $10^6$ to 16 x $10^6$ dyne/$Cm^2$) covered on the damping fluid. The detail of design was not shown in the report. They did not observe drag reduction with any of their coatings. Some of the coatings showed static divergence at high test speed.

Uram and co-workers[24] in the Davidson Laboratory conducted careful tests on a slender cylindrical body with a compliant surface designed by Kramer who initiated this investigation. The purpose of the test was to assess the drag reduction capability under more controlled conditions and reporduce Kramer's original results. The test body was approximately 84 inches long consisting primarily of three sections: (1) an afterbody approximately 41 5/8 inch long which was fitted with fins; (2) an instrument section containing a strain gage balance, pressure sensing device, etc.; (3) an interchangeable hollow forebody 39 inch long. Compliant coating was placed in this part of the body. The material property of the coating was not reported in the paper. The bodies were tested in the velocities of 19 to 50.7 ft/sec. The resulting drag was almost identical to that of rigid body. They concluded that Kramer's previous results could be erroneous, because Kramer did not subtract the form drag of his bodies in the original test.

Taneda and Honji[45] investigated the effect of flexible

wall on the boundary layer stabilization by measuring skin-friction in the Reynolds number range from 6 x $10^5$ to 1 x $10^7$ in their towing tank. The coatings were made of porous synthetic rubber (commercial rubber with 5 - 10 mm thick) covered with thin vinyl sheet (0.2 mm thick). The material property of the cover sheet was not reported and that of the rubber form was measured in a manner of static pressure vs. elastic deformation. The rubber form deformed 40 - 65% at the pressure of 30 g/$Cm^2$. The test was conducted in the transition region (laminar to turbulent boundary layer) and in fully turbulent boundary layer. In both cases, the flexible surface had always larger skin-friction than the rigid plate. However, they did not conclude that it was unlikely to reduce drag by compliant wall, because the shapes of the reference and compliant plate were not exactly identical.

In 1960's Lissaman and Harris[30] examined the compliant coatings to determine Reynolds stress and skin-friction in the turbulent boundary layer. The compliant surface was composed of polyvinylchloride film ( 6 and 35 mil thick) stretched over different damping fluids (water and water/polyox of 10,000 c.p.). The experiment was conducted with the flat plate mode in the water tunnel. The material property was not carefully studied. The only material property reported was Young's modulus of the vinyl films (3,000 - 6,000 psi). The experiments showed that there were no major differences between

the hard plate and compliant skin results. More interesting point of the results was that wide variations in the skin compliance parameters (thickness, tension and damping fluid viscosity) produced no discernible change in boundary-layer characteristics.

Vicoelastic homogeneous compliant coatings were carefully examined in the rotating disc experiment[5], and on the flat plate in water tunnel[6]. The compliant materials used in both investigation were polyvinyl chloride plastisol prepared by heating mixtures of PVC resin, a plasticizer (DØP or di-2-ethylhexyl phthalate) and a dibuthylin maleate stabilizer. The shear moduli of the coatings were 5,ØØØ - 124,ØØØ dyne/$Cm^2$. The dynamic shear moduli of the coating were not grealy changed and the loss tangent was always much less than 1 in the frequency range of $1Ø^{-2}$ to $1Ø^{2}$ Hz. The experiments were conducted in the fully turbulent boundary layer in both rotating disc and flat plate models. The static divergence of the compliant surface was observed, which developed when quotient (free stream velocity) x (square root of liquid density) / (square root of the shear modulus of the compliant material) exceeded a critical value. Below the critical condition surface compliance did not affect the flow in any measurable way, whereas above it the skin-friction was significantly increased. Hansen and Hunston[5,6] attributed the increase of drag by the compliant surface to two possible

reasons: One is that the wave structure is essentially stationary relative to the disc or free stream velocity of the water. The other is that the height of the wave crests is large compared to the viscous sublayer thickness which would prevail on a smooth, rigid surface under the same flow conditions. Consequently, the wave structure appears to have the effect on turbulent flows as a rough, rigid surface, ie., by virture of the roughness elements extending into the buffer zone of the turbulent boundary layer, the rates of turbulent energy generation and dissipation are altered so as to increase the friction drag. R. Brown[16] also observed large stationary wave of compliant surface on the rotating cylinder model, when the rotating cylinder exceeded a critical speed. The coating used consisted of air-filled, closed cell rubber whose shear storage modulus was 12 psi and loss tangent was more than 10. Very recently, Dickinson et al[25] in the David W. Taylor Naval Ship R & D Center designed two multilayer "Kramer" type coatings and a coating of a closed-cell neoprene form The coatings were examined in the water-tunnel in the Reynolds number of $1 \times 10^7$ to $6 \times 10^7$. The "Kramer" type coatings were made of bottom layer of Neoprene rubber (40 mil) covered by 15 mil thick natural rubber, and the two layers were glued by adhesive. Hard paint was sprayed on the natural rubber. (ca. 1 mil thick). The anisotropic coating was comprised of 1/4 in. thick layer of neoprene closed-cell form. The shear modulus of the form was about 6 psi at low pressure. The

mechanical property of the coating materials of the "Kramer" type coating was not reported. One of the "Kramer" type coatings failed at lower test speed of water tunnel. The drag of the second Kramer coating was within the 2% rms scatter of the smooth, solid plate drag at all velocities tested. The surface of the closed-cell neoprene form was rough, and the drag was 14-20% higher than the reference at low velocities. Above a critical velocity where the transverse stationary wave appears, the drag rapidly increases with increasing velocity.

Drag reduction in a pipe fitted with a compliant wall was examined by Dinkelacker.[46] The wall was composed of the polyurethane foam filled with water or air and thin natural rubber film (Ø.5 mm thick). The material property of the coating was not mentioned. The results of the test were inconclusive. Some of the results obtained seemed to indicate reduction in turbulent or reduction in drag (he measured velocity fluctuation and pressure fluctuation on wall).

(2) Successful Coatings

Kramer's original coating[2,3] was 'stubbed coating', which consisted of three layers and four components: thin natural rubber diaphragm (top layer with 2Ø mil thick) that was supported by a multilude of tiny rubber stubs of 4Ø mil in diameter and height with an 8Ø mil center-to-cener spacing of the stubs. A thin inner rubber layer (bottom) was bonded to

the base of the stubs. The space between stubs was filled with damping fluid, various viscosities of silicone oil. The material property of the diaphragm was reported in stiffness, pci, (pounds per cubic inch) by measuring the load on one square inch of the coated surface that would lead to a compression of one inch of a rigidly supported flat sample of the coating. (The actual deflections were 5 to 10 mil). The stubbed coating was placed on the cylinderical towing body which was towed by a motor boat in the ocean water. The measured drag of the compliant surface was affected by the stiffness of diaphragm and the viscosity of the damping fluids. There were optimum viscosities for each diaphragms. For instance, a coating with a diaphragm whose stiffness was 1,600 pci, showed the best performance with the damping fluid of viscosity of 1,200 ctsk. A coating of an 800 pci (equivalent to 100 psi) diaphragm revealed the highest drag reduction with the 300 ctsk silicone oil. On the other hand, with the softest diaphragm (600 pci) there was no optimum viscosity in the range from 10 to 400 ctsk to achieve drag reduction. There was not substantial drag reduction with the softest diaphragm coating. Among the results the medium stiffness coating with 300 ctsk damping fluid revealed the best performance, 59 percent drag reductrion compared with rigid wall friction drag at Reynolds number of $1.5 \times 10^7$. Kramer postulated that the compliant drag reduction was due to the stabilization of the laminar boundary layer by the "distributed

damping". The transition Reynolds number of laminar-turbulent would be delayed to the higher Reynolds number.

The stubbed coating revealed aging effect and other adverse influences. The performance of the one-year old coating was much worse than that of the original coating. The deficiency was removed by a drastic change in the coating design, called the "ribbed coating". The ribbed coating consisted of a diaphragm that is supported by a multitude of ribs which are supposed to be aligned with the average direction of the ambient flow. The thickness of the top layer (natural rubber diaphragm) was varied from Ø.Ø2 inch to Ø.Ø5 inch with a damping fluid of viscosity of 1Ø,ØØØ ctsk. There was optimum thickness to achieve the best performance of the coating (medium thicknes, Ø.Ø3 inch diaphragm showed the highest drag reduction for about 4Ø% at Reynolds number 1.5 x $1Ø^7$). The ageing effect of the coating was eliminated in the ribbed coating.

Klinzing et al[42] demonstrated the compliant coating drag reduction in a flexible tube. The flexible pipe was made of a silastic tubing encased by a polyurethane foam. The material property of the silastic tubing was E = 15Ø psi and thicknes Ø.Ø6 inch and that of the foam was not reported. A definite decrease in the skin-friction of flexible wall pipe was seen to exist in the region of Reynolds number from 1Ø,ØØØ to 2Ø,ØØØ (ca. 2Ø% reduction). They attributed the phenomenon to delay

of transition of laminar-turbulent boundary layer to the higher Reynolds number.

There is a successful experiment[17,47] of flexible pipes on the turbulent boundary layer. The compliant wall pipe was prepared in the following manner. A polythylene pipe (wall thickness of 160 microns) was imbedded in a container filled with damping fluid. Water and air were used as damping fluid. Average 25% of drag reduction was achieved with compliant wall pipe in Reynolds number of $2 \times 10^4$ to $10^5$ (Water as damping fluid). And a significant reduction of velocity fluctuation near the compliant wall was observed. Therefore, their conclusion was that the compliant surfaces influenced the friction and characteristics of turbulent flow. Unfortunately, they gave no information about the material property of the flexible wall at all.

During the years 1966 through 1969, several successful experiments[11-15] in turbulent air fluid flow were obtained by Blick and his students at the University of Oklahoma. Although there was a re-evaluation[32] of the Okalahoma experiments with water substrates, Blick and coworkers's works are still very encouraging for the compliant coating drag reduction. In 1965 Fisher and Blick[11] measured the turbulence intensity over a compliant wall in the wake of a small fense in a wind tunnel. The coating consisted of a 0.057 mm thick polyvinyl chloride membrane stretched over a 9.5 mm deep reservoir of damping

fluid. The damping fluids used were air, water and SAE 30 weight automobile oil. It was observed that the compliant surface had lower turbulence intensities than the hard surface. The ability of the compliant wall to damp out the turbulence seemed to increase with an increase in viscosity of the damping fluid as oil was the best damping fluid followed by water, and then air. The next experiment of Blick et al[12] indicated that it was possible to reduce the turbulent skin-friction drag by using a compliant surface of thin polyvinyl chloride material covering a fluid reservoir 7.9 mm deep. Drag reductions upto 40% were obtained at a Reynolds number of 0.8 x $10^6$. The damping fluids used were water, water solution of polyvinyl alcohol (50, 8,000 cp of viscosities) and air. The coating of the damping fluid of 8,000 cp solution indicated the best performance in drag reduction. However, the difference in drag reduction when various damping fluids were employed was not significant (38% reduction with air, 40% with solution of 50 cp and 43% with solution of 8,000 cp). Smith and Blick[41] extended the skin-friction measurements to include polyurethane foam (dry or soaked with water) covered with polyvinyl chloride sheet (0.064 mm thick). The measurement was made in a wind tunnel at a Reynolds number of approximately 0.8 x $10^6$. The results are summarized in Table I. It is interesting to note that the bare form produced skin-friction much higher than the smooth hard plate, but when the PVC skin was covered on it the friction were reduced. The

reason may lie on the roughness effect of the form. When the form was dry the finer form provided higher drag reduction than the coarse one. However, once the forms were soaked by water, the forms with larger pores (coarse forms) experienced additional reduction, while the fine form (32 ppc) experienced an increase above its dry form skin-friction value.

Table I. Skin Friction Coefficients on Form Surfaces[41]

| Material | No Film (open pores) | Covered with PVC skin(dry) | Water soaked covered w/ PVC skin |
|---|---|---|---|
| Polyurethane foam* (32 ppc) | +72% | -33% | -21% |
| Polyurethane foam (16 ppc) | +107% | -26% | -37% |
| Polyurethane foam (10 ppc) | +200% | +2% | -30% |

* ppc = pores per centimeter

. Values are compared with the skin-friction coefficient of hard smooth wall at the same Reynolds number.

Blick and Walters[13] measured the variations of the turbulence intensity from the upstream edge of compliant plate to the downstream by using a hot wire anemometer. In general the compliant wall turbulence was lower than the hard wall turbulence. The longitudinal turbulence energy spectrum was

also measured with hot wire at various depths in the boundary layer. Generally, the compliant coatings were found to reduce the energy primarily at high frequencies (greater than 100 Hz).

In the later experiment of Blick and co-workers,[15] the skin friction was measured over a wide wind tunnel speed range of 18 to 22 ft/sec with two basic types of compliant coatings: (1) polyvinyl chloride skin covering a shallow layer of water and, (2) a polyvinyl chloride skin covering a thin layer of polyurethane foam. Drag reduction upto 38% were measured over the whole test speed. The largest drag reduction occurred when polyurethane foams of small number of pores per inch (27 ppi and 40 ppi) were saturated with water. Hot wire anemometer results showed reductions in turbulence intensity, Reynolds stressess, and spectrum of turbulent energy over the type (2) compliant coatings.

Recently, Kanarskiy and Teslo observed upto 60% drag reduction by the compliant coatings in the turbulent boundary layer. And they also pointed out the coating affected the turbulence microscale. The investigation was carried out with four surfaces in the water tunnel: (1) compliant polyurethane foam covered with a 600 micron-thick rubber film; (2) same form, covered with 1 micron-thick polyethylene film; (3) noncovered form; (4) a rigid aluminum plate. The form covered with 1 micron-thick polyethylene film and noncovered form reduced the mean level of pressure fluctuations by 60 and 41

percent, respectively, at low flow speed (Ø.2 m/sec). On the other hand, in flow over the rubber film-covered form, the mean level of pressure fluctuations was 3Ø percent higher than over the rigid surface. At higher flow velocities they observed surface bulging.

2. Skin-Friction Drag on Rotating Disc (Turbulent Flow Around a Disc Rotating in Free Space)[48,49]

The flow adjacent to the surfaces of a rotating disc becomes turbulent (at the maximum radius) at Reynolds numbers $Re = UR/\nu$ exceeding $2.5 \times 1Ø^5$, where R denotes the radius and $U = \omega R$ is the tip velocity of the disc. Owing to friction, the fluid in the immediate neighborhood of the disc is carried by it and then forced outwards by the centrifugal acceleration. Thus, the velocity in the boundary layer has a radial and a tangential (circumferential) component, and the mass of fluid which is driven outwards by centrifugal forces is replaced by an axial flow.

According to the definition of the Reynolds number for rotating disc, the local Reynolds numbers of the rotating disc at each radii from center to the tip differ from each other. As the radii change from the tip to the center of the disc, the local Reynolds numbers decrease by the factor of $r^2$, where r is local radius of the disc. Figures 5(i), (ii) and (iii) show

schematic diagrams of rotating disc at three rotating speeds which correspond to the Reynolds numbers (determined by tip radius of the discs) of (i) well below $2.5 \times 10^5$, (ii) equal to $2.5 \times 10^5$ and (iii) well above $2.5 \times 10^5$. In the Figure 5(i), laminar boundary layers are formed on both sides of the disc, because the Reynolds number at the tip of the disc is well below the Reynolds number of transition from laminar to turbulent boundary layer. At the Reynolds number of $2.5 \times 10^5$ the boundary layer at the tip of the disc begins to show the transition, while the other surfaces remain in the laminar boundary layers. When the Reynolds number is much higher than the transition Reynolds number, $2.5 \times 10^5$ (Figure 5(iii)), there exist three distinct boundary layers on the rotating disc. On the outward of the disc (close to the disc tip), turbulent boundary layer is formed. On the other hand, the surfaces near the center of the disc remain laminar boundary layer. The transition occurs in between two boundary layers.

To make a theoretical derivation of friction drag on a rotating disk,[49] we consider a ring-shaped element of a boundary layer of thickness, $\delta$ on a rotating disc, located between the radii r and r + dr. For such element the increment of momentum in the radial direction is

$$\frac{d}{dr}(2\pi r\rho \int_0^{\delta} v_r^2 \, dz \,) \, dr$$

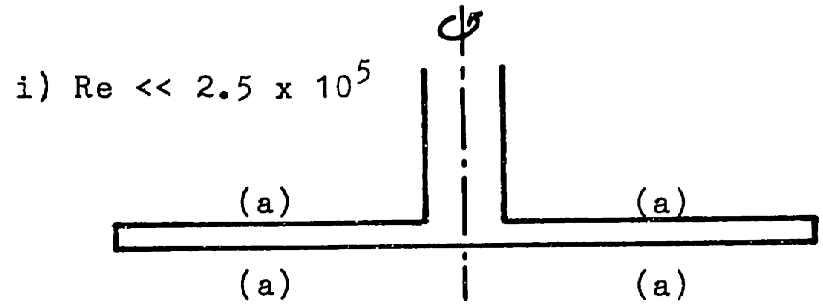


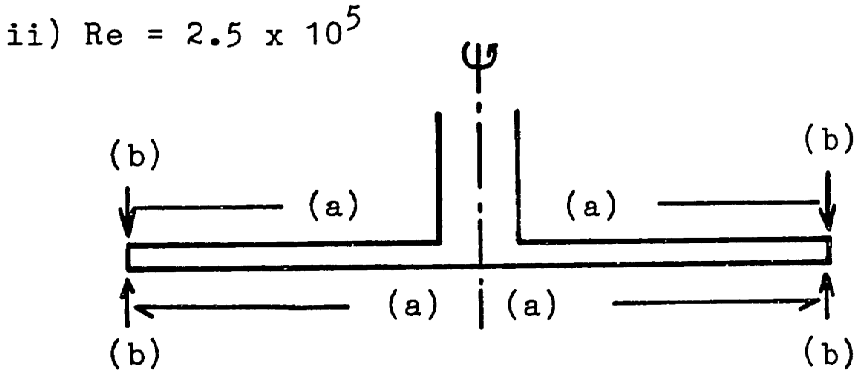


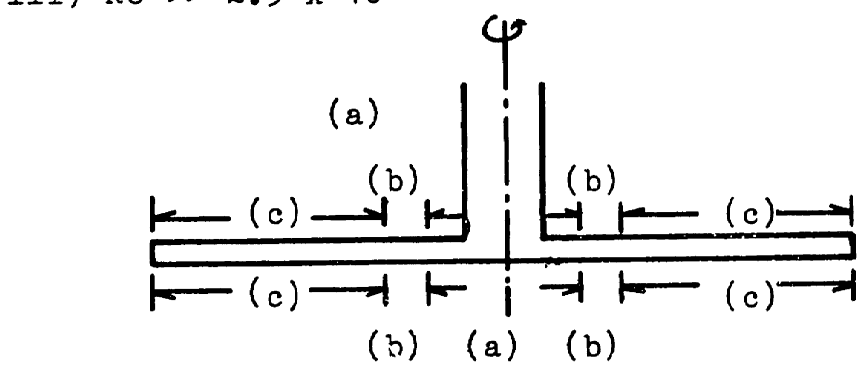


Figure 5. Schematic Diagram of Boundary Layers of the Rotating Disc: (a) laminar boundary layer, (b) transition region, and (c) turbulent boundary layer.

where, $\rho$ is the density of fluid, $v_r$ is radial velocity component.

The centrifugal force acting on the element can be expressed as

$$- 2\pi r \left(\rho \int_0^{\delta} \frac{v_\phi^2}{r} \, dz \right) dr$$

where, $v_\phi$ is circumferential velocity component.

The resultant of these two forces must be balanced by the frictional force $2\pi r \tau_r dr$ where, $\tau_r$ is the radial component of stress. Therefore,

$$\frac{d}{dr} \left( r \int_0^{\delta} v_r^2 \, dz \right) - \int_0^{\delta} v_\phi^2 \, dz = -r \frac{\tau_r}{\rho} \qquad (1)$$

Now, we obtain a second equation by evaluating the increment of angular momentum about the axis of rotation:

$$\frac{d}{dr} \left( 2\pi r^2 \rho \int_0^{\delta} v_r v_\phi \, dz \right) dr$$

This must be balanced by the momentum due to the frictional forces in the circumferential direction, which is $-2\pi r^2 \tau_\phi dr$,

$$\frac{d}{dr} \left(r^2 \int_0^{\delta} v_r v_\phi \, dz \right) = - \frac{\tau_\phi r^2}{\rho} \qquad (2)$$

To determine the skin-friction of rotating disc in a turbulent flow the integral relation eq. (1) and (2) are used assuming a power low for the distribution of flow velocities in the boundary layer, namely, the 1/7 th power, which is observed in flow through pipes in a certain range of Reynolds numbers.

$$v_r = \alpha r\omega \left(\frac{z}{\delta}\right)^{1/7} \left(1-\frac{z}{\delta}\right)$$

$$v_\phi = r\omega \left(1 - \left(\frac{z}{\delta}\right)^{1/7}\right) \qquad (3)$$

Where, $\alpha$ and $\delta$ are unknown quantities. The radial and circumferential velocity profiles satisfy the following boundary condition at the wall.

$$\text{at } z = 0: \quad v_r = 0, \quad v_\phi = r \ ,$$

and at the outer boundary of the layer

$$\text{at } z = \delta \ : \quad v_r = v_\phi = 0$$

Since $\alpha$ means the ratio between the radial and the circumferential components of the relative velocity in the boundary layer and thus, also the ratio between the corresponding components of the frictional stress.

$$\tau_r = -\alpha \tau_\phi \qquad (4)$$

The resultant relative velocity u of the medium near the surface of the disc is then

$$u = \sqrt{v_r^2 + ( v_\phi - r\omega )^2} = ( 1 + \alpha^2 )^{1/2} (\frac{z}{\delta})^{1/7} r\omega \qquad (5)$$

(Note that near the disc (z --> Ø) we obtain

$$\frac{v_r}{r\omega} = \alpha (\frac{z}{\delta})^{1/7} \quad , \quad \frac{v_\phi - r\omega}{r\omega} = - (\frac{z}{\delta})^{1/7}$$

Using the empirical 1/7 th-power low as found for a pipe we have $\frac{u}{v_*} = 8.74 ( \frac{v_* z}{\nu} )^{1/7}$

where $v_* = \sqrt{\tau_0/\rho}$ is friction velocity.

$\tau_0$ is wall shear stress.

And inserting u = U for z = $\delta$ we get,

$$\tau_0 = 0.0225 \rho u^2 (\frac{\nu}{u\delta})^{\frac{1}{4}} \qquad (6)$$

From equation (4), (5), and (6)

$$\tau_r = 0.0225 \rho \alpha^{\frac{7}{4}} (r \omega)^{\frac{7}{4}} (\frac{\nu}{\delta})^{\frac{1}{4}} \{1 + \frac{1}{\alpha^2}\}^{\frac{3}{5}}$$

$$\tau_{\phi} = -0.0225\,\rho(r\omega)^{\frac{7}{4}}(\nu/\delta)^{\frac{1}{4}}\{1+\alpha^2\}^{\frac{3}{5}} \qquad (6)'$$

Now, we calculate the equation (1) and (2) considering eq. (3) and (6)', we obtain an equation which determines $\alpha$ and $\delta$ :

$$\frac{d}{dr}(0.207r^2\omega^2\alpha^2\delta) - 0.0278r^2\omega^2\delta = -0.0225\alpha^2r^3\omega^2\left(\frac{\nu}{\alpha\omega r\delta}\right)^{\frac{1}{4}}\left(1+\frac{1}{\alpha^2}\right)^{\frac{3}{5}}$$

$$\frac{d}{dr}(0.0681r^4\omega^2\alpha\delta) = 0.0225r^4\omega^2\left(\frac{\nu}{r\omega\delta}\right)^{\frac{1}{4}}(1+\alpha^2)^{\frac{3}{5}}$$

Further, putting

$$\delta = \beta r^{\frac{3}{5}} \qquad (7)$$

Now, we obtain a system of algebraic equations in $\alpha$ and $\beta$ :

$$0.7456\alpha^2\beta - 0.0278\beta = -0.0225\,\alpha^2\left(\frac{\nu}{\alpha\beta\omega}\right)^{\frac{1}{4}}\left(1+\frac{1}{\alpha^2}\right)^{\frac{3}{5}}$$

$$0.3133\alpha\beta = 0.0225\left(\frac{\nu}{\beta\omega}\right)^{\frac{1}{4}}(1+\alpha^2)^{\frac{3}{5}}$$

Dividing the first equation by the second we get

$$1.0859\alpha^2 - 0.0278 = 0$$

whence, $\alpha = 0.162$

The corresponding value of $\beta$ obtained is

$$\beta = 0.525 \left(\frac{\nu}{\omega}\right)^{\frac{1}{5}}$$

so that the thickness of the boundary layer is

$$\delta = 0.525r \left(\frac{\nu}{r^2\omega}\right)^{\frac{1}{5}} \qquad (8)$$

For the components of the local coefficient of friction we obtain the following:

$$\frac{\tau_\phi}{\rho(r\omega)^2} = -\frac{r}{\alpha\rho(r\omega)^2} = 0.0267\ Re^{-0.2} \qquad (9)$$

where, Re is Reynolds number,

$$Re = \frac{r^2\omega}{\nu}$$

Now, we calculate the torque on one side of a disc of radius R:

$$M = 2\pi R^2\rho \int_0^\delta v_r v_\phi\, dz = 0.0364\ R^5\omega^2\rho\left(\frac{\nu}{R^2\omega}\right)^{\frac{1}{5}} \qquad (10)$$

If we define the drag coefficient as

$$C_M = \frac{2M}{\frac{\rho}{2}\omega^2 R^5} \qquad \text{(for 2 sides)} \qquad (11)$$

The drag coefficient becomes

$$C_M = 0.146\ Re^{-0.2} \qquad (12)$$

The result agrees well with experimental data (See Figure 6) except for the region of large Reynolds number.

To obtain better agreement with experiment Dorfman[48] calculated the drag coefficient using a universal logarithmic velocity profile in the boundary layer. The drag coefficients were calculated in the three different ranges of Reynolds number:

i) $10^4 \leq Re \leq 9 \times 10^4$

$$C_M = 0.0229\ Re^{-0.239}\ (1 + 0.395\ Re^{-0.08})^{0.241} \qquad (13)$$

$$\frac{\delta}{R} = 0.0853\ Re^{-0.043}\ (1 + 0.395\ Re^{-0.08})^{0.46} \qquad (14)$$

$$\alpha = -\frac{\tau_r}{\tau_\phi} = 0.629\ Re^{-0.043}\ (1 + 0.395\ Re^{-0.08})^{-0.043} \qquad (15)$$

ii) $9 \times 10^4 \leq Re \leq 9 \times 10^6$

$$C_M = 0.1136\ Re^{-0.181}\ (1+0.21\ Re^{-0.232})^{0.318} \qquad (16)$$

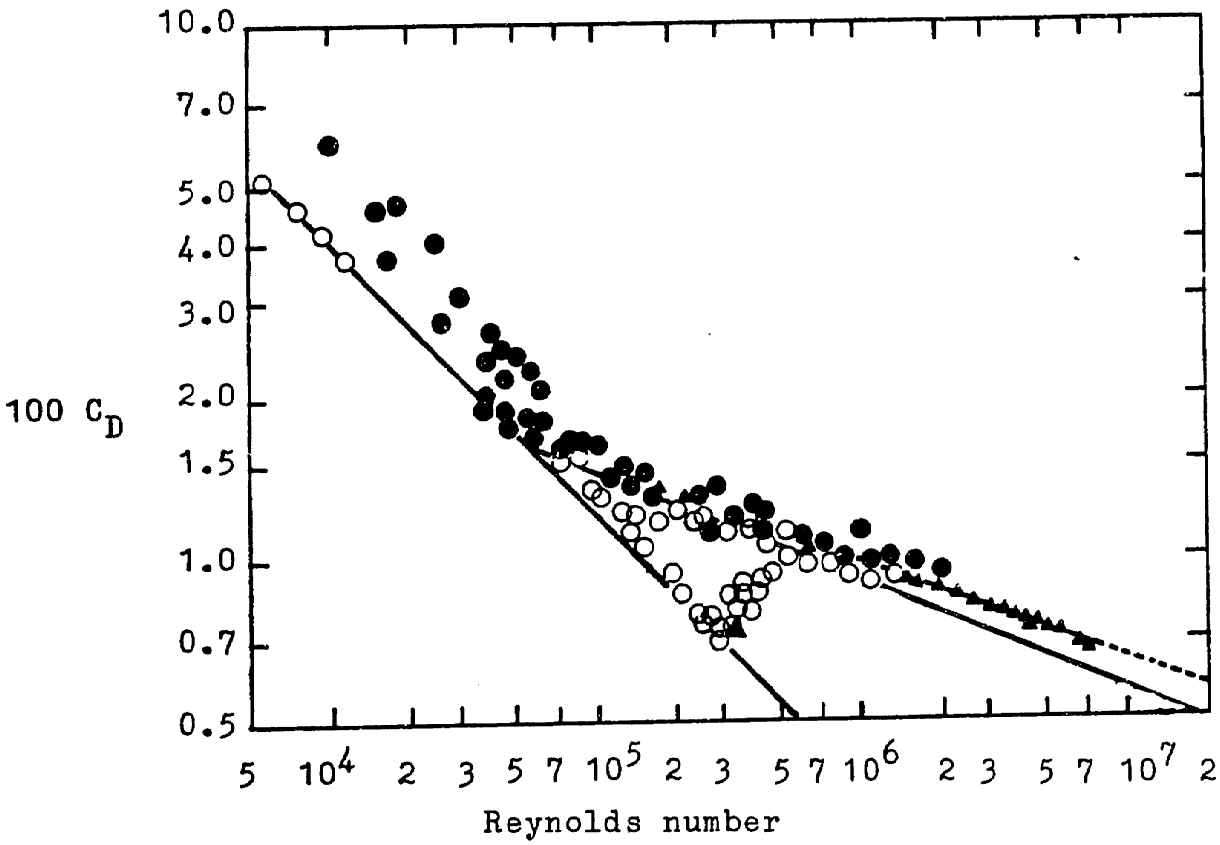


Figure 6. Drag Coefficient for a Disc Rotating in Liquid at Rest.[48]

Line 1: laminar flow,
Line 2: turbulent flow (Equation (12)), and
Line 3: turbulent flow (Equation (16)).

The marks are experimental data.

$$\delta/R = 0.0643\ Re^{-0.016}\ (1+Re^{0.032})^{0.485} \quad (17)$$

$$\alpha = 0.4565\ Re^{0.016} \quad (18)$$

iii) $6.4 \times 10^{7} \leq Re \leq 3.3 \times 10^{9}$

$$C_M = 0.042\ Re^{-0.122} \quad (19)$$

$$\delta/R = 0.0515 \quad (20)$$

$$\alpha = 0.342 \quad (21)$$

Furthermore, he denoted that the values of $C_M$ for the three intervals considered can be combined in the general formula.

$$C_M = 0.982\ (\log Re)^{-2.58} \quad (22)$$

and

$$\delta/R = 0.05 + (\log Re)^{-2.7} \quad (23)$$

$$\alpha \simeq 0.33 + 3(\log Re)^{-2.5} \quad (24)$$

In the present study the experimental results of rigid disc have been compared with Equation (16).

## 3. Chemistry of Forming Low Modulus Silicone Networks

Elastomeric networks possess the ability to sustain large

deformations without rupture and to recover rapidly to their original dimensions with no permanent deformation. Networks owe their long-range elasticity to the polymer chains of which they are comprised, which are connected of thieir ends in junctions. The deformation of a network is accommodated through the configurational rearrangements of the polymer chains. These same chain configurations provide an entropic driving force to restore the material to its original dimension upon removal of the strain. Since the entire process is accomplished without the breakage of chemical bonds and since the chain ends are connected in junctions, no permanent deformation is observed. It is crucial to elastomeric behavior that the long polymer chain possess sufficient internal mobility to undergo the required configuratiional arrangements during deformation. When the polymer chains are sufficiently above their glass transition temperature ($T > T_g + 50^\circ C$), reasonably rapid deformation under stress and recovery upon removal of stress is achieved.

Figure 7 illustrates the schematically on the elastomeric network. The points where the polymer chains are joined into network are referred to as the junction sites or crosslinks are shown by the X's in Figure 7. The number of chain ends terminating in a junction site is the functionality of that junction. The junctions used in the present study were tetrafunctional. In order for a network to exist the average

junction functionality must be at least three. Difunctional junctions act only as chain extending agents (See Figure 8(a)). Furthermore, any junction which is not joined to the network by at least three polymer chains is viewed as an elastically ineffective junction because it will not follow the network deformation. The ineffective junctions are shown in Figure 8(a) and 8(b) as ○ . In the present study, to lower the modulus of the network the network was formed in the presence of nonfunctional molecules (diluent) which are chemically almost identical to the chain polymer except that there are no group at the chain ends by which they can be connected to junctions. (Refer to Figure 8(d)). The nonfunctional diluent lowers the modulus and varies the ratio of loss to storage modulus (loss tangent) of the network as well. The dangling chain ends (loose end) of network (See Figure 8(b)) also increased the loss tangent in the compositions formed in this study (though it does not <u>generally</u> follows that the loss tangent increases).

Vinyl terminated polydimethylsiloxane and tetrafunctional hydrogen silane react to form a network in the presence of appropriate catalyst at low temperature. Silicone hydrides add to gaseous olefins in a hydrosilation reaction. In the absence of any catalyst, the reaction requires high temperatures and pressures.[51] The reaction therefore, is usually catalysed, either by radial initiators or, more commonly, by certain

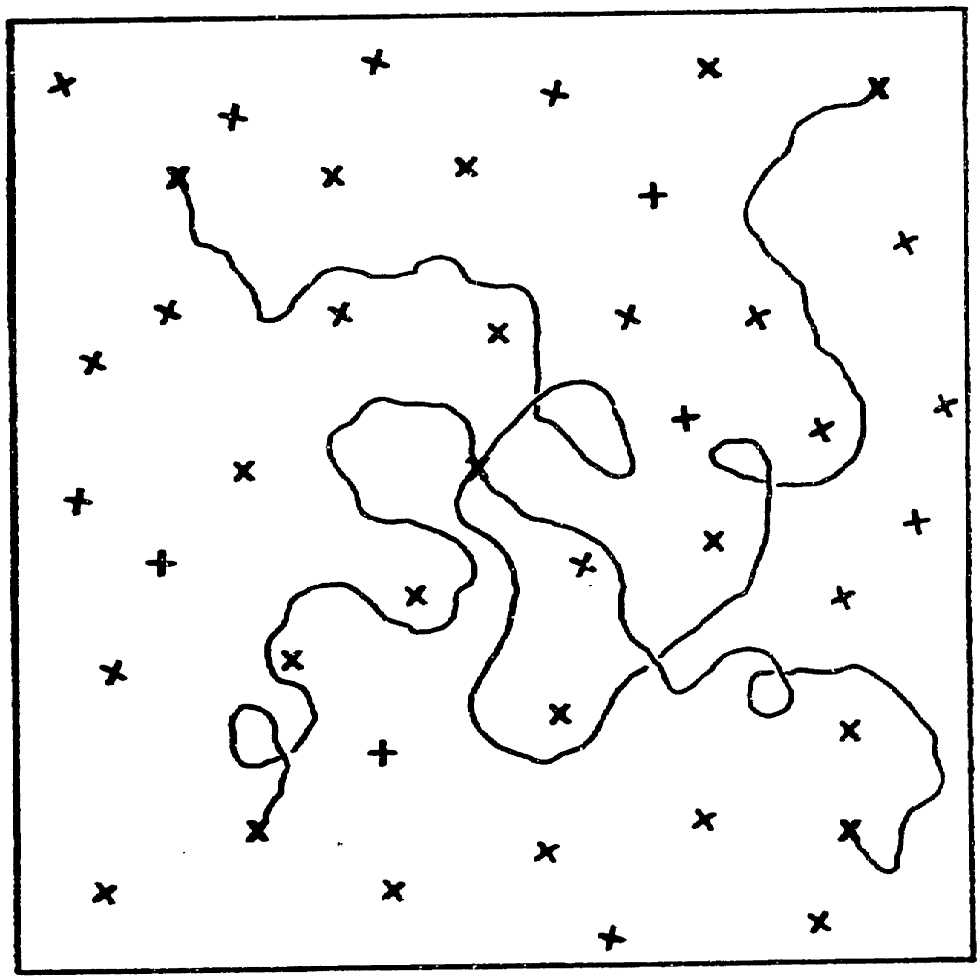

FIGURE 7. Network Topology; + = Tetrafunctional Junction

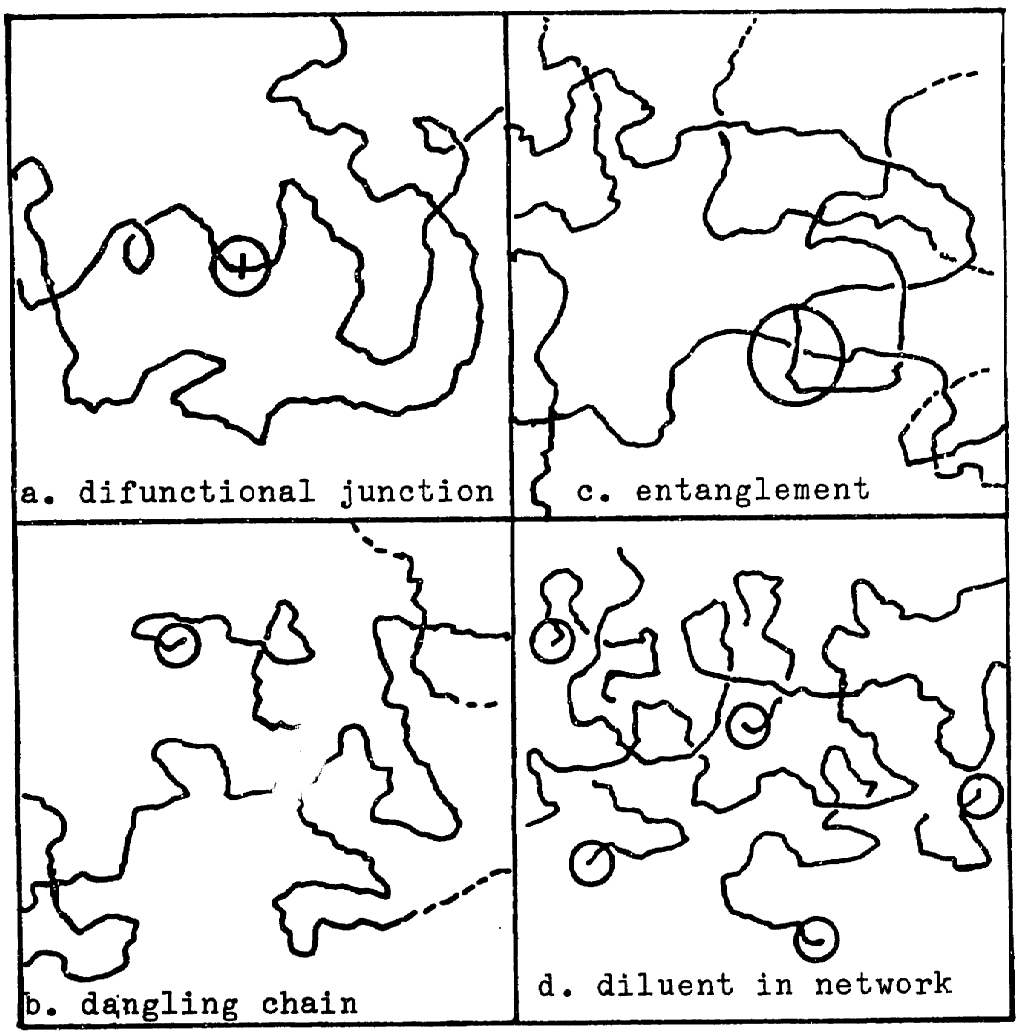


Figure 8 . Structural Components of Networks

transition metals and their complexes.

$$CH_2{=}\ CH_2 \xrightarrow[250\text{-}300^{\circ}C\ ,\ 100\text{-}150atm]{MeCl_2SiH} MeCl_2Si(CH_2CH_2)_nH \qquad (1)$$

Radical initiators, like di-t-butyl pexoxide, react with silicon hydrides to give silyl radicals (See Equation (3)). In the presence of olefins a chain reaction then sets in (Eq. (4) and Eq. (5)). Because of the weak Si-H bond, silicon hydrides are efficient hydrogen donors to radicals (Eq. (5)).

$$Bu - O - \overset{\curvearrowleft}{O} - Bu \xrightarrow{100\ -\ 140} 2BuO^{\bullet} \qquad (2)$$

$$MeCl_2Si - H \ + \ {\bullet}OBu \longrightarrow MeCl_2Si^{\bullet} \qquad (3)$$

$$MeCl_2Si^{\bullet} \ + \ CH_2{=}CH_2 \longrightarrow MeCl_2Si\text{-}CH_2CH_2^{\bullet} \qquad (4)$$

$$MeCl_2SiCH_2CH_2^{\bullet} + HSiCl_2Me \longrightarrow MeCl_2SiCH_2CH_3 + MeCl_2Si^{\bullet} \qquad (5)$$

With the discovery that transition metals and their complexes catalyse hydrosilation, the thermal and peroxide-initiated reactions described above have been largely, superseded. Typically, chloroplatinic acid, $H_2\ PtCl_6 \cdot 6H_2\emptyset$ is used as catalyst at room temperature.

$$H_2C{=}\overset{H}{\underset{R^1}{C}} \xrightarrow[H_2PtCl_6]{R_3^2SiH} R_3^2\,Si - \overset{H}{\underset{H}{C}} - \overset{H}{\underset{H}{C}} - R^1 \qquad (6)$$

Like radical-initiated hydrosilation, the catalysed reaction shows a strong preference for terminal addition.

In outline, the mechanism of the reaction[50] involves coordination of the olefin on to the metal (7) ⟶ (8), followed by addition of silane to metal (8) ⟶ (9); rearrangement to a σ - bonded platinum species (9) ⟶ (10) is followed by transfer of the terminal carbon from platinum to silicon (10) ⟶ (11).

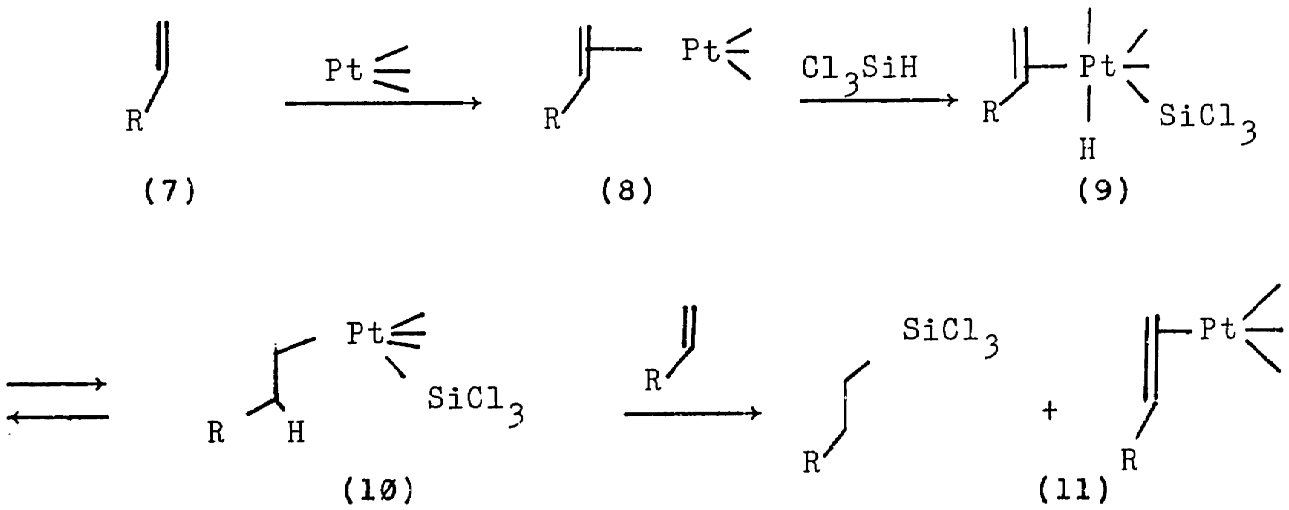


The basic reaction of hydrosilation is employed in one form of Low Temperature Vulcanizing (LTV) silicone rubber compositions.[51,93] Divinyl terminated polydimethylsiloxane is used as chain molecule and tetrafunctional hydrogensilane as junction site.

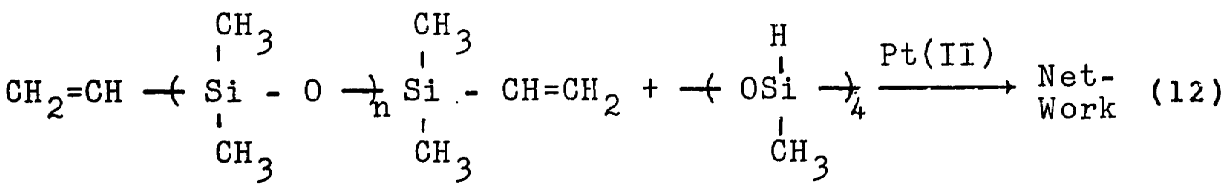


(12)

The theory of rubber elasticity[52] predicts that the equilibrium elastic modulus of an ideal rubber should increase linearly with the number of elastically effective chain per unit volume, and thus in the case of networks synthesized from $\alpha,\omega$-difunctional chains, inversely as the chain length (molecular weight). Secondly, the same theory leads to the conslusion that at fixed chain length (mol. wt. of $\alpha,\omega$-difunctional chains) the equilibrium modulus should vary $v_2^{\frac{2}{3}}$, where $v_2$ = volume fraction of a diluted network that becomes covalently connected (ie., $1 - v_2$ = fraction of diluting material). Very compliant material can thus be achieved by creating very long chain molecules (thereby using low numbers of elastically effective molecules per unit volume), and then in addition diluting the chain-junction mixture, prior to reaction, with non-reactive diluent of the same chemical type (e.g., dimethylsiloxane) thereby insuring compatibility.

## 4. Rubber Elasticity: Prediction of Modulus at Thermodynamic Equilibrium

The phenomenon of rubber elasticity have been under investigation for almost two centries.[54] Yet, there still remains much controversy as to the correct molecular theory to explain elastomeric behavior. These theories relate to an

elastomer's network structure to its equilibrium mechanical properties. In the molecular theories of rubber elasticity there are mainly two competing theories which are Flory dual network theory[55] and entanglement theories.[57-59]

The dual network theory holds the molecular model based on the supposition that in simple elongation, a real network undergoes a transition between the two extremes of affine and phantom behavior. In a theoretical affine network,[54] the effects of the macroscopic strain are transmitted to the network chains through junctions in which the chain ends are terminated. It is, therefore, the displacement of the junctions which will eventually determine the end-to-end distance of the strained network chains. On the other hand, the phantom network chains act only to impart force between junctions in which their ends terminate.[56] These phantom chains may pass through each other freely and two or more chains may occupy the same volume. James and Guth[56] demonstrated that for the "phantom" network, (i) the mean positions of junctions are determined by the system's macroscopic dimensions, (ii) displacements of these mean position are affine in macroscopic strain, and (iii) that fluctuations from these mean positions are Gaussian and of mean magnitude independent of strain. The phantom and affine molecular models differ the reduced modulus by the factor of 2 in a tetratfunctional network.

Flory's dual network theory[55] suggests that the fluctuations of junction about its mean position may be sufficiently impeded by interactions with chains emanating from spatially, but not topologically, neighboring junctions. Thus, the junctions in a real network are more constrained than these in a phantom network, but may not be so constrained as to behavior totally affine. In a typical tetrafunctional network, it may be shown easily by simple calculation of end-to-end distance and mean spatial distance of junctions that the junctions directly connected by network chains to a given junction (its topological neighbors) are not in general its nearest spatial neighbors. It is due to the spatial interpenetrations of topological domains in low functionality networks. Therefore, Flory suggests that the junctional fluctuations predicted for a phantom network may be impeded drastically in a real network due to random interspersion of the chains emanating from the junction with neighboring chains. The junction-chain "entanglements" may be presumed to restrict the locations of the junctions to the environments of neighboring members of the network when the network is strained. They may thus enforce greater displacements on the junctions under strain than the phantom model prescribes, and hence, render their locations more affine in the macroscopic strain. At small strains the locations of the junctions are dominated by the entanglements in which they are involved. Hence, their displacements may approach those prescribed by the

macroscopic strain (affine network). At higher strains, and/or at greater dilutions, the constrains due to entanglements become less severe, Øand the phantom network behavior is approached.

The network molecular theory of rubber elasticity competing with Flory dual network theory is entanglement theories. Graessley[57], Langley[58] and Kan and Ferry[59] have argued that the chains interact with chains themselves as well as junction, while Flory considers topological interactions among junctions and chains only. Their arguments are based on the rubbery plateau which is observed for high molucular weight linear polymers in dynamic mechanical testing.[60,61] The plateau has been attributed to entanglements between long chains and is a consequence of the "non-phantom" nature of the chains. If during network formation a portion of these entanglemens are permanently trapped, the resulting modulus will be greater than that due to the chemical formation of network chains alone. Langley suggested that the two modulus components are additive for small strains: ie., the small strain modulus of network, (G) is the sum of the modulus, ($G_c$) due to the chemical junctions and that ($G_e$) from the permanently entangled chains.[60]

$$G = \lim_{\alpha \to 1}[f] = G_c + G_e \qquad (1)$$

where, $\alpha$ is elongation ratio ($l/l_0$)

[f] is reduced stress ( = $f/A(\alpha - \bar{\alpha}^2)$)

and A is Area of cross-section.

$G_e$ is generally taken as the product of $G_e^{max}$, the maximum possible contribution of entangled chains to the modulus, and $T_e$, the fraction of the maximum actually obtained:

$$G_e = T_e\, G_e^{max} \qquad (2)$$

Dossin and Graessley[57] suggested that $T_e$ is equivalent to the probability that any pair of interacting units are each part of elastically active chains. Therefore, $T_e$ is simply the probability that all four paths leading from interacting chains are connected to the network. $G_e^{max}$ is expected to be closely related to $G_N^0$ and should be dependent on the condition of network formation, however, the exact dependence of $G_e^{max}$ on these parameters is still under study. For the network chain contribution to the modulus, $G_c$, an adaptation of the Flory dual network theory was utilized by Graessley[57]:

$$G_c = \upsilon\, kT/V\, (1 - 2h/\phi) \qquad (3)$$

where, h is an empirical constant between one and zero depending on the extent to which the junction fluctuations are impeded in the network (h = Ø, affine behavior; h = 1, phantom

behavior). $\upsilon$ is crosslinking density of network (# of junctions/unit volume), k and T are Boltzman constant and absolute temperature, V and $\phi$ are volume of the network and junction functionality, respectively. Therefore, the quations (1), (2) and (3) give the small strain modulus according to entanglement theory:

$$G = \upsilon\, kT/V\ (1 - 2h/\phi) + T_e^{max}\, G_e^{max} \qquad (4)$$

In addition to the molecular theories rubber elasticity, there are some phenomenological theories which are based on purely formal postulates or stress-strain relationships. Among the phenomenological theories Mooney-Rivlin theory[62-64] is the most comprehensive and practically useful to analyze the rubber networks.

$$\sigma = (2C_1 + 2C_2\,\alpha^{-1})(\alpha - \alpha^{-2}) \qquad (5)$$

The above eq. (5) is known as the Mooney-Rivlin equation, where $C_1$ and $C_2$ are constants which are determined by experiments, and $\sigma$ is stress. The equation fits experimental data exceedingly well in uniaxial extension, however, it fails in compression and does not accurately describe other deformations (for instance, shear biaxial extension).

A number of experiments[65-69] have been performed to support the theories mentioned above. Mark[69] who had studied the rubber elasticity in a series of experimental works[65-67,69] concluded that chain-chain interactions (entanglements) did not make a substantial contribution to eiher the small or large strain equilibrum tensile modulus and that the basic hypothesis of Flory dual network theory was correct. However, later investigators[68,53] pointed out Mark's experiments could be interpretted differently. That is, his results could have agreed with the entanglement theory, too.

Recently, Meyers et al[53,70] performed careful experiments with end linking reaction of $\alpha, \omega$ -divinyl polydimethylsiloxane and polyfunctional junctions to examine the theories of rubber elasticity. The results of small strain and large strain of the networks supported the hypothesis of entanglement rather than the Flory's dual network theory.

## 5. Dynamic Mechanical Properties of Dilute Networks

To study the viscoelastic behavior of polymers various techniques have been used. Stress relaxation, creep behavior and dynamic experiment are the most frequently used techniques. The experimental values of each techniques are correlated so that it is possible to calculate one value from others. The dynamic experiments is usually done by employing

periodic strain or stress to the materials. When the strain is varied sinusoidally it is found that the stress will also alternate sinusoidally but will be out of phase with the strain (if the material shows linear viscoelatic behavior). A dynamic experiment at frequency $\omega$ (radians/sec) is qualitatively equivalent to a transient experiment at time $t = 1/\omega$. The constitutive equation for linear viscoelasticity in simple shear is based on the principle that the effects of sequential changes in strain are additive:[71,20]

$$\sigma_{21}(t) = \int_{-\infty}^{t} G(t-t')\dot{\gamma}_{21}(t')dt' \qquad (1)$$

where $\dot{\gamma}_{21} = \partial\gamma_{21}/\partial t$ is the shear rate, $G(t)$ is the relaxation modulus, and $\sigma_{21}$ is shear stress at time t. The integration is carried out over all past times t' up to the current time t. For the dynamic experiment the constitutive equation becomes:

$$\text{Let} \qquad \gamma(t) = \gamma^0 \sin \omega t \qquad (2)$$

where $\gamma^0$ is the maximum amplitude of the strain. Then,

$$\dot{\gamma}(t) = \omega\gamma^0 \cos \omega t \qquad (3)$$

Substituting in equation (1), denoting t-t' by s, we have

$$\sigma(t) = \int_0^{\infty} G(s)\omega\gamma^0 \cos[\omega(t-s)]ds$$

$$= \gamma^0[\omega\int_0^{\infty} G(s)\sin \omega s ds] \sin \omega t + \gamma^0[\omega\int_0^{\infty} G(s)\cos \omega s ds] \cos \omega t \qquad (4)$$

The integrals converge only if $G(s) \longrightarrow \emptyset$ as $s \longrightarrow \infty$ ; otherwise, they must be formulated somewhat differently. It is clear that the term in sin $\omega t$ is in phase with $\gamma$ and the term in cos $\omega t$ is 90 degree out of phase; $\sigma$ is periodic in $\omega$ but out of phase with $\gamma$ to a degree depending on the relative magnitudes of these terms. The quantities in brackets are functions of frequency but not of elapsed time, so equation (4) can be written:

$$\sigma(t) = \gamma^0(G'\sin \omega t + G''\cos \omega t) \qquad (5)$$

Thereby, defining two frequency-dependent functions - the shear storage modulus $G'(\omega)$ and the shear loss modulus $G''(\omega)$.

The stress, $\sigma(t)$ can be written in an alternative form displaying the amplitude $\sigma^0$ of the stress and the phase angle $\delta$ between stress and strain. From trigonometric relations,

$$\sigma(t) = \sigma^0 \sin(\omega t + \delta) = \sigma^0 \cos \delta \sin \omega t + \sigma^0 \sin \delta \cos \omega t \qquad (6)$$

Comparing Eq. (5) and Eq. (6),

$$G'(\omega) = (\sigma^0 / \gamma^0) \cos \delta \qquad (7)$$

$$G''(\omega) = (\sigma^0 / \gamma^0) \sin \delta \qquad (8)$$

and $$G''/G' = \tan \delta \qquad (9)$$

In any dynamic measurement at a given frequency two independent quantities, either G' and G" or tan $\delta$ and $\sigma^0 / \gamma^0$ are obtained.

It is usually convenient to express the sinusoidally varying stress as a complex quantity, then the modulus is also complex,

given by[,1]

$$\sigma^*/\gamma^* = G^* = G' + iG'' \qquad (10)$$

$$| G^* | = \sigma^0/\gamma^0 = \sqrt{G'^2 + G''^2} \qquad (11)$$

This corresponds to a vectorial resolution of components in the complex plane. It is evident that G' is the ratio of the stress in phase with the strain to the strain, whereas G" is the ratio of the stress 90 degree out of phase with the strain to the strain.

The physical meaning of storage modulus, $G'(\omega)$ is a quantity of the energy stored and recovered per cycle of periodic deformation and the loss modulus, $G''(\omega)$ is a measure of the energy dissipated or lost as heat per cycle, when different systems are compared at the same strain amplitude. The loss tangent, $\tan\delta$ which is demensionless and conveys no physical magnitude but is a measure of the ratio of energy lost to stored in a cyclic deformation is very useful to study the viscoelastic properties of polymers.

A dynamic measurement at frequency is qualitatively equivalent to a transient relaxation modulus, G(t) at $t = 1/\omega$ . For the viscoelastic liquids such as polymeric solution or linear amorphous polymers, $G'(\omega)$ approaches zero with decreasing frequency (terminal zone), this means that the phase

angle between stress and strain approaches 90 degrees as the stored energy per cycle of deformation becomes negligible compared with that dissipated as heat. Increasing the frequency, rubbery plateau zone is appeared if the molecular weight of the polymer is sufficiently high. The plateau zone is understood as the effect of the entanglement of the polymer chains. There is a transition from rubbery to glassy state as further increase of the frequency. In the transition regime, the storage modulus undergoes dramatic change over several powers of 10.

The introduction of chemical crosslinks into uncrosslinked polymers (polymer solution or amorphous linear polymer) converts them from a viscoelastic liquid to a viscoelastic solid. The viscoelastic solid shows charateristic properties as follows: the viscosity becomes infinity, the material aquires an equilibrium modulus, therefore, the properties in the rubbery plateau and terminal zones change profoundly. However, the properties in the transition zone may change very little.[72]

In the frequency regions where $G'(\omega)$ changes slowly (plateau zone) the behavior of polymer is nearly perfectly elastic; ie., little energy is disspated in periodic deformations, thus, in such regions, $G''(\omega)$ tends to be considerably less than $G'(\omega)$. This effect is prominent in the locations of $G''(\omega)$ for the glassy state polymers and

crystalline polymers, whose $G'(\omega)$ curves are relatively flat throughout.

At high frequencies, the motion of dashpots (viscous element) becomes negligible compared with that of the the springs (elastic element) in the spring-dashpot model[73] of viscoelastic materials; then $G''(\omega)$ should approach zero. On a molecular basis, this would correspond to the absence of any molecular or atomic adjustments capable of dissipating energy within the period of deformation. However, around transition zone $G''(\omega)$ shows maxima which represents high dissipation of deformation energy upto certain frequency and beyond the frequency the backbone configurational changes diminish. At very low frequencies (terminal zone), $G''(\omega)$ for a viscoelastic liquid is proportional to $\omega$ as for a simple Newtonian liquid. On the other hand, the crosslinked network and crystalline polymer do not indicate such behavior at very low frequencies but revealed certain constant low $G''(\omega)$.

As mentioned above, loss tangent is a useful measure of the viscoelastic behavior of polymers. ($\tan \delta = G''/G'$). For the viscoelastic liquid $\tan \delta$ is large and in fact becomes inversely proportional to the frequency in the low frequency region (terminal zone). Because in the terminal zone G" of the viscoelastic liquid is proportional to $\omega$ and G' to $\omega^2$, respectively. Regardless of crosslinks in the system, all the amorphous polymers have values in the transition zone which are

in the neighborhood of tan $\delta$ = 1, ranging from Ø.2 to 3. The glassy and semicrytalline polymers have values in general around Ø.1.[77] The loss tangent determines macroscopic physical properties as the damping of free vibrations, the attenuation of propagated waves, and the frequency width of a resonance response.

For the idealized networks which have uniform strands and no defect in the structure, the dynamic mechanical properties are estimated by Mooney[81]:

$$G' = \upsilon RT[1 + \sum_{1}^{N} \omega^2 \tau_p^2 / (1 + \omega^2 \tau_p^2)] \qquad (12)$$

$$G'' = \upsilon RT \sum_{1}^{N} \omega \tau_p / (1 + \omega^2 \tau_p^2) \qquad (13)$$

where, $\upsilon$ is effective chain density of network, $\omega$ is frequency (rad/sec) and $\tau_p$ is major relaxation times.

A real network always possesses some defect or irrequlariti̇es in the structure: (1) the presence of dangling chains due to either the finite molecular weight of the precursor or incompletion of end linking reaction of chain molecules; (2) the presence of trapped entanglements; (3) the presence of sol fraction. The dangling chains and sol fraction do not contribute to the equilibrium modulus because they can not store elastic energy at equilibrium. On the other hand, the trapped entanglements contribute to the equilibrium modulus

as mentioned in the previous section.

If the dangling chains or the sol fraction consists of relatively short, unbranched molecules, its contributions to the dynamic moduli can be estimated by the following equations.[80]

$$G' = (\rho RT/M) \sum_{1}^{N} \omega^2 \tau_p^2 \quad /(1 + \omega^2 \tau_p^2) \qquad (14)$$

$$G'' = (\rho RT/M) \Sigma \ \omega \tau_p \quad /(1 + \omega^2 \tau_p^2) \qquad (15)$$

where, $\rho$ and M are the density and molecular weight of polymer, $\omega$ and $\tau_p$ are the frequency (rad/sec) and $p^{th}$ relaxation time of polymer, respectively. The net contribution of the short dangling chain and sol fraction to the network moduli can be the calculated value multipied by the weight fractions of dangling chains and sol fraction. However, it is uncertain whether the major relaxation times are the same for a loose molecule threaded through a network as they are in a linear polymer.[72]

In the case of longer dangling chains or sol fraction which exceed the critical length to form entanglements, the viscoelastic behavior of the network becomes more complicated. Langley and Ferry[79] examined the viscoelastic properties of polydimethylsiloxane networks with various crosslinking densities in the wide range of frequency. They have observed the maxima in tan $\delta$ and the inflections in the stroage compliance, J' in the relatively low frequency range, which

they termed 'secondary loss peak'. The maximum of the secondary loss peak decreased and shifts to higher frequencies with increasing crosslinking density. The phenomena were attributed to rearrangements of configurations by slippage of untrapped entanglements. The sources untrapped entanglements are long linear molecules unattached to the network and long dangling chains. Furthermore, a quantitative analysis was made to calculate the contribution of untrapped entanglements to the total dynamic moduli. The value of $J_{eN}$, dynamic storage compliance in the plateau zone, was compared with equilibrium compliance, $J_e$.

$$G_{eN} = 1/J_{eN} = \upsilon' RT \qquad (16)$$

$$G_e = \upsilon RT \qquad (17)$$

and $$G_{eN}/G_e = \upsilon'/\upsilon \qquad (18)$$

where, $G_{eN}$ is the storage modulus in the plateau zone, $\upsilon'$ is the density of effective network chains terminated either by chemical crosslinks or by entanglements, either trapped or untrapped, whereas $\upsilon$ is the density of effective network strands terminated by chemical crosslinks or trapped entanglements. The values of $\upsilon$ and $\upsilon'$ are calculated by employing equilibrium swelling technique and compared with the ratios of $G_{eN}$ to $G_e$. Excellent agreement was reported. Ferry et al.[82,83] also studied various stages of crosslinking

reaction for polybutadiens-sulfur system. In this study, they also observed the slow relaxation (low frequency losses) which persisted past the gel point and diminished as further crosslinking reaction.

In the extensive studies[84] of viscoelastic behavior of lightly crosslinked network, mixtures of butyl rubber with linear polyisobutylene of high molucular weights were carefully examined. A comparison with the properties of a butyl rubber without polyisobutylene showed contributions to the dynamic loss attributable to the raplating linear species. A simple blending law[86] which had some success in mixtures of linear polymers with different molecular weights was introduced to express the storage moduli of the mixtures:

$$G'_{bl}(\omega) = V_{11}G'_{11}(\omega\lambda_{11}) + V_{22}G'_{22}(\omega\lambda_{22}) \quad (19)$$

where the subscripts bl, 11, and 22 referred in their systems to the blended system, the linear polybutylene, and a butyl rubber network of similar character to that present in the blended system in the absence of linear species. The time shift factors $\lambda_{11}$ and $\lambda_{22}$, which turned out to be unity, are the ratios of relaxation times of species 1 and 2 in the blended system to those in the isolated components. $V_{11}$ and $V_{22}$ are weighting factors. A similar relation was applicable to $G''(\omega)$. The second term of Eq. (19) was replaced by the equilibrium modulus of the mixture, $G_e$ and $G'_{11}(\omega\lambda_{11})$ was

achieved by the viscoelastic test of linear species. The second term of $G''_{bl}(\omega)$ would be zero assuming network did not contribute to the total loss at very low frequencies. Then the relations were,

$$G'_{bl}(\omega) = V_{11}G'_{11}(\omega\ \lambda_{11}) + G_e \qquad (20)$$

$$G''_{bl}(\omega) = V_{11}G''_{11}(\omega\ \lambda_{11}) \qquad (21)$$

The calculated values were compared with experimental ones. The weighting factor, $V_{11}$ was approximately equal to 2/3 power of volume fraction of linear molecule. That is, the dynamic moduli of the mixture was proportional to the volume fraction of linear molecule to a power of about 2/3. The time required in stress relaxation for the portion of the modulus attributable to the reptating species to decay to half its plateau value was proportional to the molecular weight of linear species to the third power.[84] In other words, the position of the low frequency loss peak which mentioned above is pushed down to the low frequency region as the molecular weight of reptating molecule increses. The succeeding work of Kramer et al[85] indicated similar behavior with the mixture of crosslinkable ethylene-propylene terpolymer and saturated ethylene-propylene copolymer. The relaxation time to decay to half its plateau modulus was approximately proportional to the 3.5 power of the molecular weight. It is interesting to note

that the proportionality of relaxation time to the 3 to 3.5 power of the molecular weight of linear molecule as is the terminal relaxation time in uncrosslinked polymers of high molecular weight.

## Experimental Procedures

### 1. Fabrication of Compliant Coatings

#### A. Synthesis of Lightly Crosslinked Silicone Network

It is convenient to utilize chain molecules of well defined molecular weight with functional end groups to vary network chain density, and it is easy to reproduce a network bearing specified properties when needed. If the end-linking reaction (chain ends to junction) goes to completion, the average chain molecular weight and molecular weight distribution between the crosslinks will be those of the chain precursor. Therefore, various molecular weights of $\alpha$, $\omega$-divinyl polydimethylsiloxanes (PDMS) were used to prestudy the dynamic mechanical properties of silicone networks with appropriate junction materials such as 1,3,5,7-tetramethyl cyclotetrasiloxane of tetrakis (dimethylsiloxy) silane.

i)
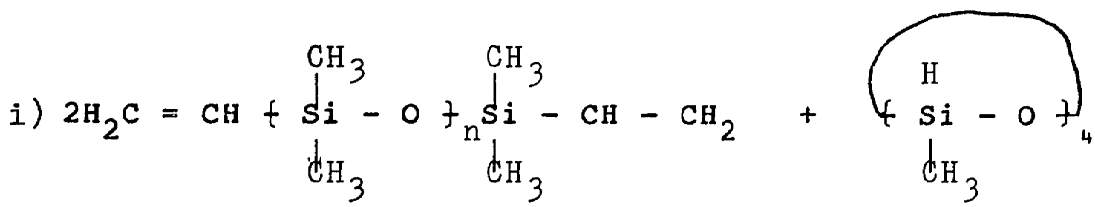

( $\alpha$ , $\omega$ -divinyl PDMS) (tetramethyl cyclotetrasiloxane)

$\xrightarrow[\text{at } 70^{0}C]{\text{Pt(II)}}$ Network Polymer or,

ii) $2H_2C = CH \{ Si(CH_3)_2 - O \}_n Si(CH_3)_2 - CH = CH_2$ + 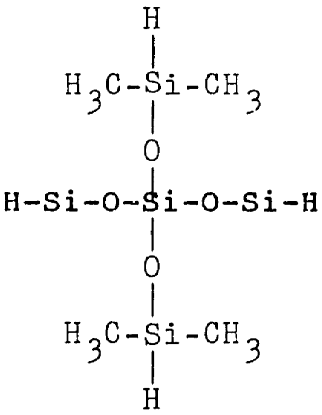

{ α ,ω -divinyl PDMS } { tetrakis(dimethylsiloxy)silane }

$\xrightarrow[\text{at R.T.}]{\text{Pt(II)}}$ Network polymer

The network was easily formed by addition reaction of Si-CH=$CH_2$ + Si-H with platinum catalyst [cis-dichloro bis (diethyl sulfide) platinum (II)],[95] $Pt[\{(C_2H_5)_2S\}_2Cl_2]$, which was synthesized previously in our laboratory[53]. The General Electric Corporation[96] courteously provided the α, ω -divinyl PDMS of various molecular weights (Mn = 7,000, 9,560, 26,400, 28,200, and 39,700). The junction molecules, 1,3,5,7-tetramethyl cyclotetrasiloxane, tetrakis (dimethylsiloxy) silane and the various molecular weights of nonreactive PDMS were purchased from the Petrarch Systems, Inc.

A distinction must be drawn between networks which are

diluted first and then crosslinked and those which are crosslinked first and then swollen. In the former, the network chains have their average random conformation in an unstrained state. In the latter, however, the chains are all elastically extended beyond their normal end-to-end distances, and topology is different with respect to proportion of loose ends, entanglement entrapment, and presence of small cyclic structure.[97]

In present study the networks were diluted by the former method. Nonfunctional polydimethyl siloxane (trimethyl terminated PDMS) was present in the crosslinking reaction as a diluent. The networks are synthesized with diluents having variable molecular weights ($M_d$; molecular weight of diluent) and variable loadings. In the later work, a chain extender, oligomeric hydrogen terminated PDMS (M.W. = 400) purchased from the Petrarch Systems, Inc., was also utilized in the network to extend the length of the network chains (about 3 - 5 times longer than the initial chain length), so that a sufficiently low compliance of the network was achieved. The ratio, R of the concentration of SiH groups in junction and the chain extender to that of the vinyl groups in the chain molecule was always kept 1.2 ± 0.05 in all networks. The SiH-ratio which was defined by the ratio of the concentration of SiH group in the chain extender to that in the junction molecule was varied from 0 to 4.

The components (chain molecules, junction molecules, chain extender molecules and diluent) of the network without catalyst were mixed using an electric driven motor stirrer (LIGHTNIN, Mixing Equipment Co., N.Y.) for at least 2 hours at about 300 rpm in a 500 ml glass beaker. The platinum (II) catalyst was added at the rate of 25 ± 5 ppm of the reactive polymers in the precursor and mixed for 10 minutes. When the precursor included a diluent of high molecular weight, an ice bath was utilized to keep the mixture cool, so that an anomalously fast gelation was prevented. If the mixture was not kept cool during mixing of catalyst, the gelation of the precursor with high molecular weight diluent ($M_d$ = 49,350, 200 phr) occurred within 15 minutes at room temperature. After the mixing the mixture was left under vacuum to evacuate the trapped air bubbles in the resin. The degased mixture was poured in a polystyrene dish and cured in an oven at $70^0$ C or in an evacuated desicator at room temperature for 24 hours. The former curing condition was used in the first part of this study with 1,3,5,7-tetramethyl cyclotetrasiloxane as junction molecule. The latter method of cure was used in most of the later studies with tetrakis (dimethylsiloxy) silane as junction molecule. The SiH groups of the chain extender and junction molecule can react to the moisture in the air and form silanol groups which react to SiH very easily in the presence of platinum (II) .[53,98] If this reaction occurs, the network cannot yield high extent of reaction and thus, it becomes

difficult to control the material properties by simply fixing the components of the precursor. Therefore, the reaction was carried out in an evacuated desicator at room temperature. For the high temperature curing ($70^{0}$C) the reaction was carried out in air or dry He environment. The material properties of the networks prepared under different environments were compared and found almost identical. Thereafter, the reactions at high temperature ($70^{0}$C) were done in the air.

## B. Characterization of Raw Materials and Networks

### (1) Characterization of Raw Materials

The number average molecular weights of $\alpha,\omega$-divinyl PDMS were determined by taking near IR spectra of vinyl end groups with Cary-14 Spectrophotometer at the wave number 4650 $Cm^{-1}$ (C=C stretching band). A trimethyl terminated PDMS of 5,000 ctsk viscosity was used as reference material. Divinyl tetramethyldisiloxane (99+ % pure, Rhome-Poulene Co.) was utilized as a calibration standard. Three standard solutions in carbon tetrachloride, ranging in concentration from 0.04 to 0.07 molar, were used to determine molar absorptivity of the $Si-CH=CH_2$ group, $\varepsilon_0$. Figure 9 shows the calibration curve of the absorbance vs. molar concentration of the $Si-CH=CH_2$ groups. The molar absorptivity, $\varepsilon_0$ was 1.693. A standard 1 Cm-quartz cell was used to take the spectrum.

The number average molecular weights were calculated as follows:(53)

$$Mn = 2\rho /C = 2\rho\, b\varepsilon_0/A \qquad (1)$$

where is the density of the polymer (Ø.972 g/ml), C is the molar concentration of vinyl group in α,ω -divinyl PDMS, b is the path length of the cell (1 Cm), and A is absorbance of the sample. Equation (1) assumes all the polymer chains terminated in vinyl groups.

Gel permeation chromatographys (GPC) of the α , ω -divinyl PDMS were obtained using a Waters liquid chromatograph equipped with $1Ø^5$, $1Ø^4$ and $1Ø^3$ Styragel at a flow rate of 2.Ø ml/min and Ø.5 ml of Ø.15 - Ø.25 wt % solution were injected. Concentrations were detected by a differential refractometer (Model R4Ø1). The polydispersity, Mw/Mn of the α , ω -divinyl PDMS was determined by the GPC. The Mw/Mn by GPC and Mn by vinyl determination are given in Table II.

To calculate the molecular weight of the chain extender, hydrogen terminated oligomeric PDMS, the molar concentration of SiH groups was measured by using a Perkin Elmer 143Ø Infrared Spectroscoph with data station. The SiH stretching vibration at 2174 $Cm^{-1}$ was monitored by using liquid NaCl cell (Research & Industrial Instruments Co., England) of Ø.5 mm gap. The solution of 25 g/l in $CCl_4$ was used for analyssis. From the Beer's Law:

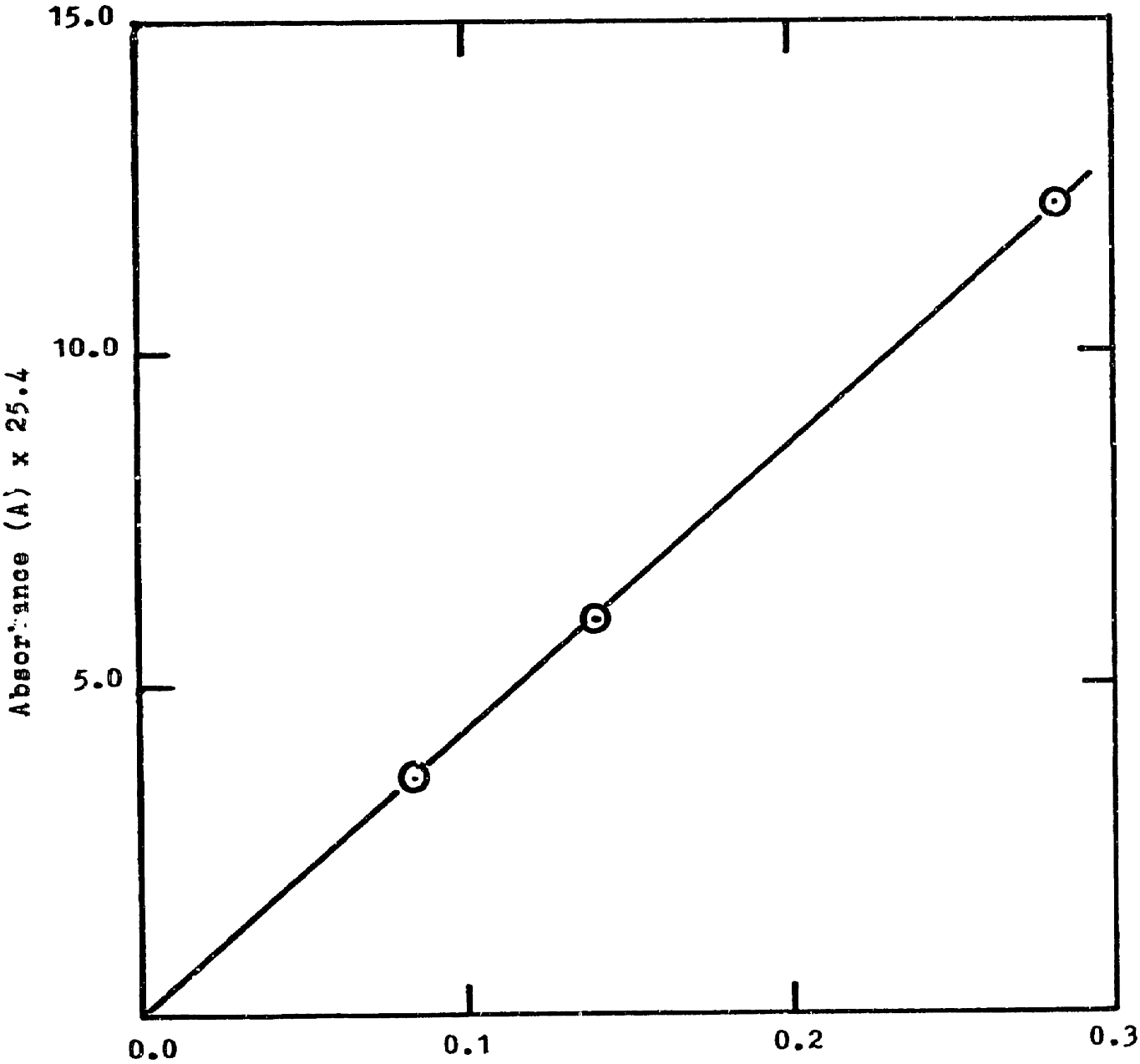


Figure 9. Calibration Line of Vinyl Group Using Cary-14 IR-II Mode at Wave Number 4,650 $Cm^{-1}$.

Table II. Characterization Data of α,ω-divinyl PDMS

| | a | b | c | d | e | f |
|---|---|---|---|---|---|---|
| Mn* | 7,000 | 8,800 | 26,400 | 28,200 | 39,700 | 83,300 |
| Mw/Mn** | 2.30 | 2.35 | 2.21 | 2.05 | 2.51 | 2.83 |

* determined by end group analysis.

** determined by GPC.

$$A = \varepsilon_0^H bc \qquad (2)$$

where $\varepsilon_0^H$ is the molar absorptivity of SiH and other parameters are defined above. $\varepsilon_0^H$ was used 15,400 l $mole^{-1}Cm^{-1}$ which was determined by using Bis (trimethylsiloxy) methylsilane (99+ %, Petrarch Systems, Inc.) as calibration standard previously in our laboratory.[53] The calculated molecular weight of the chain extender was 400.

(2) Characterizations of Networks

(i) Extraction and Determination of Sol Fraction

A Soxhlet extractor was used to extract unreacted polymer (sol) from the undiluted or diluted network to determine the sol fraction and estimate the extent of crosslinking reaction. After extraction by benzene and evaporation of the benzene, the mass fraction of the extractable which were not incorporated into the network (unreacted chain molecule and diluent, if present) was obtained by weighing the residue. The sol fraction was calculated by subtracting the portion of diluent as loaded from the total extractable.

Miller and Macosko[68] derived equations describing the structure of networks formed by the end linking reaction such as the networks in the present study. They have calculated the extent of reaction of the functional groups in the chain molecule by using sol fraction of the network. A brief

derivation of the relation between sol fraction and extent of reaction is attatched in the Appendix B. In Table III the sol fractions and the extend of reaction, $\varepsilon$ are listed for the prestudied networks.

(ii) Determination of Apparent Chain Density

A direct observation of chain density, $\upsilon/v$ was considered by measuring equilibrium shear modulus, $G_e$ of the networks close to the zero strain limit (actually at 1% shear strain). A Rheometrics Eccentric Rotating Disc Mechanical Spectrometer was utilized to measure the equilibrium shear modulus of networks:

$$G_e = A_1 \upsilon / V \, RT \, (V/V_0)^{2/3} \qquad (3)$$

where, $A_1$ is structure factor of network at close to the zero strain limit,[55] R is gas constant, T is absolute temperature, and V and $V_0$ are the volumes of strained and unstrained network which are usually assumed unity (ideal rubber behavior). The structure factor, $A_1$ was assumed unity for tetrafunctional network which has been observed directly by extensive experiments[70] with silicone networks. To accomplish this the spectrometer was brought to 1% shear strain, and held at this strain until an equilibrium rate of stress was obtained (10 to 30 min).

C. Measurement of the Mechanical Properties of Networks and Compliant Coatings

An Eccentric Rotating Disc (Rheometrics) Mechanical Spectrometer[99,100] was utilized to measure the dynamic mechanical properties of the homogeneous networks in shear mode in preliminary studies. Circular specimens of 2.5 Cm in diameter were tested at 1% shear strain in the frequency range from 0.1 to 16 Hz. The properties are reported in the storage modulus and tan $\delta$ ( = loss modulus/storage modulus).

For the composite coatings, in contra distinction to the homogeneous networks, the compression mode was used rather than the shear mode. A Dyna Stat® was used to measure the dynamic storage modulus and loss tangent in compression mode. A circular specimen of 2.5 Cm in diameter was placed in between two aluminum discs of 3.8 Cm in diameter and oscillated at 1% compressive strain from 0.1 to 100 Hz. The thickness of the specimen was measured by micrometer. Data were taken at successive frequencies automatically under command of a DEC PDP-11 computer. To measure the properties of the composite compliant coating the bottom layer (screen material) of the coating was removed from the backing of velvet. (Refer to Figure 13, the schematic diagram of the compliant coating).

The tensile property of the top film of the compliant coating was measured by using an Instron® tensile tester. Dumbbell shape specimens were punched out from the sheet and

extended at the speed of 1 mm/min. The thickness of the specimen was measured by using an Ames Model 66 foot micrometer. The width of the specimen was also measured using a precision ruler. (Take average of three point along the test region). The thickness and width were used for calculating the cross-section of specimen. The dimensions of the dumbbell-shaped specimen are illustrated in Figure 10.

## D. Fabrication of Composite Compliant Coatings

The composite compliant coatings were made of lightly crosslinked silicone networks with various dynamic properties and the viscous rayon velvet fabric as backing material to meet the recommended conditions[1,38] for drag reduction. A number of investigators[5,6,16,17,32,47,76] who reported drag increase with their coatings observed a kind of surface divergence as rippling waves of large amplitude and large wavelength. Ash and Bushnell[38] suggested that small amplitude and wavelength of surface motion are necessary to achieve drag reduction by compliant wall. Previous experimental works[2,3,4,11-15,40] shared as a common feature of successful coatings, that is, most of the successful coatings consist of a thin and relatively stiff layer on the top of the coating.

Therefore, in the present study, the velvet was utilized to achieve anisotropic structure, and a thin films were attached on the top of the coating. It was difficult to

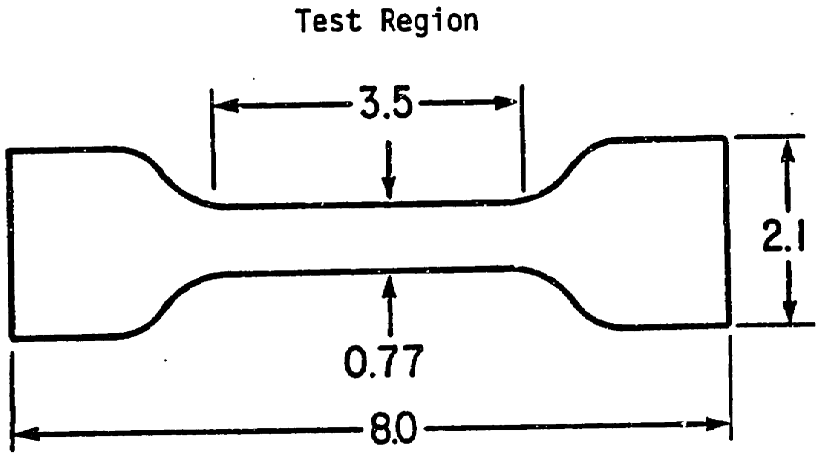


Figure 10. Dumbbell Specimen of Tensile Test of Films.

achieve smooth and bubble-free surfaces of the coating. When the precursor was poured and cured on the velvet fabric, many air bubbles were trapped in the matrix and resulted in rough surface. Because of the fiber piles and backing fabric, the area of interface between precursor and fibers is extremely high, so that there are a lot of trapped air in the interface. The trapped air tends to come out of the matrix gradually. However, if the surface is covered with a film, the escaping air will be trapped beneath the cover film. And there are also lots of bubbles still remaining in the matrix. To solve the bubble problem the substrate on which compliant material was coated was specially designed and a loading apparatus was also made to make bubble-free smooth coating.

Figures 11 (a), (b) and (c) are pictures of the specially designed substrate of the compliant coating (compliant disc). Figure 11 (a) is the inner disc on which the coating is placed. The outer disc, Figure 11 (b) holds the inner disc. The discs were made of a brass plate. The inner disc has a number of holes on the plate through which the troublesome air bubbles are evacuated if the disc is loaded upside down in a container of the silicone mixture. The detail of the coating precedures is shown later. The outer disc has a part where the holder is connected to rotate the disc in a water chamber. When the discs are assembled the total thickness of the coating can be controlled by rotating the height controlling disc

(Figure 11 (c)). The inner disc rests on the height controlling disc, so that the height of the inner disc is varying by rotating the height controlling disc. The height controlling disc has threads on its tip which varies about 1.1 mm per turn (22 tpi thread). After setting the height of the inner disc, the discs are tied by set nuts and support screws. A schematic diagram of the compliant disc (side view) is illustrated in Figure 12. Figure 13 shows the detail of the compliant coating. The coating has 4 distinct layers: (1) the top film, (2) pure network, (3) velvet and network, and (4) fiber glass screen layer on the inner disc. The thickness of the pure network layer can be varied by rotating the height-controlling disc. The average height of velvet fabric was about 2.5 mm. The velvet fabric was glued on the fiber glass screen material by using Epoxy resin. The other side of the screen material was cemented on the inner disc by using the same epoxy resin. Epon 828 and Ancamine 1618 as crosslinking agent were mixed in stoichiometric equivalence (100 : 60 by weight) for 20 min at room temperature. The mixture was used for attaching the velvet on the screen and the screen on the inner disc. The epoxy was cured at 90$^{0}$C for more than 10 hours and postcured at 110$^{0}$C for 2 hours to complete the crosslinking reaction of epoxy. If this reaction does not go to completion, then the unreacted epoxy or the amine in the crosslinking agent will severely inhibit or block the reaction of SiH and vinyl silane to form the compliant network. Therefore, it is very

(a) Outer disc, Top(Left picture) and Bottom(Right picture).

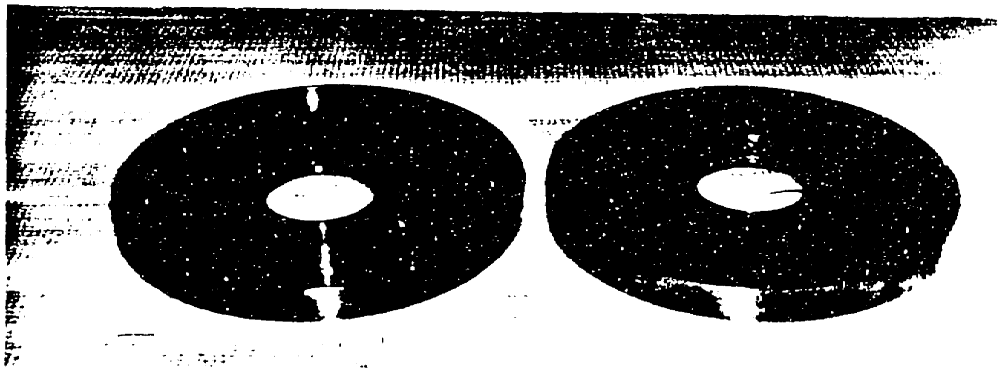

(b) Inner disc, Top(Left picture) and Bottom(Right picture).

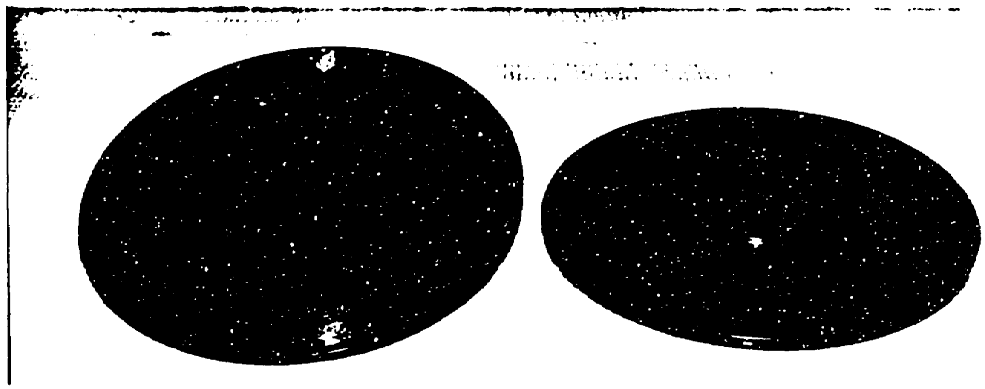

(c) Height controlling disc, Right picture.

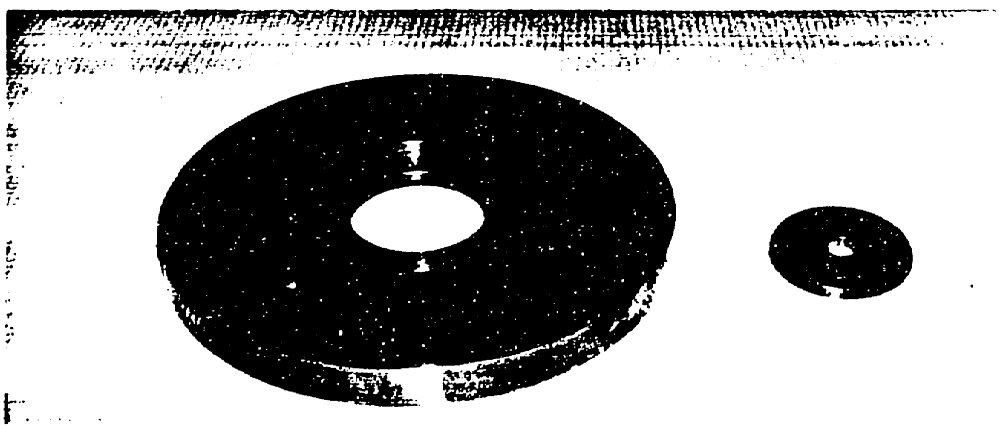

Figure 11. Pictures of brass discs for composite compliant coating.

important to get a complete reaction of the epoxy resin, with excess of neither epoxy nor amine groups.

The role of the screen material is to allow escape of air bubbles. If the velvet was attached to the solid inner brass disc directly, the epoxy would form a complete film on the back of the velvet fabric, which would prevent the trapped air from coming out of the matrix.

The detail of the coating procedure is as follows:

[A] Attachment of Velvet Fabric on the Inner Disc

1. Cut a velvet fabric and screen material into about 11" x 11" square and put them in the oven at about 90$^{0}$C for 1 hour to release possible residual stress in those materials (and remove moisture in the velvet).

2. The inner disc is kept in the oven at 90 C before the epoxy is used.

3. Mix Epon 828 (100 part by weight) and Ancamine 1618 (60 parts by weight) thoroughly by using an electric motor driven stirrer (LIGHTNIN Mixing Equipment Co., New York) for 20 min at room temperature.

4. Take the inner disc, velvet and screen material out of the oven and spread the epoxy mixture on the both sides of screen material. It is important to leave the the

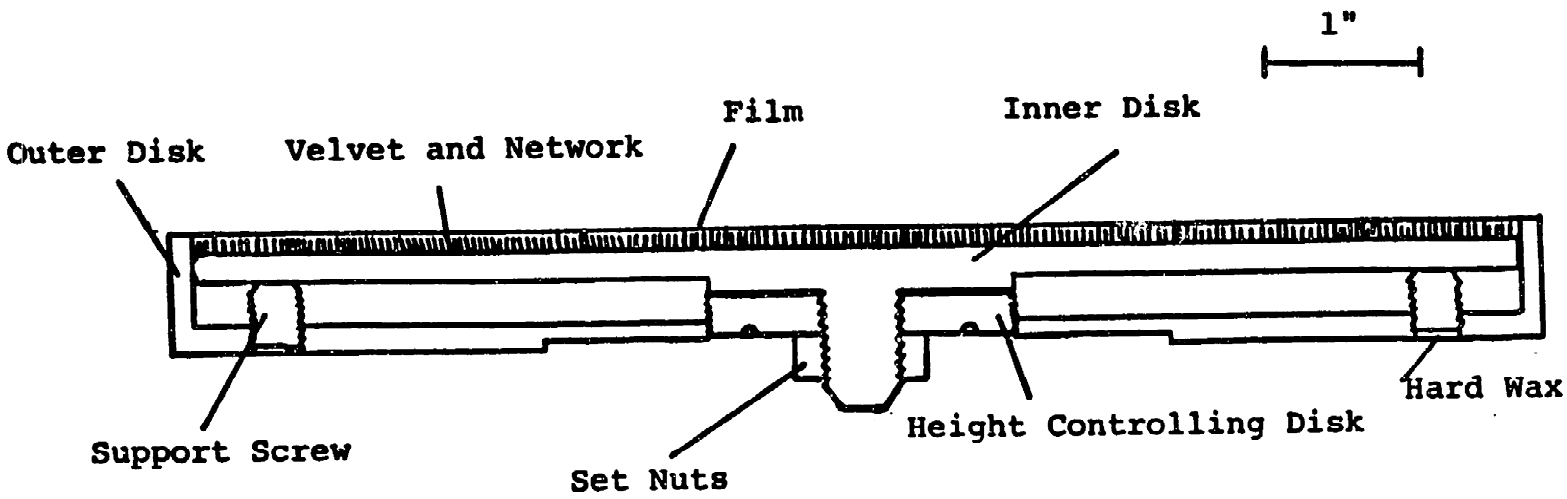


Figure 12. Scheme of Compliant Disk (Side View)

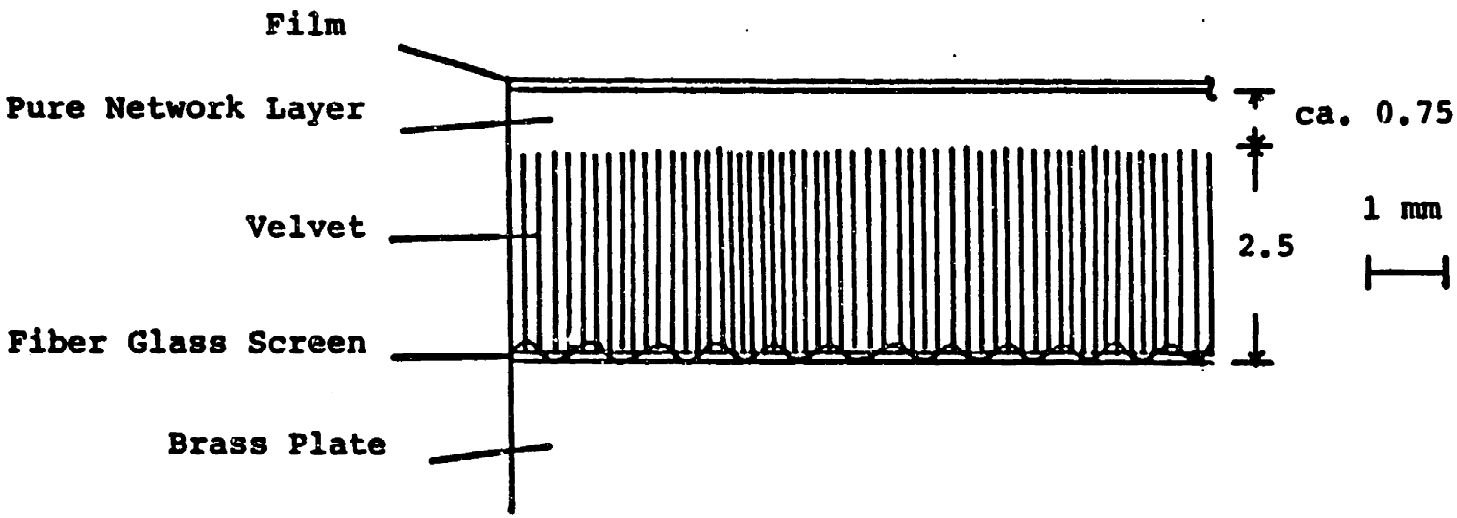


Figure 13. Detail of Compliant Coating

holes in between warp and weft of the screen material for the good ventilation. (The excess epoxy mixture on the screen is removed by air blowing).

5. Put the glued screen in the oven at 90 $^{0}$C for 3 - 4 min to make the epoxy reacted and sticky enough to attach the velvet and the brass disc.

6. Take the glued screen out of the oven and put the velvet and the inner disc on each side of the screen.

7. Bring the velvet attached to the inner disc back to the oven at 90 $^{0}$C and cure the epoxy for at least 10 hours at this temperature and then postcure it at 110 $^{0}$C for 2 hours.

[B] Assembling discs

1. Assemble the height controlling disc in the outer disc.

2. Put the inner disc with velvet fabric (from process [A]) in the outer disc with the surface up.

3. Rotate the height controlling disc, and adjust the level of the fiber tip in velvet equal to the rim of outer disc by using plastic level on it.

4. Set the thickness of the pure resin layer (refer to Figure 13) by rotating the height controlling disc appropriate angle. (360 degree corresponds to about 1.1

mm).

5. Fix the position by screwing the set nuts in Figure 12. And adjust 6 support screws on the outer disc to make the discs assemble firmly.

6. Put the assembled disc upside down on the table and mask the holes of the support screws by employing hard wax (Paraffin Wax). After a molten paraffin is poured in the holes and hardened the excess paraffin is removed by brade and polished to flush with outside of the holes.

[C] Preparation of Precursor of Silicone Networks

1. Premix the $\alpha, \omega$-divinyl PDMS (Mn = 26,400), hydrogen terminated oligomeric PDMS, tetrakis (dimethylsiloxy) silane and appropriate diluent by using an electric motor driven stirrer (LIGHTNIN, Mixing Equipment Co., N.Y.) at about 300 rpm in a 500 ml glass beaker for at least 2 hours. When the diluent of a high molecular weight ($M_d$ = 49,350) is mixed in, an ice bath is equipped outside of the beaker. The molar ratio of $[SiH]_{Total}/[Vinyl]$ is kept always 1.2 ± 0.05.

2. Add the Pt(II) catalyst at the rate of 25 ppm of the reactive resin in the premixture obtained in process (1) and mix them together by the same stirrer stated above for 10 min.

3. Put the precursor under vacuum for about 5 min to take the trapped air out of the precursor. (The container of the precursor should be more than twice larger than the amount of the precursor otherwise, during the degassing under the vacuum the resin is foaming out of the container).

4. Pour the bubble-free precursor very carefully in a plexiglas container of which bottom is covered with a thin film which becomes the upper membrane surface of the composite coating. (see Figure 14). The container consists of two separable plexiglas plates (1/2" thick and 12" x 12" square plate). The thin film is placed on the bottom plate and the top plate which has a circular hole of 9 inch diameter concentric with the center of the plate is put on the bottom plate. The thin film on the bottom plate becomes the top layer of the our compliant coating. When the diluent is very low molecular weight ($M_d$ = 1,200, very low viscosity like water), the bottom and top plates are clamped to prevent the precursor from leaking out of the container through the interface.

5. Load the assembled compliant disc very slowly by using the loading device shown in Figure 14. The compliant disc is lowered by turning the top handle counter-clockwise. Since the assembled compliant disc is hung upside down, the surface wihch contacts the precursor in the reservoir

is velvet fabric glued on the inner disc via the screen material. Therefore, the precursor wets the velvet from its tip to the bottom. There are a number of holes (1/4" in diameter) on the inner disc, through which the trapped air is vented out.

6. Lower the compliant disc until the rim of the outer disc hits the film covered on the bottom plate of the container; And leave it for 24 hours at room temperature to form complete network.

7. After 24 hours the compliant disc is released from the loading device and the plexiglas container; the edge of the film is cut off to fit on the outer disc. The edge of the outer disc is cleaned by paper tissue wetted with isopropanol. Now, a compliant coating is ready for test.

The loading device shown in Figure 14 consists of 5 parts which are main frame, control handle upper rod with threads, lower rod, and universal joint in between upper and lower rods. As shown in Figure 14 the lower rod is screwed in the back side of the assembled disc. The universal joint allows the disc to keep horizontal regardless of the upper rod level. The control handle can bring the upper rod up and down, thus the disc by rotating clockwise and counter-clockwise, respectively. In this manner it is possible to load the disc

in the precursor container very slowly while maintaining it and horizontal.

## 2. Measurement of Skin-Friction Drag

### A. Rotating Disc System in a Large Chamber

To measure the skin-friction drag of the composite compliant coatings and reference hard disc, a rotating disc system in a large plexiglas chamber was designed and set up as shown in Figure 15. A 1 1/2 hp-DC motor was installed vertically on steel support columns. The motor shaft was connected to the sample holder (Figure 16) which holds the discs by using 8 flat-head screws. Two nearly frictionless bearings held the shaft of the sample holder to suppress vibrations of the discs.

After the discs were attached on the sample holder they were lowered into, and then rotated in, a large cylindrical water reservoir. The dimensions are: 17" ID, 9" height, wall thickness 1/2", as shown in Figure 17. The dimensions of the discs and plexiglas water reservoir are almost identical with those used by Hansen and Hunston.[5] The shear stress (vector sum of the tangential and radial component) of the disc is that chamber was almost identical to that in the free space unbounded continuum (within 6% uncertainty).[101] Daly and Nece[102] presented experimental data and semi-empirical theory for the effect of the enclosure on Newtonian flow over smooth

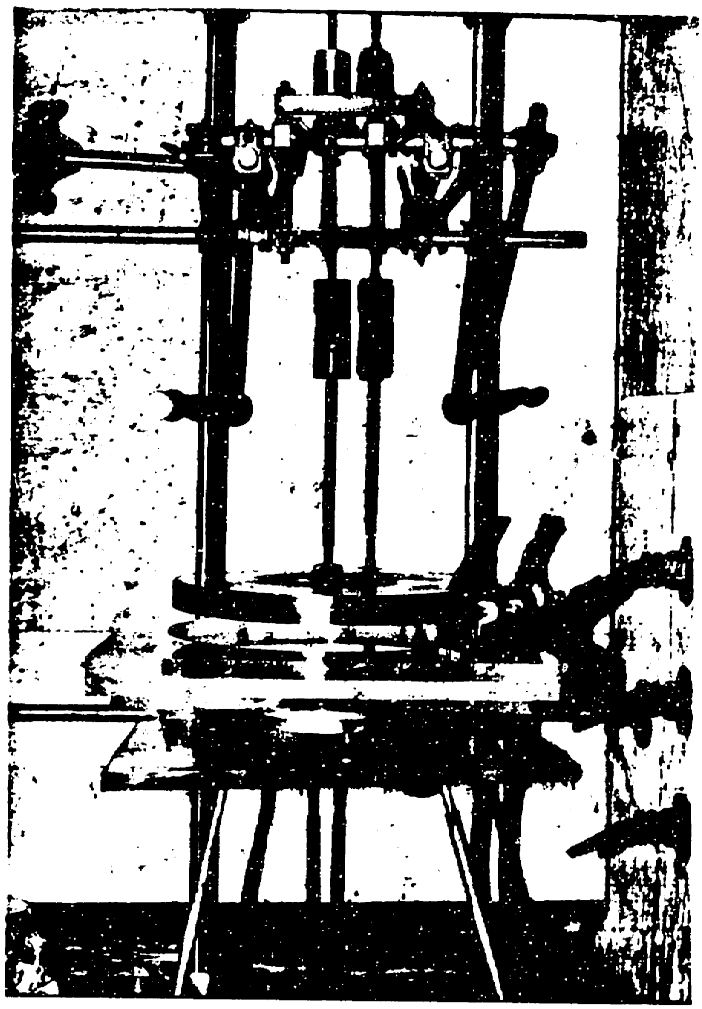

Figure 14. Set-up for Composite Compliant Coating (Disc Loading Device).

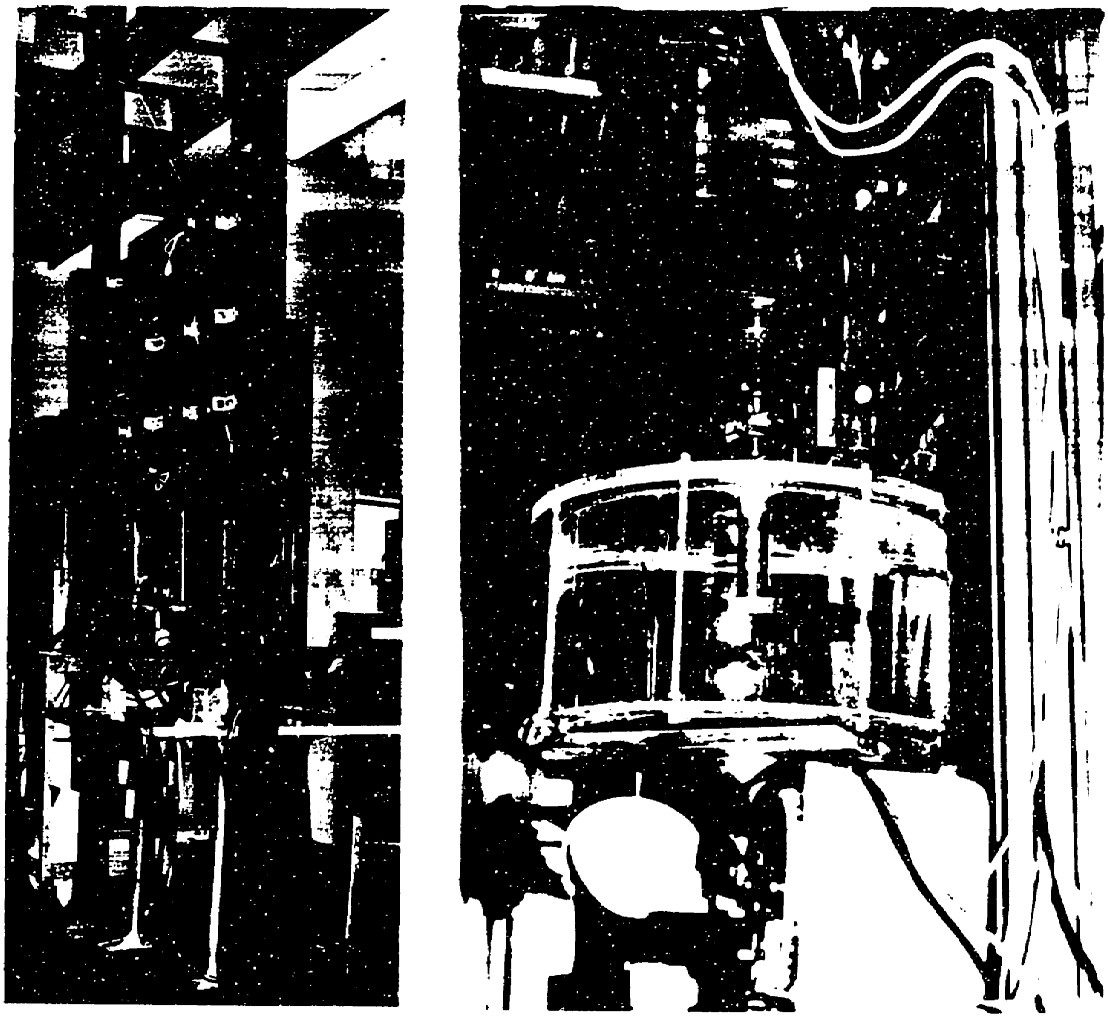

Figure 15 . Experimental Apparatus of Rotating Disc for Drag Measurement

discs. The general effects of an enclosure on flow over a rotating disc are to reduce the shear stress components, the drag, and the drag coefficient as compared with free disc results.[48] This is due to the development of side and end-wall layers on the cylindrical enclosure surrounding disc. Outside of the boundary layers the core of the fluid rotates approximately as a solid body with angular velocity of $\beta = K\omega$ where $0 < K < 0.5$. The coefficient K depends essentially on the relative dimentions h/R and S/R where h and S are the distances from the surface of the disc to the top of enclosure and from the edge of the disc to the side wall of the enclosure (see Figure 17). The K value approaches zero when the enclosure is sufficiently large compared to the disc. Roschke[101] estimated K = 0.06 for the experimental conditions of Hansen and Hunston,[5] which thus includes those of this study. Thus, the drag coefficients of the disc in the enclosure differ by only a few percent from those expected in an unbounded continuum (free space).

The rotational speed of the disc was controlled by using a motor controller (Ja-Lor Electronics Inc., MA) and measured using a stroboscope (Type 1531-A, General Radio Co., MA). The skin-friction of rotating disc was calculated from the torque exerted by the DC motor in combinations with rotational speed. The torque to rotate the disc in water was measured by means of the current of the armature of the motor. There is a linear

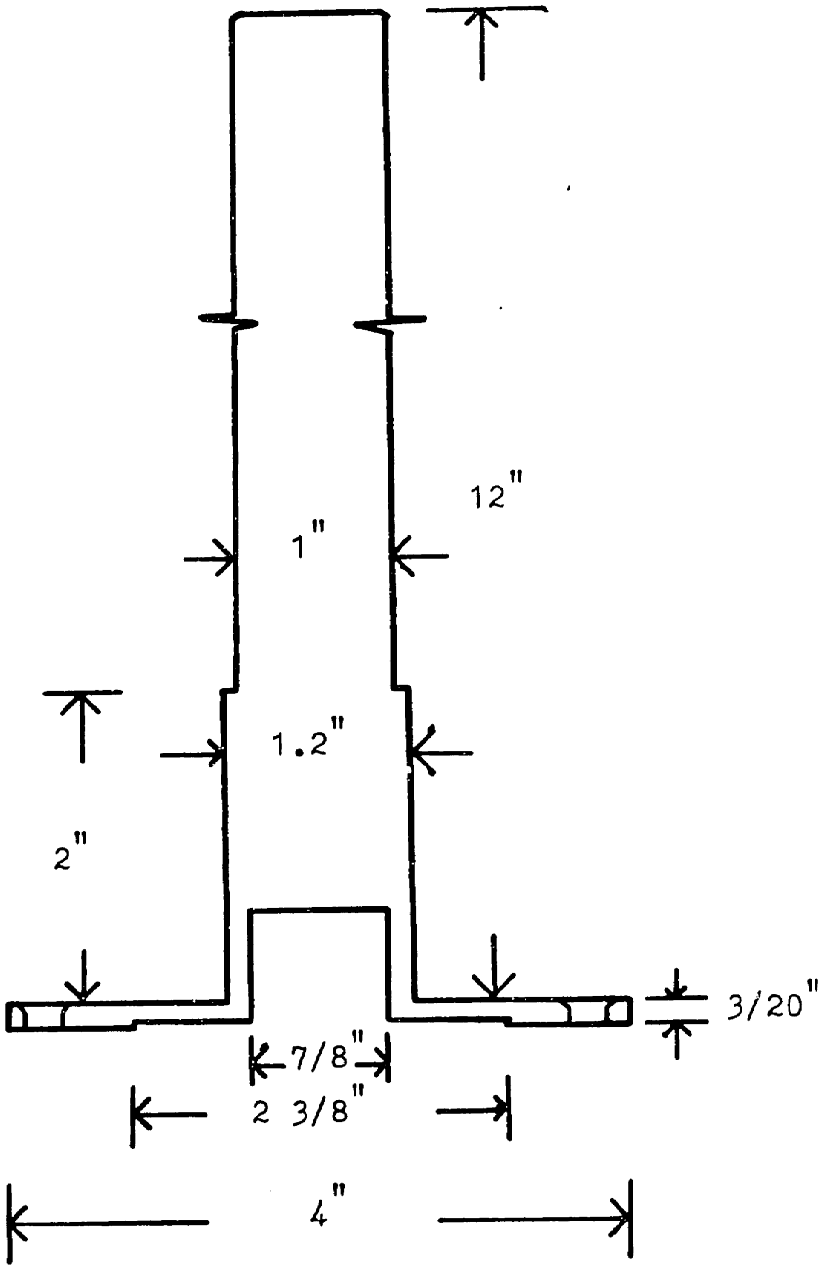


Figure 16. Schematic Diagram of Sample Holder (Side View).

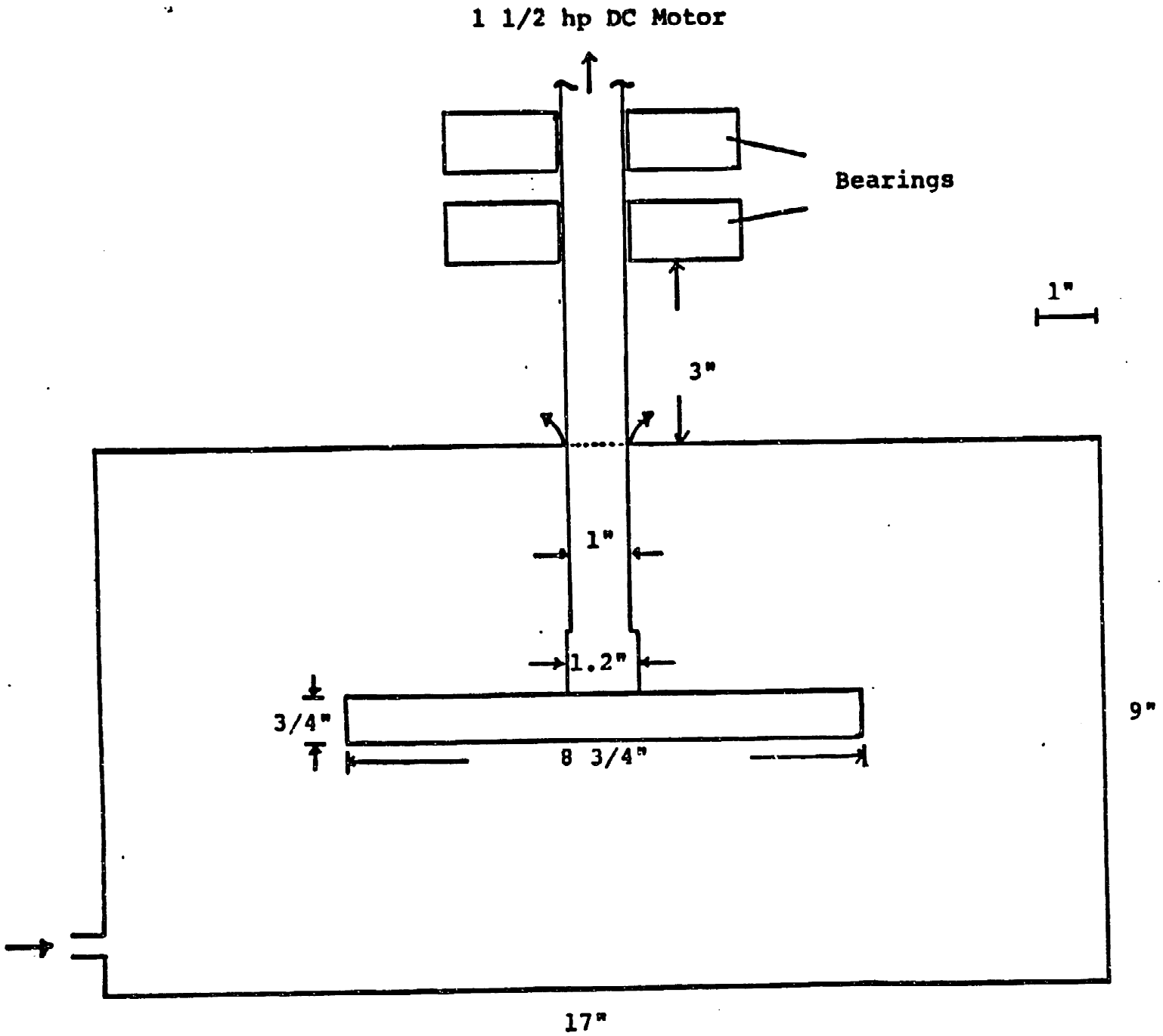


Figure 17. Scheme of Experimental Apparatus

relation between the motor current and the torque of the motor.(102)

$$T = K_T I \qquad (1)$$

where T is motor torque in Nm, I is current of the armature in amp, and $I_T$ is motor torque constant in Nm/A. If the $K_T$ is known for a DC motor, then the torque will be directly obtained by measuring the armature current. There are two ways to obtain the motor torque constant, $K_T$: One is to measure the current and torque directly by using a dynamometer while the motor running at a constant speed. By running at several different speeds the $K_T$ can be obtained. Another way of determining $K_T$ is to calculate the value based on the measurement of the voltage constant, $K_E$. The torque constant is always related to the voltage constant in the following way.(102)

$$K_T = K_E \quad [\text{Unit: Nm/A; Volt/rad sec}^{-1}] \qquad (2)$$

$$\text{or } K_T = 9.5493\ K_E \quad [\text{Unit: Nm/A; Volt/rpm}] \qquad (3)$$

It is easier to obtain $K_T$ by the latter method, which was used in the present study.

The voltage constant, $K_E$ was obtained by running the motor as a generator (driven by another motor) and measuring the generated voltage, $E_g$, while measuring the rotating speed, n by

the stroboscope. The voltage constant was then calculated:

$$K_E = E_g / n \quad [\ V/rad\ sec^{-1},\ rad\ sec^{-1}] \qquad (4)$$

The calculated $K_E$, thus $K_T$ was Ø.943 Nm/A for the 1 1/2 hp DC motor used for the rotating disc.

$$T = Ø.943\ I \quad [Nm;\ \ Nm/A,\ A] \qquad (5)$$

The plexiglas reservoir had a removeable top cover cylindrical wall and bottom plate fixed on the wall. The top cover had a hole of > 1" in diameter in the center through which the shaft of sample holder was running and was tightened to the cylindrical wall by using eight 3/8" bolts and nuts. A natural rubber gasket was used in between the cover and cylindrical wall to prevent water leaking when operated at high speed. There is an inlet/outlet pipe on the bottom of the cylindrical wall which is connected to the faucet.

The reservoir was brought up and down by using a heavy duty jack (for automobiles) hooked up with thick aluminum plate on the top (1" thick plate). When the disc was loaded and unloaded the reservoir was lift up and dropped down by using the jack.

B. Drag Measurement on the Rotating Disc

The procedure of measuring the friction drag on the rotating disc is as follows:

1. Attach the disc on the sample holder which has been connected to the motor shaft through the cover plate of the reservoir. A level is used to make sure the disc is connected horizontally.

2. Bring the other part of reservoir up (side wall and bottom) to make the disc stay in the center of the reservoir. And attach the cover plate on the cylindrical wall.

3. Fill the water in the reservoir and leave the water running slowly to overflow through the edge of the center hole on the top plate during the drag measurement. When the test speed increases the air is asperated into the tank through the gap of the center hole due to the negative pressure around the rotating axis. To avoid this problem water is allowed to run slowly during the measurement.

4. Rotate the disc at a predetermined testing speed and measure the armature current, I by using a digital multimeter (75 multimeter John Fluke MFG Co., Inc., Washington). Set the next speed by the stroboscope and adjust the motor controller to fit the speed and measure the corresponding current, and so on.

Initially there was a problem in deducting the torque arising from the bearings from the total measured torque,

because the bearing drag coming from two bearings on the sample holder was related both to the rotating speed of the shaft and the temperature of the bearings. However, it was found that the bearing drag showed constant values above 40° C at each rotating speed. Thus, to avoid the complexity due to the temperature dependence of the bearing drag all measurements were done at the bearing temperatures above 40° C. The relation of the bearing drag to the rotating speed above 40 C is shown in the next section.

C. Calculation of Drag Coefficient of Compliant Coatings

To separate the real torque of the rotating disc from the meaured torque (armature current) the rigid reference disc was rotated in the air at various speeds. At each speed the torque was measured and plotted against the rotating speeds as shown in Figure 18. Neglecting the air friction drag, the torques obtained were assumed the drag forces due to the bearings and internal friction of the motor itself. And it was further assumed that there were two linear relations between the drags and the rotating speeds as shown in Figure 18. The linear relations for calibration were:

(i) $\omega \leq$ 1,200 rpm

$$K = 0.00017\ \omega + 0.525 \qquad (6)$$

(ii) 1,200 rpm $\leq \omega \leq$ 1,500 rpm

$$K = 0.000117\ \omega + 0.5831 \qquad (7)$$

where K is the current due to the bearing drag and the internal friction of the motor. The torques of the rotating disc were calculated by subtracting K values from the measured current in the experiment. The K values were calculated by using Equations (6) and (7) for appropriate rotating speed.

Since the composite compliant coating was placed only on one face (the underside) of the disc, it was necessary to calculate hypothetical drag coefficients of the coating as if both surfaces were compliant coatings. In the present study two reference discs were utilized to achieve more accurate and reasonable values of the hypothetical drag coefficients of the coatings. Reference disc #1 was prepared by forming a bulk undiluted silicone network of high crosslinking density and high modulus ($E = 1.0 \times 10^7$ dyne/$Cm^2$) on the compliant disc in place of the low modulus material. Therefore, reference disc #1 was geometrically identical with the compliant coatings except for the hardness of the coating. Reference disc #2 was made of polished brass whose dimensions were exactly the same as reference disc #1. However, there is a small difference on the shaft side of reference disc #2. As shown in Figures 19(a), (b) and (c), the sample holder was flushed on the rear surface of the reference disc #1 or compliant disc. However, the flat screw heads on the sample holder reference disc #1 and in the compliant disc set-up were still exposed to the water and thus contributed some degree of additional drag. On the

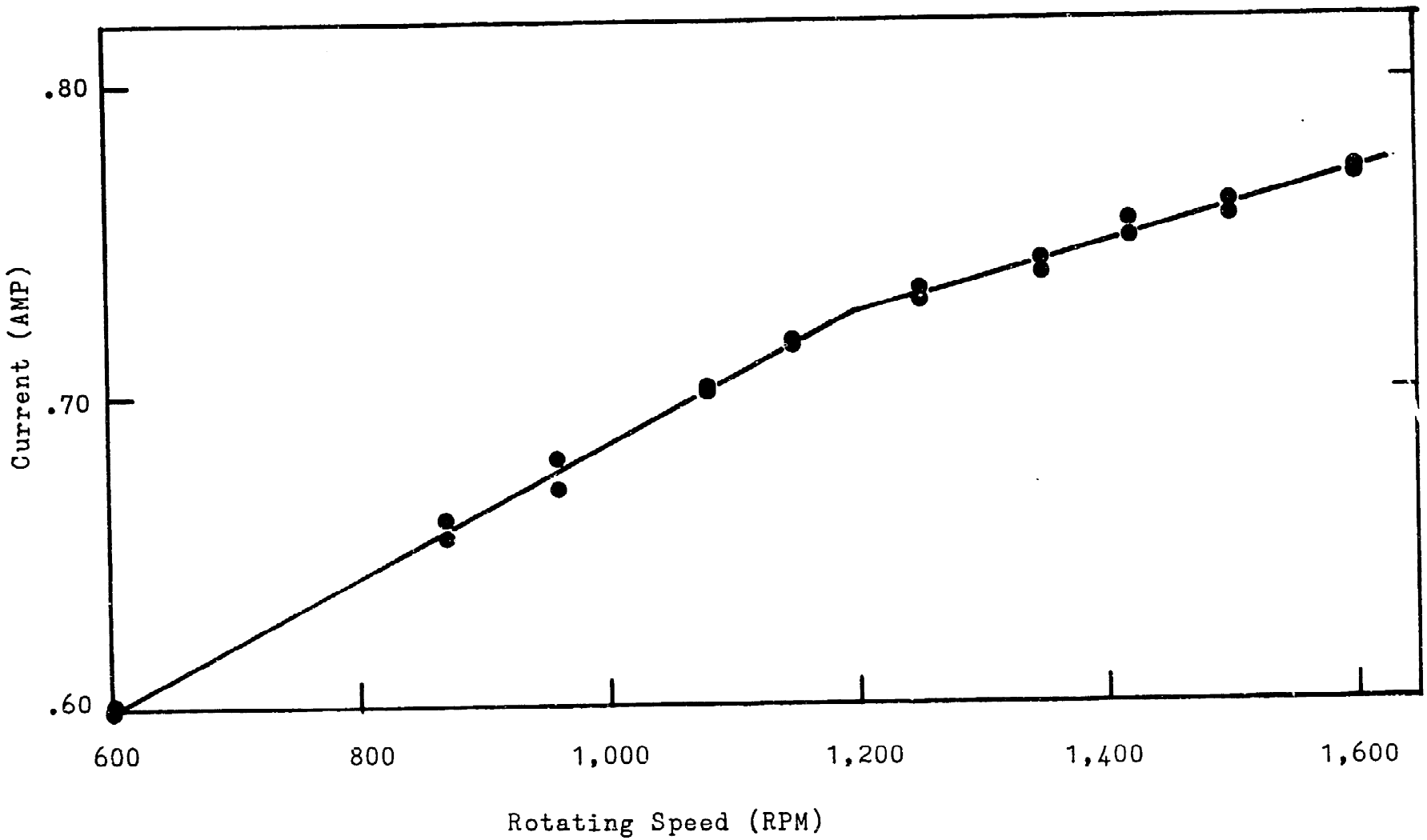


Figure 18. Armature current due to the bearing drag and internal friction of motor with respect to the rotating speed at the bearing temperature higher than 41°C.

other hand, with reference disc #2 (solid disc) the heads of the screws on the sample holder were covered by a smooth hard coating flushed with the upper surface (on the shaft side). Therefore, reference #2 was truly smooth on both sides, and its drag coefficient could then be directly compared with the theoretical predictions[49] (see the Equation (16) in section 2 in Literture Survey).

In the derivation of the hypothetical drag coefficients of the compliant coatings, the following assumptions were made:

(1) Neglect the drag forces on the shaft of the sample holder (the diameter was only 1 inch) and the edge of the disc (3/4 inch height).

(2) The drag of the hard coating on the reference 1 is equal to that on the brass surface of reference 2.

Now, if we define,

$T_1$ = Torque of reference 1 (both sides drag)

$T_2$ = Torque of reference 2 (both sides drag)

$T_3$ = Torque of compliant disc (coating on the face only)

$$T_2 = F_2 + B_2 \qquad (8)$$

$$F_1 = F_2 = T_2/2 \qquad (9)$$

$$B_1 = T_1 - F_1 = T_1 - T_2/2 \qquad (10)$$

$$F_C = T_3 - B_C$$

$$= T_3 - B_1$$

$$= T_3 - T_1 + T_2/2 \qquad (11)$$

where, the subscripts 1, 2 and 3 denote reference 1, reference 2 and compliant coating, and F and B are the torque on the face of the disc and that on the rear of the disc as shown in Figures 19(a), (b) and (c).

Finally, the hypothetical drag coefficients of the compliant coating are:

$$C_D = 2T/\ \omega^2 R^5$$

$$= 4FC/\ \omega^2 R^5$$

$$= 4(T_3 - T_1 + T_2/2)/\ \omega^2 R^5 \qquad (12)$$

where, $C_D$ = Hypothetical drag coefficient of compliant coating. (Both sides coating)

T = Hypothetical torque of compliant coating. (Both sides coating)

$\omega$ = Angular velocity of the disc (rad/sec)

R = Radius of disc (11.11 Cm).

The drag coefficients of the compliant coatings reported in the present study are the calculated hypothetical drag coefficients as if both sides of the disc had identical compliant coatings and those of the reference are experimental values of reference disc #2.

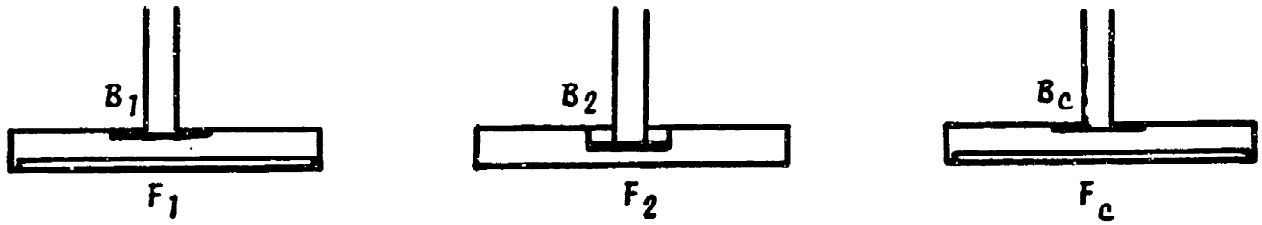


Reference Disc #1
(Hard Coating)
Screw Heads

Reference Disc #2
(Smooth Brass)
No Screw Head

Compliant Coating Disc

Screw Heads

Figure 19. Schematic diagrams of reference discs and composite compliant disc with sample holder attached on them.

## Results and Discussions

### 1. Dynamic Mechanical(Dynamic Mechanical Properties of Lightly Crosslinked Silicone Networks

#### A. Dynamic Shear Moduli and Loss Tangent by Eccentric Rotating Disc

In the preliminary study material properties of silicone networks, a number of silicone networks were synthesized, characterized and examined the dynamic mechanical properties with various crosslinking densities. To find appropriate material properies for favorable drag reduction by compliant coating it was necessary to vary the material properties of coating over a wide range, ie., soft to hard coatings (G') and low to high damping materials (G" or tan$\delta$ ).

The dynamic shear storage and loss moduli were measured at a fixed dynamic strain (1%) and four different frequencies (Ø.16, 1.6, 8.Ø, and 16 Hz) by utilizing the Eccentric Rotating Disc Mechanical Spectrometer at room temperature. Figure 2Ø shows the results of shear storage moduli of the networks composed of various molecular weights of chain molecules (Mn = 7,ØØØ to 39,7ØØ) at the frequencies of Ø.16 and 16 HZ, respectively. The storage moduli of the networks decreased monotonically with the increase of initial molecular weights of chain molecules (decreasing network chain density). The

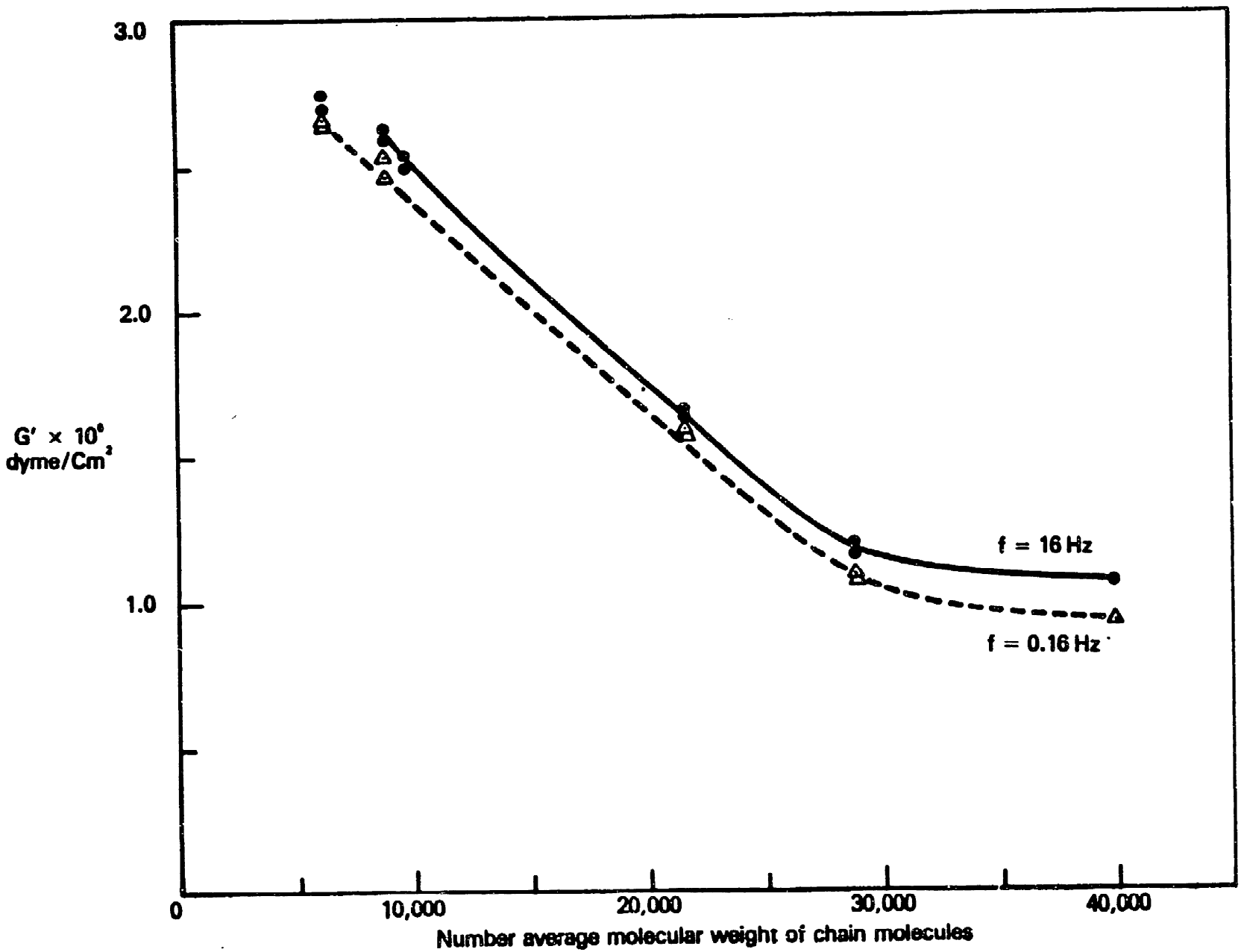


Fig.20. Variation of storage shear moduli with various molecular weights of $\alpha,\omega$-divinyl poly (dimethyl siloxane).

frequency dependence of storage moduli was not very large for all examined undiluted networks. The lowest storage modulus observed was around $10^6$ dyne/$Cm^2$ at 16 Hz with the chain molecule of Mn = 39,700 which was almost the upper limit to synthesize bubble free network. Because of high viscosity and relatively fast gelation rate of the precursor, it was diffcult to avoid trapping air bubbles in the network with higher molecular weight chain molecule. In Figure 21 the trend of damping factors (tan $\delta$ = G"/G') of the undiluted networks is shown with various dynamic frequencies. The tan $\delta$ of the network in which the molecular weights of the chain molecules were varied up to Mn = 28,600 are almost independent of the frequency and remained below 0.05. For the network composed of the longest chain molecule (Mn = 39,700) the damping factor increased slightly as a function of frequency. Networks formed from the three shorter chain molecules revealed higher extent of reaction of vinyl groups ( $\varepsilon$ = 0.86 - 0.875) than that of the network with longest chain ( $\varepsilon$ = 0.825) as shown in Table III. The relatively high losses of the network with the lonest chain molecule may be due to the higher sol fraction and unreacted free ends (dangling chains) in the network. In either undiluted network the tan $\delta$ was not very high. Furthermore, as the extent of network chain density increases in the network with the longest chain molecule, the damping factors should decrease almost to zero. Thus, it is not feasible to gain high loss factors by stopping crosslinking short of complete

Table III. Characterization of Silicone Networks

| Sample | $\bar{M}_n$ of $\alpha,\omega$-divinyl PDMS | Diluent | | $W_s$ | $\epsilon$ | $v_{2f}$ | $G_e(\epsilon=0.01)$ ( $\times 10^{-5}$) (dyne/$Cm^2$) | $\nu/V_0$ (mole/$Cm^2$) |
|---|---|---|---|---|---|---|---|---|
| | | Mol. Weight | Dilution, Ratio (phr) | | | | | |
| I-1 | 8,800 | - | - | 0.033 | 0.875 | - | 19.8 | 7.91 |
| I-2 | 21,600 | - | - | 0.038 | 0.868 | - | 12.4 | 4.96 |
| I-3 | 28,600 | - | - | 0.044 | 0.860 | - | 7.54 | 3.01 |
| I-4 | 39,700 | - | - | 0.079 | 0.825 | - | 4.66 | 1.85 |
| A-1 | 7,000 | 1,200 | 97 | 0.039 | 0.867 | 0.479 | 4.55 | 1.82 |
| A-2 | 7,000 | 1,200 | 208 | 0.088 | 0.818 | 0.289 | 1.06 | 0.424 |
| A-3 | 7,000 | 1,200 | 290 | 0.130 | 0.792 | 0.217 | 0.509 | 0.203 |
| A-4 | 7,000 | - | - | 0.040 | 0.865 | - | 17.0 | 6.79 |
| B-1 | 7,000 | 49,350 | 111 | 0.167 | 0.774 | 0.395 | 1.51 | 0.603 |
| B-2 | 7,000 | 49,350 | 200 | 0.181 | 0.768 | 0.273 | 0.236 | 0.0943 |
| B-3 | 7,000 | 49,350 | 410 | 0.185 | 0.765 | 0.195 | 0.0799 | 0.0319 |
| C-1 | 28,200 | - | - | 0.105 | 0.805 | - | 4.67 | 1.87 |
| C-2 | 28,200 | 1,200 | 44.7 | 0.127 | 0.792 | 0.596 | 1.43 | 0.571 |
| C-3 | 28,200 | 1,200 | 98.8 | 0.055 | 0.847 | 0.468 | 0.552 | 0.221 |
| C-4 | 28,200 | 1,200 | 212.1 | 0.082 | 0.822 | 0.287 | 0.0799 | 0.0319 |

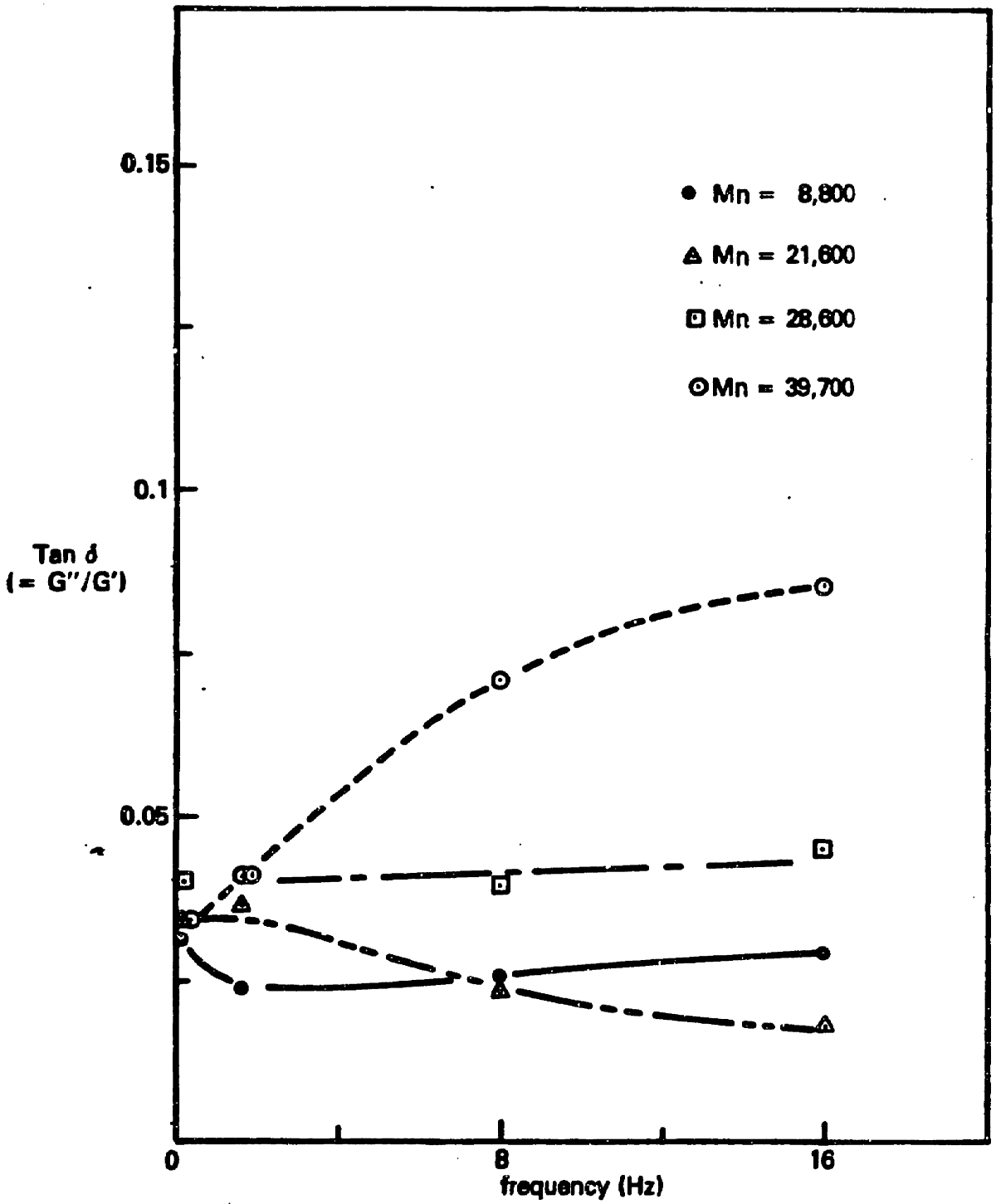


Fig. 21 Frequency dependence of damping factors (G''/G') for various molecular weights of chain molecules at room temperature.

reaction.

Therefore, we turn to networks with diluents. Figure 22 shows the double log plots of storage moduli versus apparent network chain densities of the preswollen networks at Ø.16 and 16 Hz. The apparent network chain density was calculated from the equilibrium shear modulus at 1% strain by using the Equation (3) in section 3.1 in the experimental section. Line (a) of Figure 22 showed the trend of storage moduli with apparent network chain densities varied by dilution (Ø - 29Ø parts per hundred reactive resin) at frequency of 16 Hz. The networks were composed of $\alpha,\omega$-divinyl PDMS (Mn = 7,ØØØ and 28,2ØØ), tetramethyl cyclotetrasiloxane and nonreative PDMS of M.W. = 1,2ØØ ($M_d$ = 1,2ØØ). Both of the networks showed the similar straight line of the double log plots. Its slope was one through the examined dilution ratios. At lower frequency (Ø.16 Hz) the network with shorter chain molecule (Mn = 7,ØØØ) showed slightly lower storage moduli than those at 16 Hz, whereas, the network with longer chain molecule (Mn = 28,2ØØ) showed much lower values (close to the equilibrium moduli) than those at 16 Hz as shown in the Figure 22. The slopes of the double log plots at the low frequency (Ø.16 Hz) also revealed a unity for both networks. It means that the storage moduli of the dilute networks decrease linearly with apparent network chain density in the range of Ø.16 Hz to 16 Hz.

At zero strain limit the storage modulus of the ideal

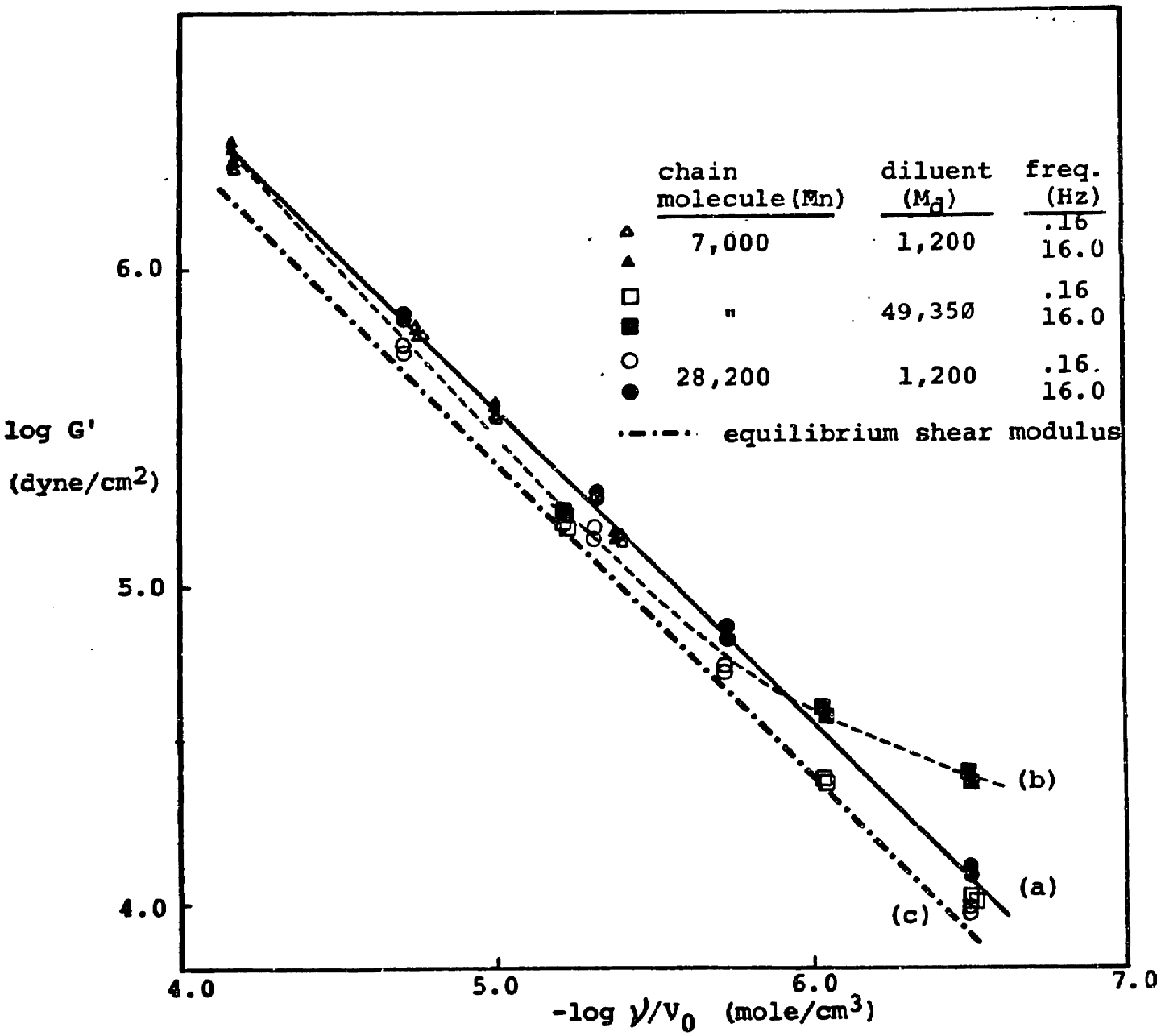


Figure 22. Variations of storage shear moduli with apparent chain densities of diluted silicone networks.

network (perfect network) was predicted as same as equilibrium modulus in the frequency range well below transition frequency from rubbery to glassy state,[91] ie., at very low frequencies. A real network, however, differs from the ideal network in that the presence of network defects in the structure. The three most important are the presence of: dangling ends due to the incomplete reaction of chain molecules, permanently trapped entanglements, and sol fraction and diluent. The dangling ends, sol fraction and diluent do not contribute to the equilibrium modulus because they cannot store elastic energy at equilibrium. The frequency dependence of storage modulus of network is mainly due to the dangling ends and unreacted linear molecules in the network at well below transition frequency. In Figure 22, the networks with longer chain molecule (Mn = 28,200) revealed higher frequency dependence of storage modulus than those with shorter chain molecule (Mn = 7,000). The reason may lie in that the former consisted of higher sol fraction (unreacted chain molecule) and much higher molecular weight of chain molecule which yields more untrapped entanglements than the latter.

The curve (b) of Figure 22 showed the double log plots of shear storage moduli verus apparent network chain densities of dilute networks at 16 Hz. The networks were synthesized with chain molecule of Mn = 7,000 and high molecular weight diluent (nonreactive PDMS $M_d$ = 49,350) loaded from 0 to 410 phr. The

trends of storage moduli were not linear with the apparent network chain density at either Ø.16 or 16 Hz. It is quite different from the results of the above networks diluted with low molecular weight PDMS ($M_d$ = 1,2ØØ) where linear relations were observed. As the dilution ratio increased (lower apparent network chain density), higher curvature was observed. As indicated by Kramer et al,[84] the reason may be due to the high fraction of high molecular weight diluent which contributes to the dynamic modulus of the network, whereas low molecular weight diluent contributes negligibly. The significant frequency dependence of storage modulus was observed at higher loading. Kramer et al.[84,85] proposed the moduli of networks with diluent were proportional to about 2/3 power of volume fraction of diluent.

Figure 23 shows the plots of damping factors, tan $\delta$ , versus various loadings of diluents ($M_d$ = 1,2ØØ and 49,35Ø) at Ø.16 and 16 Hz respectively. The base network polymer was composed of $\alpha,\omega$-divinyl PDMS of Mn = 7,ØØØ as a chain molecule. The distinct difference of damping property between the two diluents employed is evident. Since the molecular weight of chain molecules used was slightly lower than the average entanglement spacing[92] of linear PDMS (M.W. 8,1ØØ - 12,ØØØ), the networks diluted with PDMS of $M_d$ = 1,2ØØ shows very low damping (Figure 23(a')). However, the network with the diluent of $M_d$ = 29,ØØØ shows very high damping at a frequency

of 16 Hz (Figure 22(b')). The high damping observed may be due to the high molecular weight of diluent in the network and incomplete of crosslinking reaction. (See Table III, group B networks ($M_d$ = 49,350) showed much higher sol fraction than group A networks ($M_d$ = 1,200)). This results are qualitatively agreed with the previous works.[79,84,85]

Figure 24 and 25 showed the frequency dependence of loss tangent of the networks with low and high molecular weight diluents, respectively. As discussed above, the networks with low molecular weight diluent showed low loss tangent (less than 0.07) at the frequencies from 0.16 to 16 Hz for all dilute networks examined in the present work (0 - 290 phr). The loss tangent with lower loadings (97 phr) decreased in a similar manner, but slightly faster than that of undilute network with the increasing frequency. The low molecular weight diluent increases the molecular mobility of chain molecules both reacted or unreacted due to plasticization, which causes the lower dilute network to exhibit slightly higher frequency dependence than bulk network. The loss tangent of the network with higher dilutions (208 and 290 phr) increased slightly at higher frequency which differed from that of the undilute and lower loading networks. It may be due to higher content of unreacted chain molecule and loose chain ends in the network than the lower loading and undilute networks. (Compare sol fractions, $w_s$ and the extent of reaction of vinyl group in

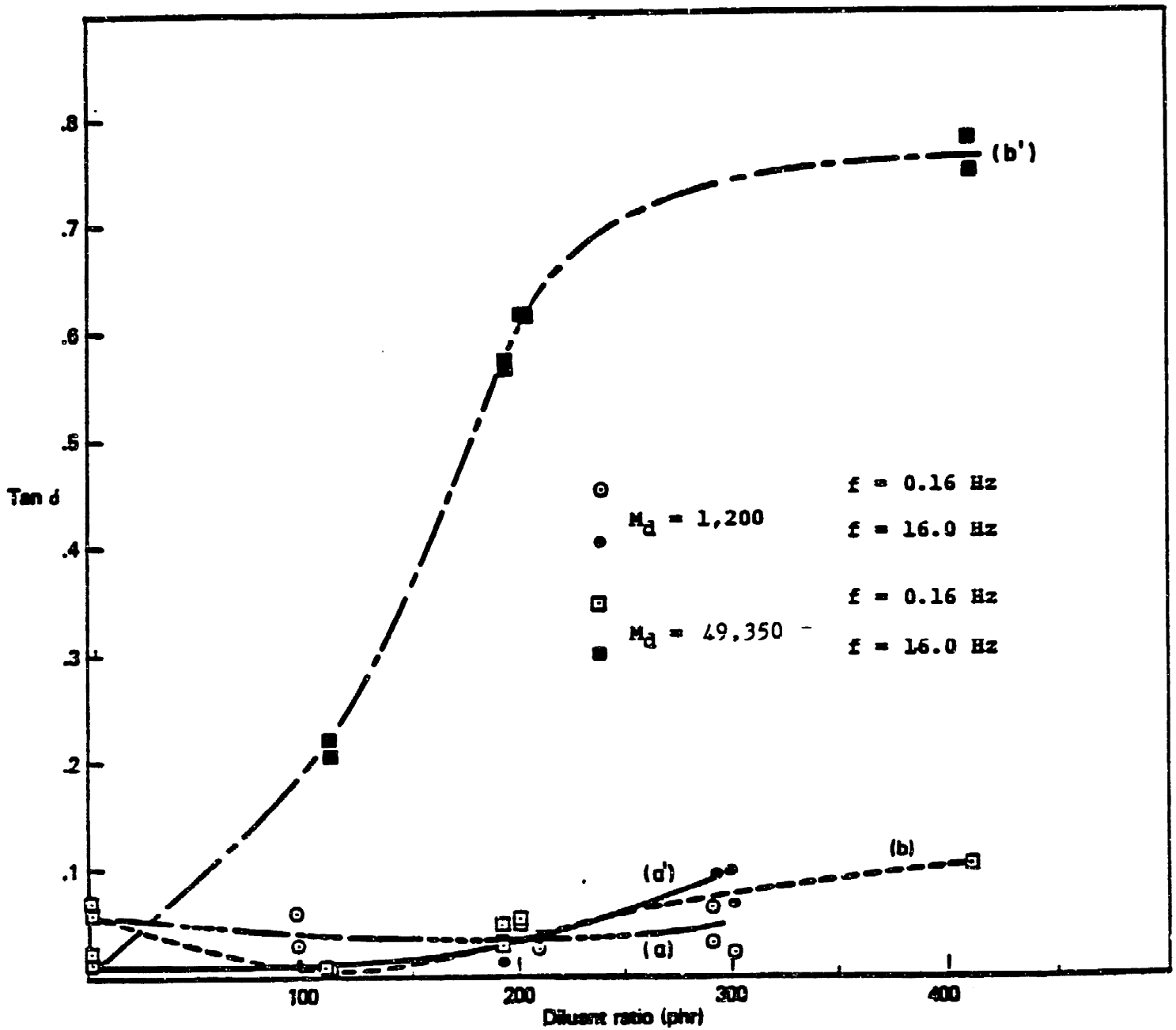


Figure 23 Variation of damping factor (G"/G') with dilution ratios of networks.
* chain molecule ; Mn = 7,000 diluents ; $M_d$ = 1,200 and 49,350.

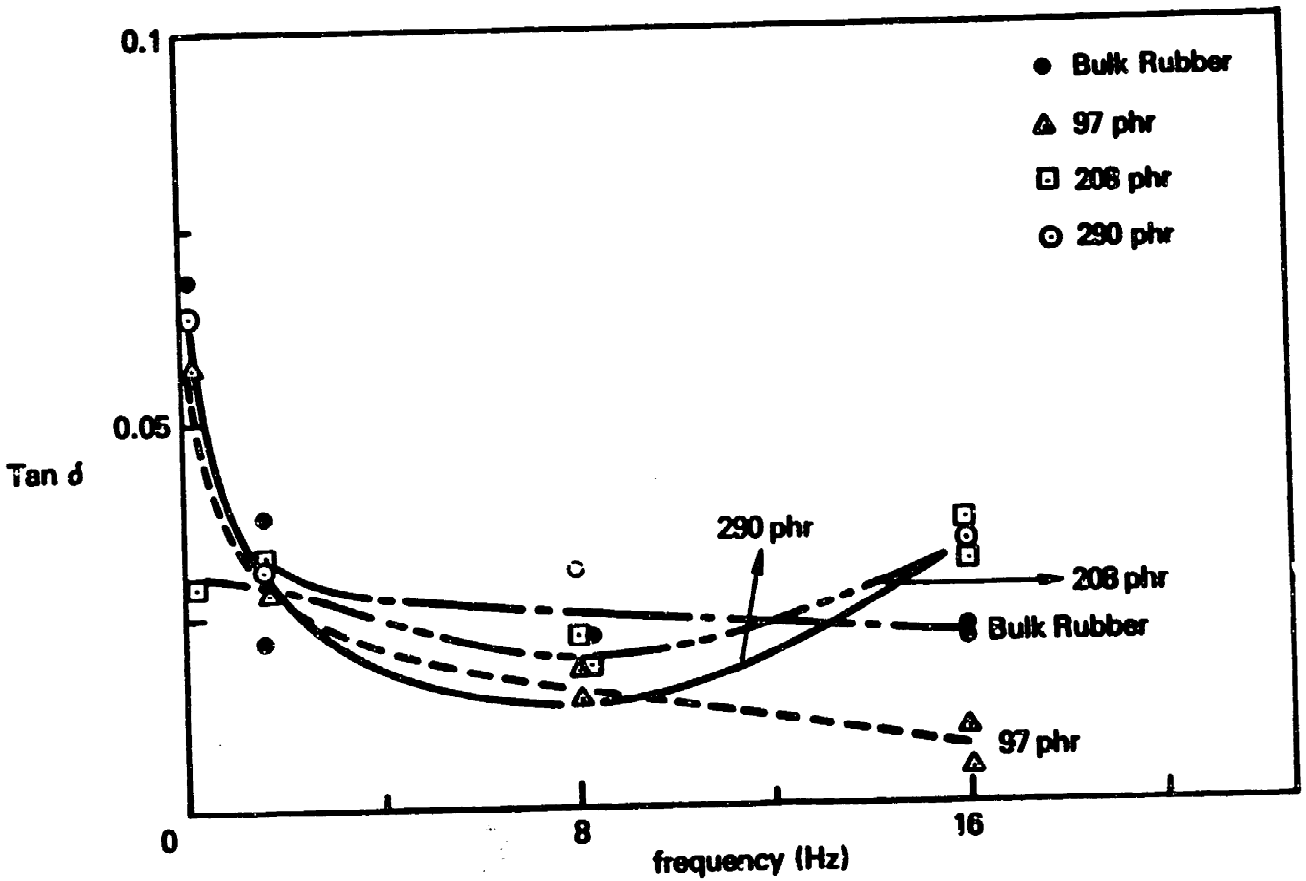


Figure 24. Frequency dependence of damping factor of diluted networks with low molecular weight diluent ($M_d$=1,200) *chain molecule ; $\bar{M}n$ = 7,000.

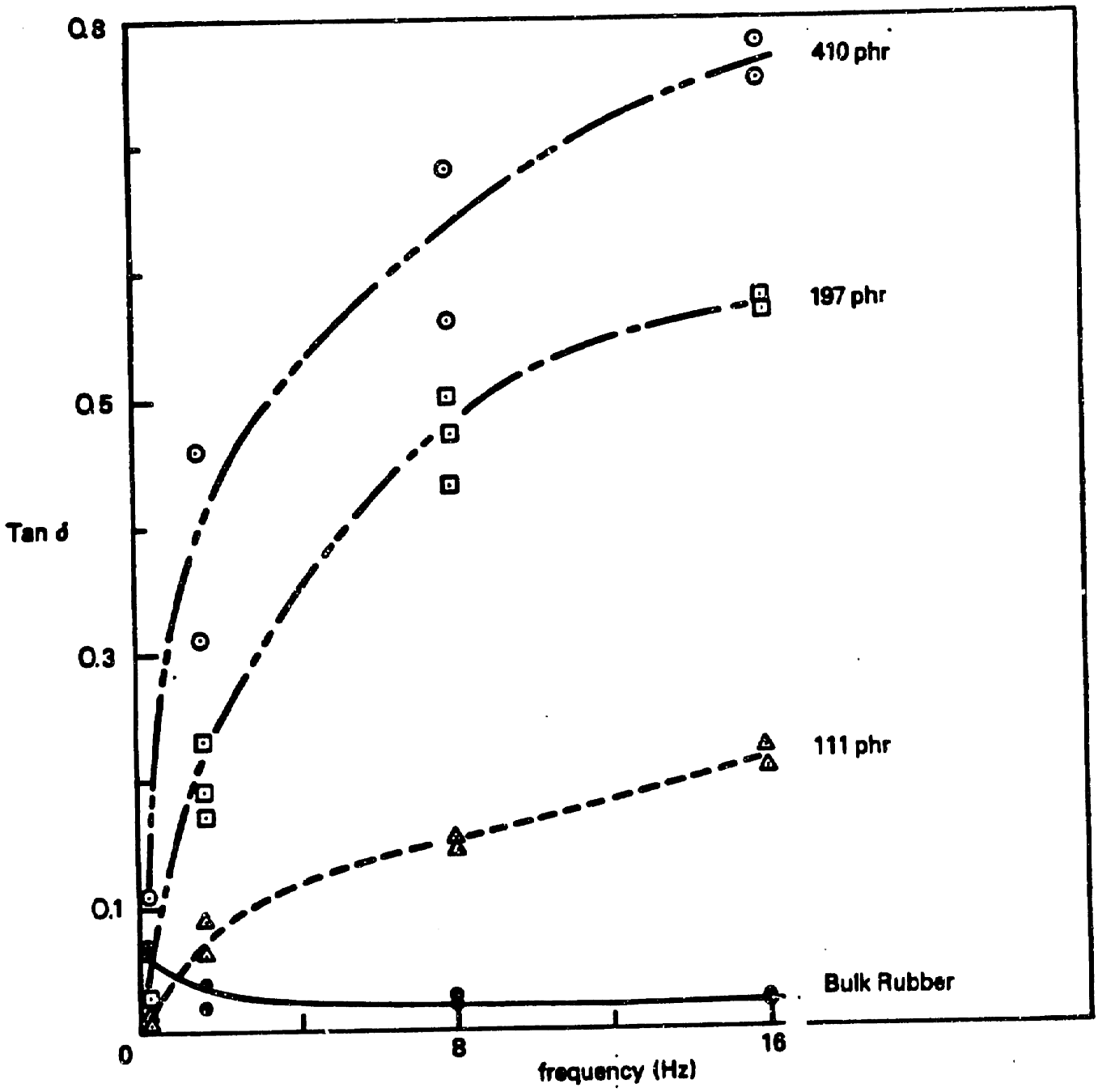


Figure 25.Frequency dependence of damping factors of diluted networks with high molecular weight diluent($M_d$=49,350) *chain molecule ; $\bar{M}n$ = 7,000.

Table III).

In Figure 25, the networks with high molecular weight diluent ($M_d$ = 49,350) showed very strong frequency dependence of loss tangent. With increasing loadings of diluent, stronger frequency dependence was observed. Langley and Ferry[79] and Kramer et al[84,85] showed similar results where the loss tangent increased with higher sol fraction and/or high molecular weight raptating molecules in the crosslinked PDMS. In Figure 26 the loss tangents at 0.16 and 16 Hz are compared with two different networks composed of the same diluent ($M_d$ = 1,200) but different molecular weights of chain molecules (Mn = 7,000 and 28,200). The frequency dependence of loss tangent was pronounced for the network with longer chain molecule (Mn = 28,200). It may be due to higher molecular weight of chain molecule contributing to the loss modulus more effectively than the lower molecular weight chain molecule as the chain molecules remain unreacted and/or dangling in the network. However, the loss tangent did not rise rapidly with increasing dilution ratio, which differed from the above network with high molecular weight diluent (group B networks in Table III).

## B. Dynamic Moduli and Loss Tangent of Composite Coatings in Compression Mode

Since composite coatings consisted of lightly crosslinked

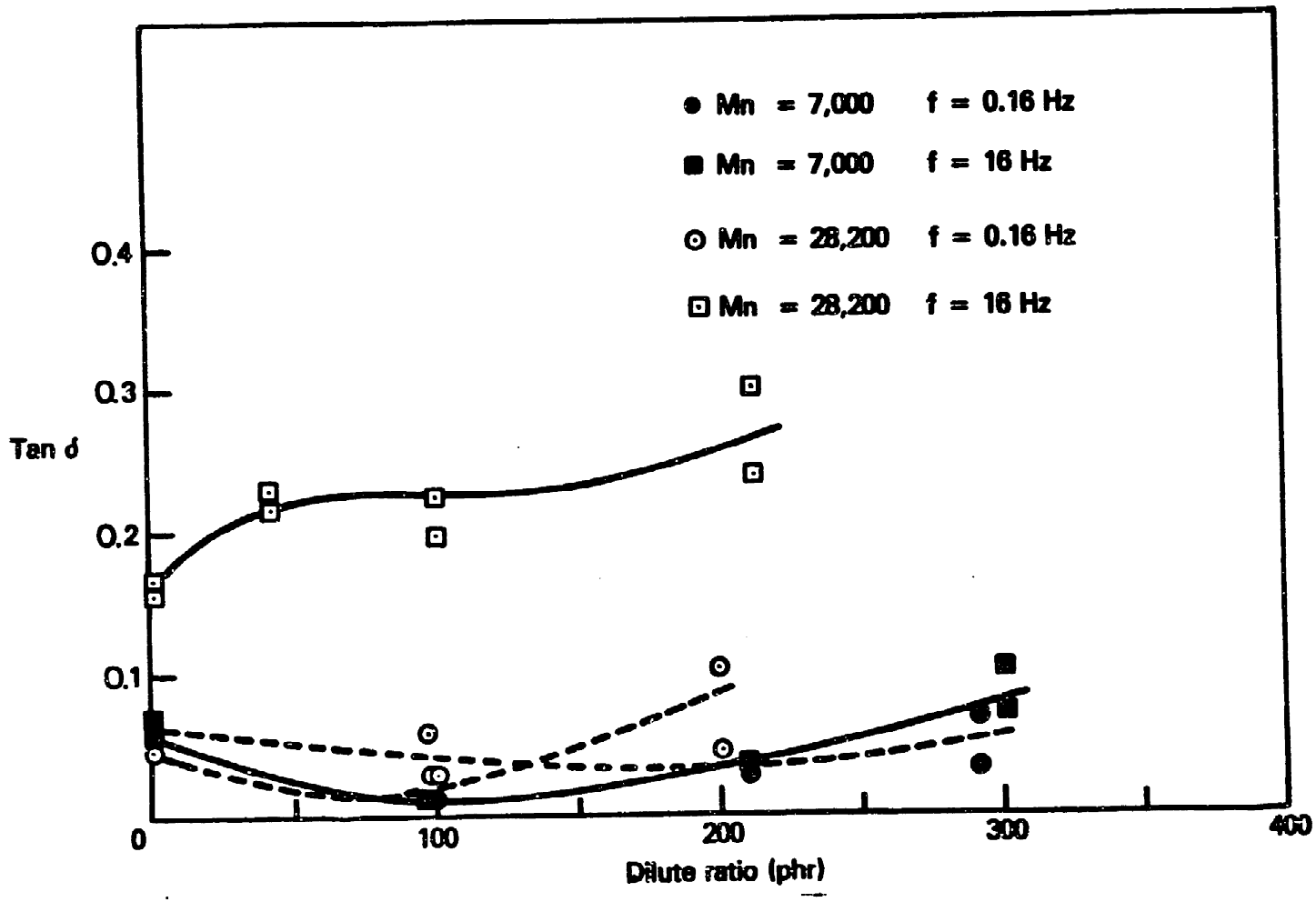


Fig.26. Variation of damping factor with various dilution ratios.

Diluent: PDMS, $M_d$ = 1,200

Base Network: Mn 7,000 and 28,200 α,ω-divinyl PDMS.

silicone networks embedded in vertical fiber pile of rayon velvet, it was necessary to study the dynamic moduli and loss tangents of the networks in compression mode.[1] Tetrakis (dimethylsiloxy) silane was used as tetrafunctional junctions instead of tetramethyl cyclotetrasiloxane which was used previously. With the former junction, the gelation time of the precursor was much shorter than the latter at room temperature.

Three different dilute networks were prepared to compare the dynamic mechanical properties in compression mode in the frequency range of 0.1 to 100 Hz. The networks consisted of the same chain molecule ( $\alpha, \omega$ -divinyl PDMS, Mn = 26,400) and junction molecule, and equal amount of diluent loaded (200 parts per hundred reactive resin).

The results of dynamic storage moduli and loss tangents of the network in the frequency range of 0.1 to 100 Hz are shown in Figure 27. The solid curves represent the storage moduli of the networks, and the dotted curves show loss tangent at 1% compressive strain. Three sets of curves revealed significant difference in the moduli and loss tangent. The network (A) with diluent of lowest molecular weight ($M_d$ = 1,200) shows very

---

1. Attempts to measure in shear mode were defected by highly unreliable, irreproduceable data possibly arising from slip between filaments (pile) of the rayon, and the silicone elastomer.

low damping and low storage moduli which are almost independent of the frequency throughout the testing frequencies. The storage moduli almost reached the equilibrium modulus of the network. The network (B) composed of the diluent of medium molecular weight ($M_d$ = 17,250) reveals moderate frequency dependence of both the storage moduli and loss tangent. At the lowest frequency (0.1 Hz) the storage modulus of the network (B) showed higher value than that of the network (A). As the frequency increased the storage moduli increased moderately and the loss tangent increased rather rapidly from 0.1 to 0.33. Finally, the network (C) consisted of the diluent of the highest molecular weight ($M_d$ = 49,350) showed strong frequency dependence of the dynamic behavior. The storage moduli of the network (C) showed the highest values over the entire testing frequencies (0.1 - 100 Hz). The damping factor (loss tangent) of the network (C) increased very rapidly with the frequency and reached around 0.4 at 100 Hz. The phenomenon is attributable to the low frequency relaxation in the network with reptating linear (unbranched) molecules for the networks (B) and (C). And for the network (A) with the diluent of $M_d$ = 1,200, the diluent worked as a low viscosty solvent in the network so that the molecular mobility of the network became much higher, ie., long time relaxation (low frequency) tended to disappear. The trend of networks (B) and (C) are qualitatively in accord with the proposal of Kramer et al.[84,85] In the proposal they suggested that the relaxation

time to decay to half of its plateau modulus was approximately proportional to the 3.5 power of the molecular weight of reptating molecule. Therefore, the higher molecular weight diluent in the network tends to reveal higher losses in the low frequency range. The trends of the dynamic mechanical properties in the compression mode are very similar to those in the shear mode discussed in the previous section. The frequency dependence of the networks are summarized in Table IV. The dynamic behavior of the networks are compared at the frequencies of Ø.1 and 1ØØ Hz.

In Figure 28, 29, and 3Ø the dynamic storage moduli and loss tangents of the dilute networks (A), (B) and (C) are compared with those of the compliant coatings with the dilute networks (A), (B) and (C) imbedded in the rayon velvet fabric. The thickness of velvet fabric is about 2.5 mm and the total thickness of the coating is 3.Ø - 3.3 mm, which means the networks cover the fiber pile tips over Ø.5 - Ø.8 mm thickness. The dynamic measurements were carried out at 1% compressive strain in the frequency range of Ø.1 to 1ØØ Hz. The storage moduli of the composites were about twice greater than those of the homogeneous networks (without velvet) at the frequency of Ø.1 Hz. As the frequency increased the storage moduli of the composites were significantly increased, whereas, those of the homogeneous networks were almost constant (network (A) in Figure 28) or moderately increased (network (B) in

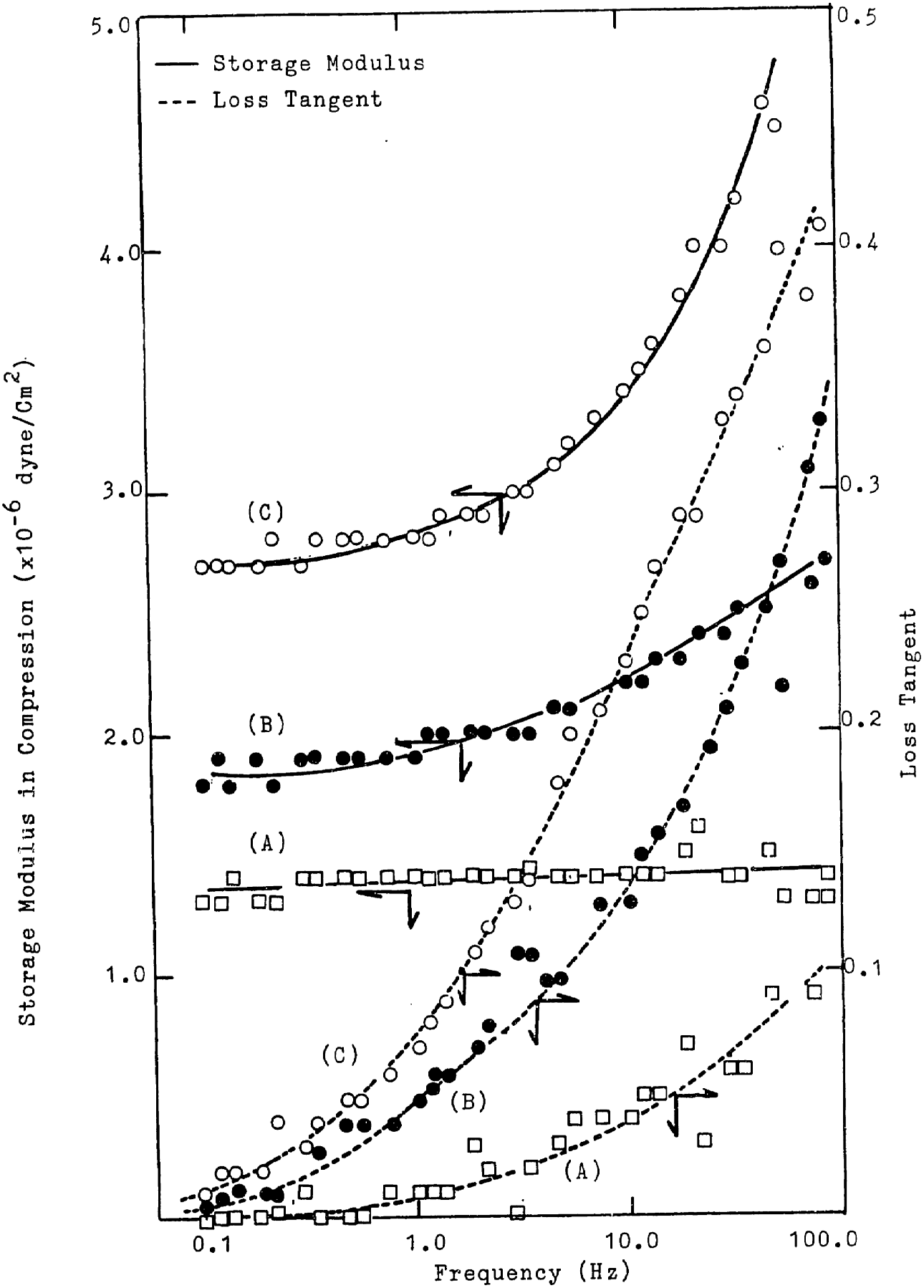


Figure 27. Dynamic Mechanical Properties of Homogeneous Silicone Network (A): 200 phr of $M_d$=1,200, Network (B): 200 phr of $M_d$=17,250, Network (C): 200 phr of $M_d$=49,350.

Table IV. Comparison of Dynamic Mechanical Properties* of Diluted Networks** with Various Diluents

| | $M_d$*** | Storage Modulus ($x10^6$dyne/cm$^2$) | | Loss tangent | |
|---|---|---|---|---|---|
| | | 0.1 Hz | 100 Hz | 0.1 Hz | 100 Hz |
| Network (A) | 1,200 | 1.55 | 1.64 | 0.018 | 0.18 |
| Network (B) | 17,250 | 1.95 | 2.85 | 0.019 | 0.34 |
| Network (C) | 49,350 | 2.46 | 4.86 | 0.051 | 0.42 |

* Measured by using Dyna Stat$^R$ at 1% strain in compression mode.

** All networks were synthesized with $\alpha,\omega$-divinyl PDMS (Mn = 26,400), tetrakis (dimethylsiloxy) silane and various diluents of 200 phr.

*** Molecular weight of diluent loaded.

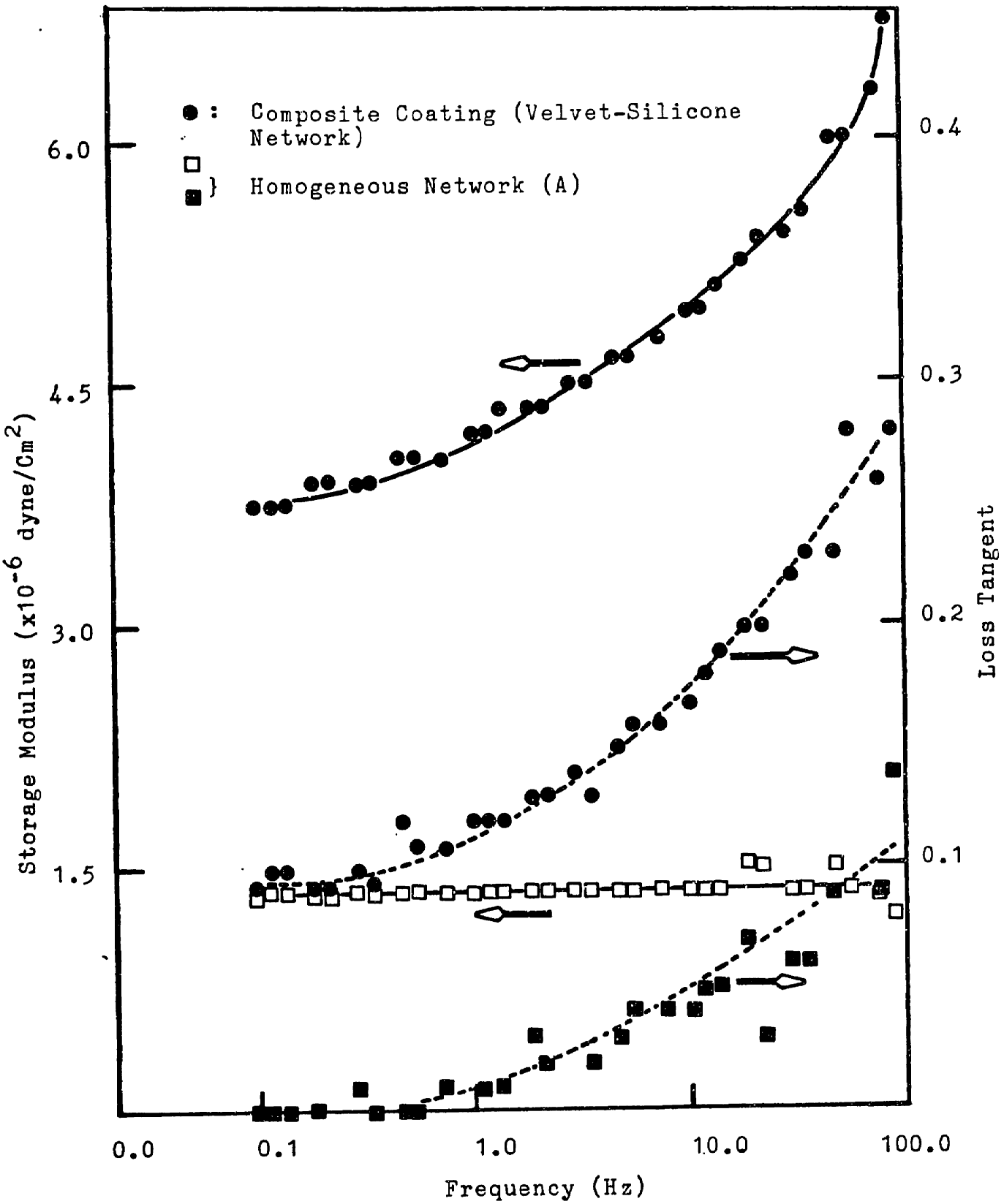


Figure 28. Comparison of Dynamic Mechanical Properties between Homogeneous Silicone Network and Composite Coating (measured in compression mode). Diluent used: 200 phr of $M_d$=1,200.

Figure 29 and network (C) in Figure 30). It is interesting to notice that the curves of the loss tangents of the composites were shifted to higher values or tan  in all coatings. However, the shapes of the curves of the composites were very similar to those of the dilute networks. The differences of the loss tangents between the composites and the dilute networks were about 0.1 throughout the frequency range. The storage moduli of the homogeneous networks and composites are illustrated in Table V-(a) at 0.1 and 100 Hz. In Table V-(b) the loss tangent of the homogeneous networks and composites are compared at 0.1 and 100 Hz.

The reinforcement effect of the fibers embedded in silicone rubber in the composites causes higher storage moduli than those of the homogeneous silicone rubber networks. The reason for the composites to reveal higher loss tangents than the dilute network may be due to the possible dissipating mechanism of the velvet fabric. The valvet fabric consists of a backing fabric (plain fabric of rayon) and the vertically running fibers stitched to the backing fabric. When the composite experiences compressive sinusoidal force, the fibers and backing fabric may be one of the sources of losses. Small scale slippage may also occur between fiber and network, which may cause higher losses in the composites, but this is not easily demonstrated.

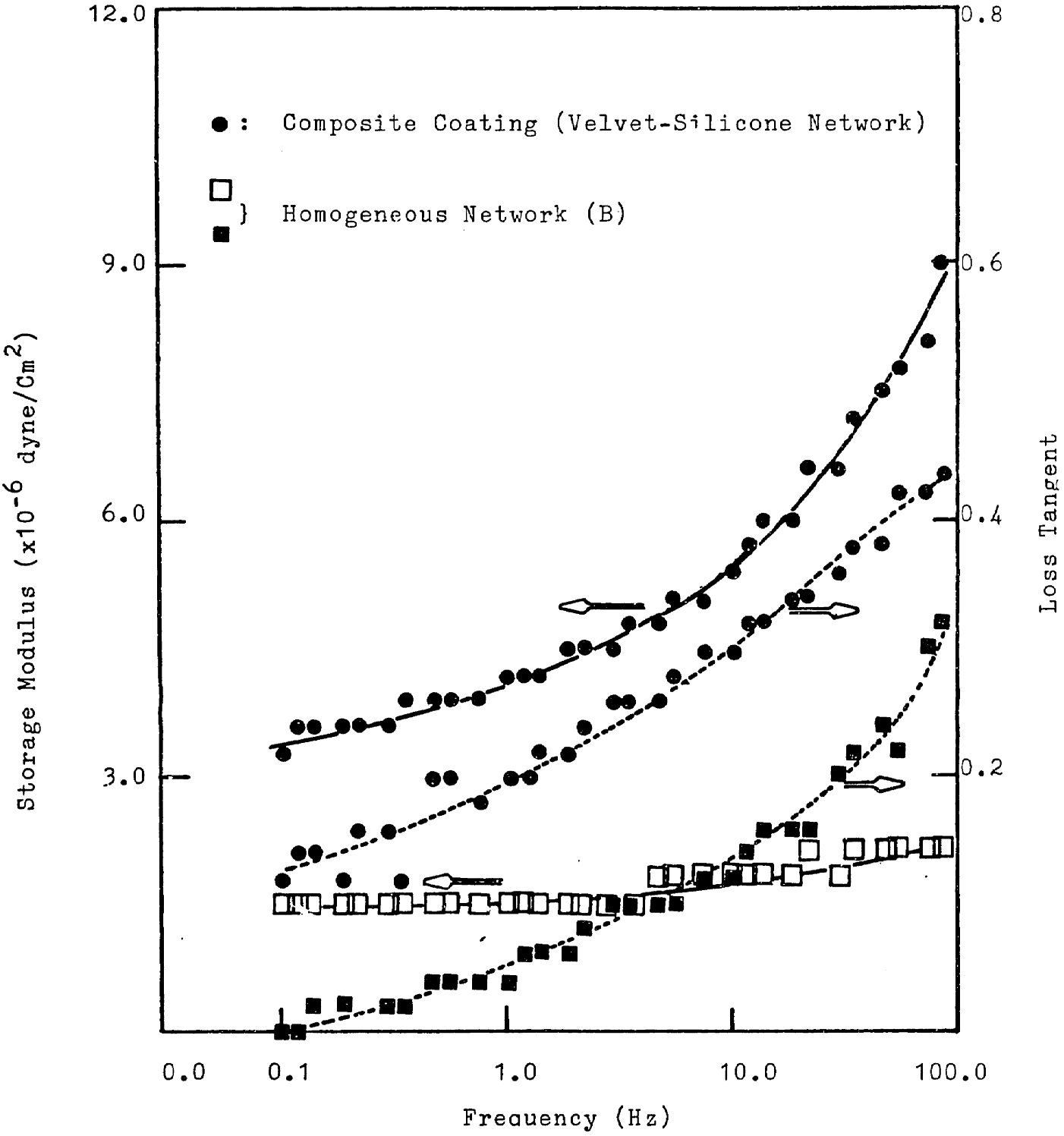


Figure 29. Comparison of Dynamic Mechanical Properties between Homogeneous Silicone Network and Composite Coating (measured in compression mode). Diluent used: 200 phr of $M_d$=17,250.

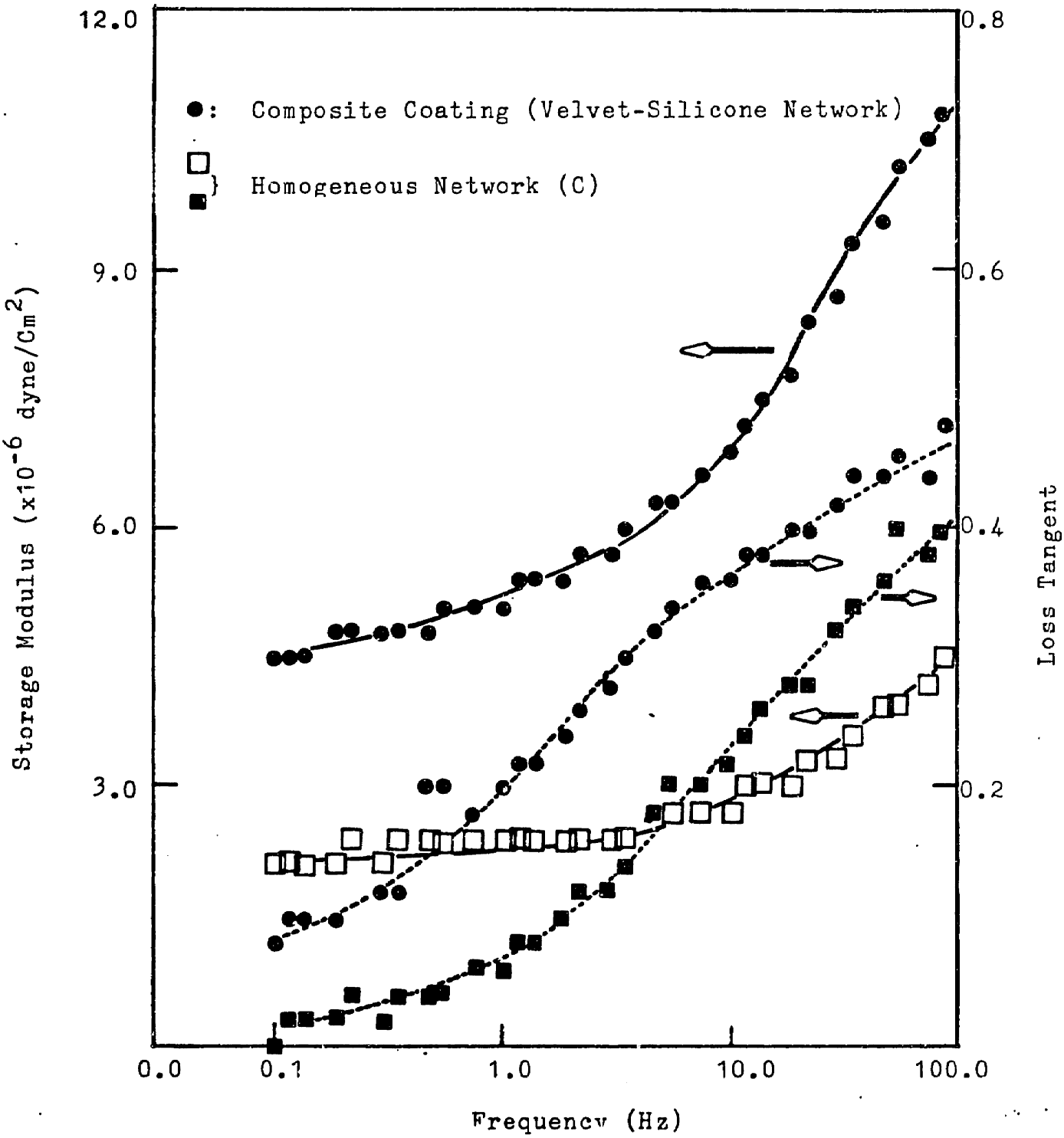


**Figure 30 .** Comparison of Dynamic Mechanical Properties between Homogeneous Silicone Network and Composite Coating (at compression mode). Diluent used: 200 phr of $M_d$=49,350.

Table V-(a). Comparison of Dynamic Storage Modulus*

Unit: $x10^{-6}$ dyne/$Cm^2$

| | $M_d$** | Dilute Network | | Composite | |
|---|---|---|---|---|---|
| | | Ø.1 Hz | 1ØØ Hz | Ø.1 Hz | 1ØØ Hz |
| Network (A) | 1,2ØØ | 1.55 | 1.64 | 3.8Ø | 6.78 |
| Network (B) | 17,25Ø | 1.95 | 2.85 | 4.18 | 1Ø.5 |
| Network (C) | 49,35Ø | 2.46 | 4.86 | 5.48 | 12.9 |

Table V-(b). Comparison of Loss Tangent*

| | $M_d$** | Dilute Network | | Composite | |
|---|---|---|---|---|---|
| | | Ø.1 Hz | 1ØØ Hz | Ø.1 Hz | 1ØØ Hz |
| Network (A) | 1,2ØØ | Ø.Ø18 | Ø.18 | Ø.Ø94 | Ø.28 |
| Network (B) | 17,25Ø | Ø.Ø19 | Ø.34 | Ø.12 | Ø.46 |
| Network (C) | 49,35Ø | Ø.Ø51 | Ø.42 | Ø.Ø97 | Ø.49 |

* Measured by using Dyna Stat® at 1% compressive strain.

** Molecular weight of diluents

## 2. Composite Compliant Coating Drag Reduction Measured by the Rotating Disc

A number of composite compliant coatings were tested on the rotating disc, and the drag forces of the compliant coatings were compared with those of smooth hard reference disc. The hard reference was geometrically identical to the compliant coatings. The composite compliant coatings thus tested consisted of four layers: (1) a fiberglass screen material next to the base plate of the disc, (2) rayon velvet fabric, (3) dilute network on the screen material, and (4) a thin film covered over the compliant parts. Figure 13 in the experimental part shows the scheme of these layers in detail.

The dynamic mechanical properties of the composite compliant coatings were measured after removing the backing screen material and the top film by using Dyna Stat®. The compression mode was employed for all coatings at 1% strain in the frequency range of Ø.1 to 1ØØ Hz. A tensile test was done to measure the mechanical properties of the top films of the coating.

Table VI illustrates the compositions, the top film used in each coatings and the dynamic mechanical properties of the coatings (composites) at 1ØØ Hz. The ratios of the concentrations of the functional groups (SiH) on chain extender to those on junction molecule (SiH-ratio) were Ø.7/Ø.3 and

Ø.8/Ø.2. The molecular weights of diluents employed were $M_d$ = 5,97Ø (1ØØ ctsk) and 17,25Ø (5ØØ ctsk). The dilution ratios of the networks were 2ØØ - 3ØØ phr (parts per hundred reactive resin). The thin films used as the top layer of the composite coatings were respectively natural rubber Ø.ØØ5 inch thick, and teflon films Ø.ØØ1 and Ø.ØØ5 inch thick. The ranges of the compression storage moduli and the loss tangents of velvet-silicone coatings were from 1.1 x $1Ø^6$ to 5.7 x $1Ø^6$ dyne/$Cm^2$, and from Ø.4 to Ø.7 at 1ØØ Hz, respectively. The compliant coating discs were rotated at speeds from 69Ø rpm to 1,5ØØ rpm, which corresponds to the Reynolds number of 8.92 x $1Ø^5$ to 1.94 x $1Ø^6$.

As mentioned above, the top film of the composite coating played a very important role to reduce the skin-friction drag on the turbulent boundary layer. Figure 31 shows the effect of the top film on the skin-friction drag. The coatings were made of three different top films on the same compliant velvet-silicone material. The network in the coating was synthesized by $\alpha,\omega$ -divinyl PDMS (Mn = 26,4ØØ), tetrakis (dimethylsiloxy) silane and chain extender (the SiH-ratio was Ø.7/Ø.3) with a diluent ($M_d$ = 5,97Ø) loaded 2ØØ phr. A group of points (a) on the top of the Figure 31 which shows extremely high skin-frictions are the results of bare coating (no top film). As indicated in the Figure 32 where the drag reduction ratios were plotted in the variouis log Reynolds numbers, the

Table VI. Compositions and Dynamic Mechanical Properties of Composite Coatings

| Sample | Composition | | | Film | | | Mech. Property** (at 100 Hz) | |
|---|---|---|---|---|---|---|---|---|
| | (SiH)* Ratio | Diluent (PDMS) (M.W.) | Dil. Ratio (phr) | Nat. Rubber (5mil) | Teflon (1mil) | Teflon (5mil) | Storage Modulus ($dyne/Cm^2$) | Loss*** Tangent |
| SC810-1 | 0.7/0.3 | 5,970 | 200 | | | | 3.39 | 0.398 |
| SC810-2 | 0.7/0.3 | 5,970 | 200 | x | | | 3.39 | 0.398 |
| SC810-3 | 0.7/0.3 | 5,970 | 200 | | x | | 3.39 | 0.398 |
| SC810-4 | 0.7/0.3 | 5,970 | 200 | | | x | 3.39 | 0.398 |
| SC829 | 0.7/0.3 | 5,970 | 200 | | | x | 5.77 | 0.479 |
| SC905 | 0.8/0.2 | 5,970 | 300 | | | x | 2.24 | 0.448 |
| SC912 | 0.8/0.2 | 17,250 | 300 | | | x | 1.13 | 0.700 |
| SC920 | 0.8/0.2 | 17,250 | 203 | | | x | 5.66 | 0.605 |

* (SiH) of chain extention mol./(SiH) of junction molecule.

** Dynamic mechanical property of coating in compression mode at 1% strain.

*** Loss tangent = loss modulus/storage modulus.

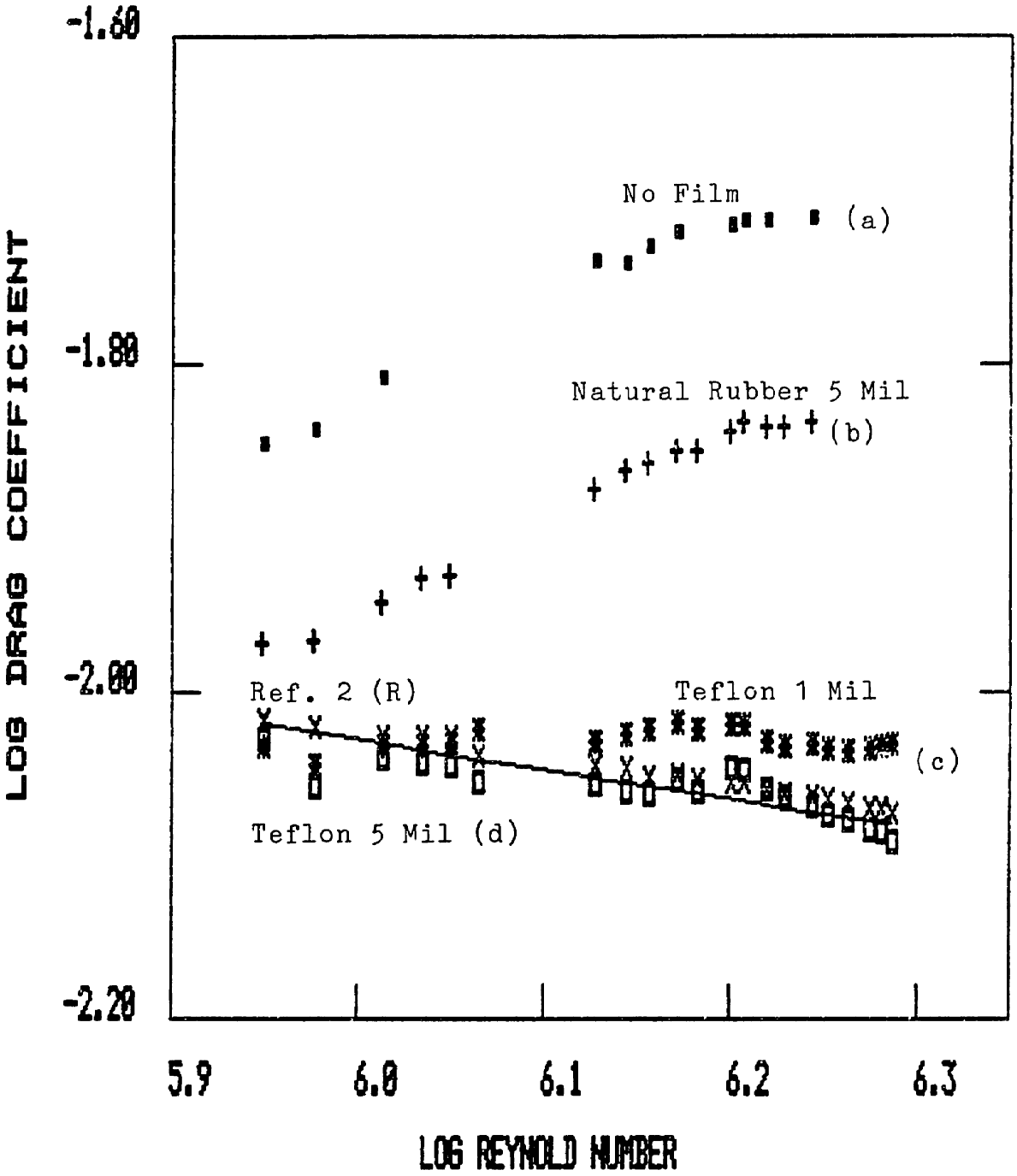


Figure 31. Log Reynolds number vs. drag coefficient of composite compliant coatings. Effect of top films on drag.

drag of the bare coating recorded upto about 126 percent increase at the highest Reynolds number tested.

Drag reduction ratio = $1 - C_{D,C}/C_{D,R}$

where, $C_{D,C}$ and $C_{D,R}$ are the drag coefficient of the compliatn coating and that of the smooth and rigid reference, respectively. During rotation the coating without the top film displayed very large wave motions whose wavelength was of the order of few centimeters and wave height was few milimeters. These motions are very similar to those that Hansen and Hunston[5,68,76] and other investigators[32] observed previously. The coating (b) covered with natural rubber sheet 0.005 inch thick showed much lower drag coefficients (Figure 31(b)) than the bare coating. The amplitude of the static wave on the coating seemed to be smaller than that of the bare coating (a). However, the static divergence appeared on the coating (b) through the whole testing speed range. The drag coefficients of the coating (b) were 11 to 68% higher than those of the reference at the Reynolds number of $8.92 \times 10^5$ to $1.76 \times 10^6$. The tensile modulus of the natural rubber film was $E = 2.13 \times 10^7$ dyne/Cm$^2$. The coating with film (c), teflon film 0.001 inch thick, revealed much lower drag coefficient than the above coatings (a) and (b) in the Figure 31 and 32. The drag equal to those of reference at low speed and coefficients of the coating (c) were slightly higher (about 9%)

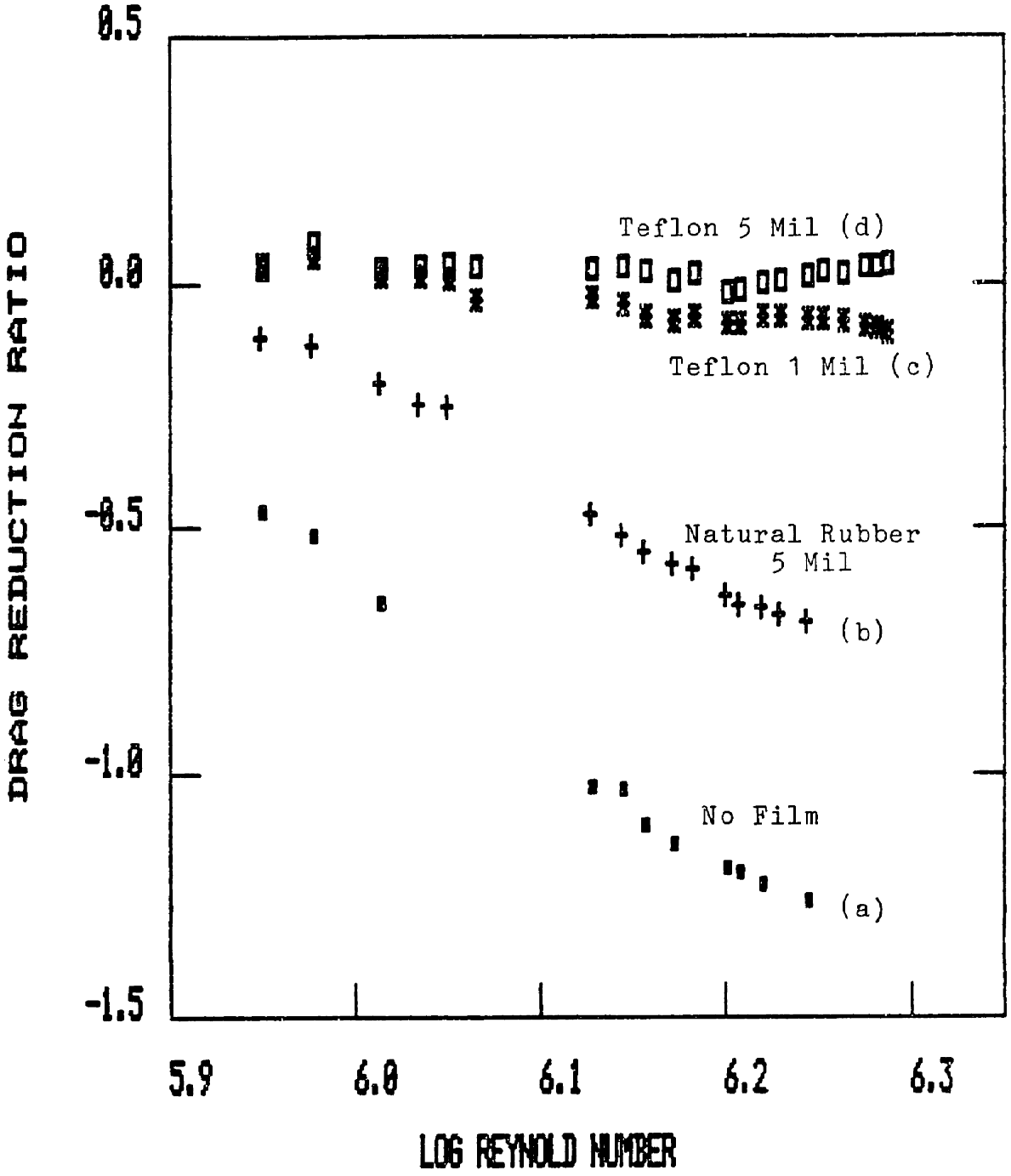


Figure 32. Log Reynolds number vs. drag reduction ratio of composite coatings. Effect of top films on drag.

than the reference at high velocities. The tensile modulus of the teflon film Ø.ØØ1 inch thick was 4.63 x $1Ø^9$ dyne/$Cm^2$. Finally, when a teflon film Ø.ØØ5 inch thick was placed on the compliant material, small drag reduction was observed through the testing velocities (within 5% drag reduction). The surface motions of the coating (d) with a teflon film Ø.ØØ5 inch were completely different from those of the bare coating, and wave height was greatly repressed.

The tensile modulus of the teflon-II (Ø.ØØ5 inch thick film) was 7.Ø x $1Ø^9$ dyne/$Cm^2$. The detail of the tensile behavior of the films is illustrated in Figure 33. In Table VII the top film effects on the compliant coating drag reduction are summarized with the mechanical properties of the films. The mechanical properties of films are reported in two quantities which are tensile modulus, E, and stiffness at 1% strain. Considering the interaction between the turbulent fluctuations and the compliant wall, the stiffness is better parameter to illustrate the effective material property for drag reduction than the tensile modulus, because the stiffness is defined as the force in gram at 1% strain on a sample Ø.77 Cm wide, therefore is proportional to the total force to deform the film.

The dynamic properties of the base compliant material without film (velvet-silicone rubber) were measured at 1% compressive strain from Ø.1 to 1ØØ Hz. The plots of (a) in

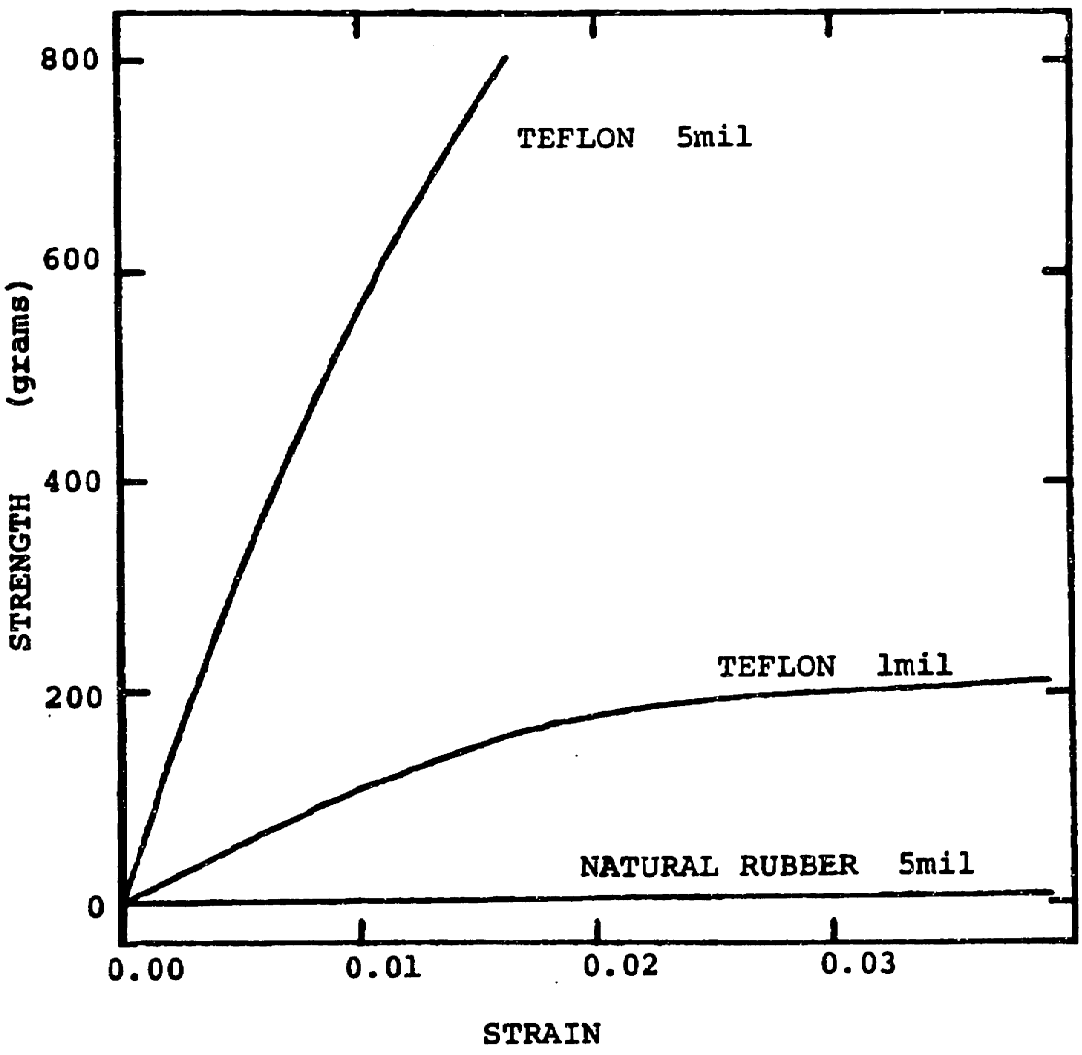


Figure 33. Tensile properties of top films of composite coatings.

Table VII. Effect* of Top Films on Skin-Friction Drag

| Film | Thick-ness (inch) | Film Property | | Drag reduction ratio** | |
|---|---|---|---|---|---|
| | | E(dyne/Cm$^2$) | Stiffness at 1% strain(g) | Re=8.92x10$^5$ | Re =1.94x10$^6$ |
| No film | - | - | - | -0.465 | -1.26*** |
| Natural rubber | 0.0056 | 2.13x10$^7$ | 2.3 | -0.115 | -0.682*** |
| Teflon-I | 0.0012 | 4.63x10$^9$ | 107.9 | -0.003 | -0.092 |
| Teflon-II | 0.0042 | 7.00x10$^9$ | 571.4 | 0.017 | 0.051 |

* Compliant network was synthesized by $\alpha,\omega$-divinyl PDMS (Mn = 26,400), the SiH-ratio of 0.7/0.3 and diluent of $M_d$ = 5,970 (200 phr).

** Drag reduction ratio; $R = 1 - C_{D,C}/C_{D,R}$, where $C_{D,C}$ and $C_{D,R}$ are drag coefficients of compliant coating and reference disc #2.

*** Test done at Reynolds number of 1.76x10$^6$.

Table VIII. Illustation of the Experimental Conditions.

| | Name of Coatigs | Variable | Constant Condition | Reference Figures |
|---|---|---|---|---|
| Test-I | (a) SC81ØT5<br>(b) SC9Ø5T5 | Dilution ratio | Low damping | 34,35,36,37 |
| Test-II | (c) SC92ØT5<br>(d) SC912T5 | Dilution ratio | High damping | 38,39,4Ø,41 |
| Test-III | (a) SC81ØT5<br>(c) SC92ØT5 | Molecular Wt. of diluent | Low dilution ratio | 42,43,44,45 |
| Test-IV | (b) SC9Ø5T5<br>(d) SC912T5 | Molecular Wt. of diluent | High dilution ratio | 46,47,48,49 |

Figures 36 and 37 show the log storage moduli and tan $\delta$ of the compliant meterial employed in this test. The storage moduli of the composite increased monotonically from $1.63 \times 10^6$ to $3.38 \times 10^6$ dyne/$Cm^2$ in the frequency of Ø.1 to 1ØØ Hz. The loss tangent of the composite also showed monotonical increase as frequency increased ( tan $\delta$ = Ø.Ø93 to Ø.4Ø in the same frequency range). The compliant material used in this experiment of top film effect on the skin-friction showed relatively low damping property. The effect of top film on the drag reduction can be attributed to; (1) the high modulus thin film restricts the large surface motion which prevents the drastic drag increase due to the surface wave formation, (2) a high modulus thin film can resonate at high frequency, one of the neccessary conditions to achieve drag reduction by compliant coating, according to Ash and Bushnell.[38]

In the succeeding experiments the dynamic properties of the compliant material have been varied with a fixed top film (teflon-II, Ø.ØØ5 inch thick) to investigate the relation of the velvet-silicone rubber material properties to drag reduction. The coatings were constructed for the following purposes:

(1) To examine effect of the softness with constant low damping.

(2) To examine the effect of the softness on the skin-friction of coating with constant high damping.

(3) To examine the effect of the damping factor on the

skin-friction with constant dilution ratio.

The purposes of this experiment are summarized in Table VIII.

Figure 34 shows double log plots of drag coefficients of the rotating discs vs. Reynolds number from 8.92 x $10^5$ to 1.94 x $10^6$. The plots of (a) and (b) in Figure 34 illustrate the drag coefficients of the compliant coating with less diluent (SC810T5; 200 phr) and that with more diluent (SC905T5; 300 phr), respectively. The plots (R) of Figure 34 denote the drag coefficient of the smooth brass disc (reference-II), which shows a good agreement with the theoretical predictions (straight line).

Both of the coatings were composed of $\alpha, \omega$-divinyl PDMS (Mn = 26,400), chain extender, and tetrafunctional junction molecules with the same molecular weight ($M_d$ = 5,970) diluent. The SiH-ratios defined by the ratio of [SiH] of chain extender to [SiH] of junction molecule were 0.7/0.3 for the former and 0.8/0.2 for the latter.

The coating (a) in Figure 34 shows slightly lower drag coefficients than the rigid reference (R) through the Reynolds number tested (around 5% reduction). On the other hand, the coating (b) shows equal or slightly lower skin-friction than the reference at the low rotating speed, however, higher drag (upto 10%) is observed as the speed increases.

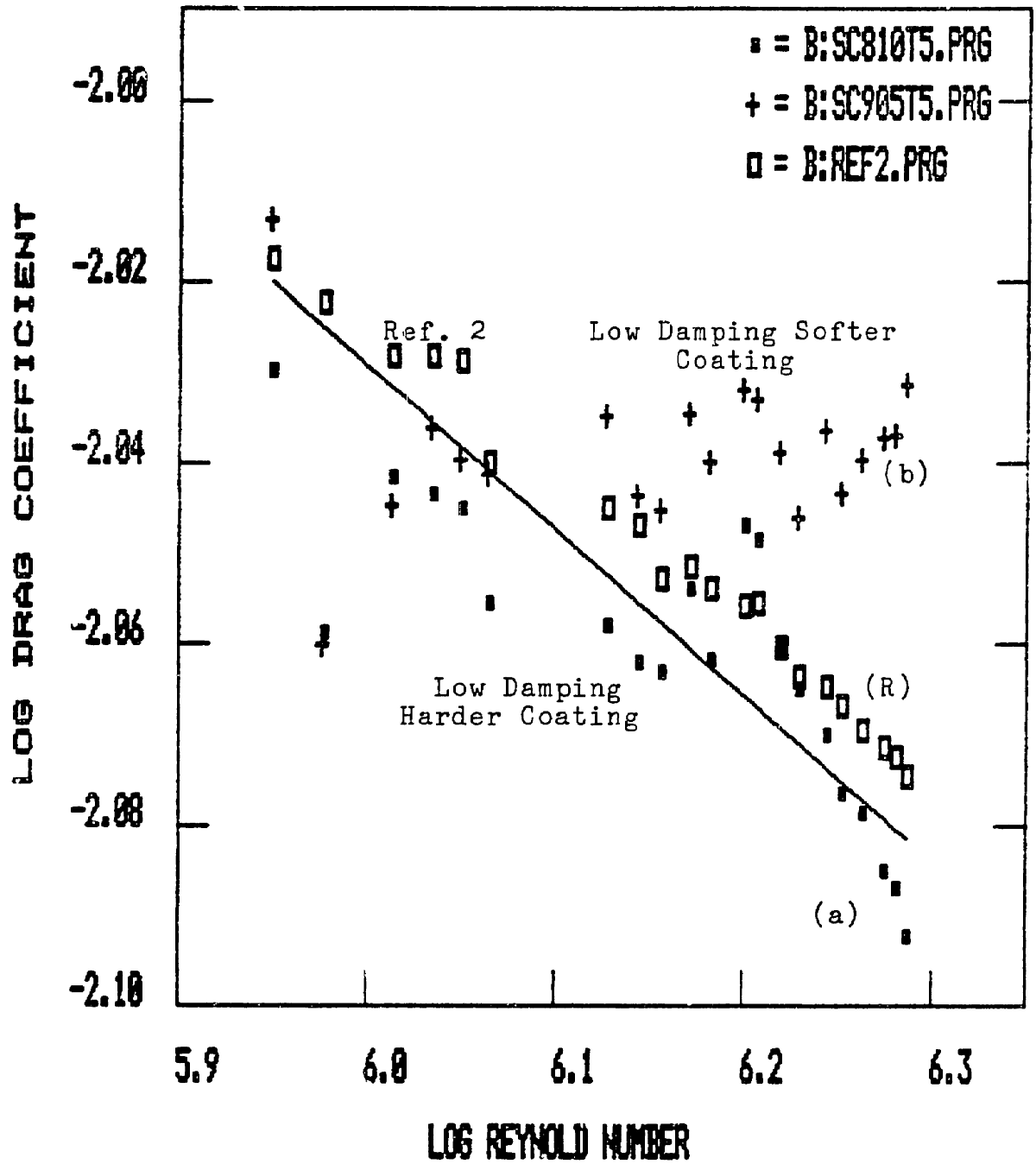


Figure 34. Log Reynolds number vs. log drag coefficient of the composite compilant coatings in test-I. (a)$M_d$=5,970 200phr, (b)$M_d$=5,970 300phr.

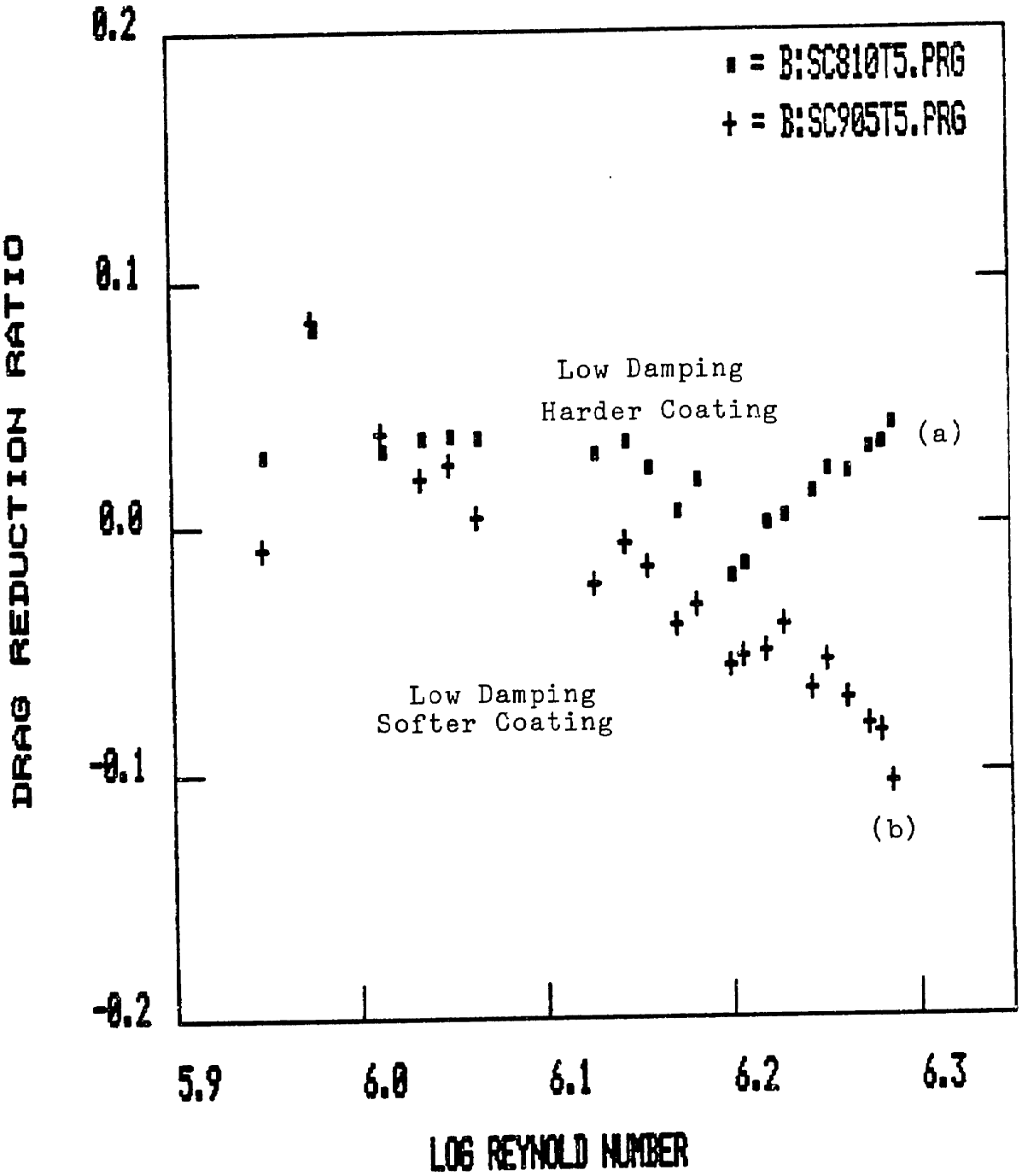


Figure 35. Log Reynolds number vs. drag reduction ratio of the composite coatings in test-I.
(a)$M_d$=5,970 200phr, (b)$M_d$=5,970 300phr.

For more quantitative study the results are replotted in a manner of the drag reduction ratio versus log Reynolds number (Figure 35). The drag reduction ratio, R is defined by the following equation:

$$R = 1 - C_{D,C} / C_{D,R} \qquad (1)$$

where, $C_{D,C}$ and $C_{D,R}$ are the skin drag coefficient of compliant coating and smooth brass reference, respectively.

The coating (a) which showed Ø - 5% drag reduction lead about 1.5 times higher storage moduli than the coating (b) at Ø.1 to 1ØØ Hz. (See Figure 36). The loss tangents of the coatings (a) and (b) were almost identical in this frequency range, as it is evident in Figure 37 (tan $\delta$ = Ø.1 - Ø.45 at Ø.1 to 1ØØ Hz).

Figures 38 and 39 show the log drag coefficients and drag reduction ratios of the compliant coatings (Test-II in Table VIII) with respect to log Reynolds number, respectively. In the present test, the softness effect of the coatings on the drag reduction was examined with high damping coatings.

The coatings (c) and (d) were composed of the networks synthesized with the same chain, chain extender and junction materials as the coatings in Test-I of Table VIII. The diluent employed in the coating (c) and (d) has higher molecular weight ($M_d$ = 17,25Ø) which exceed the value of entanglement spacing of PDMS ($M_e$ = 8,8ØØ - 12,ØØØ).[92] Therefore, the coatings must

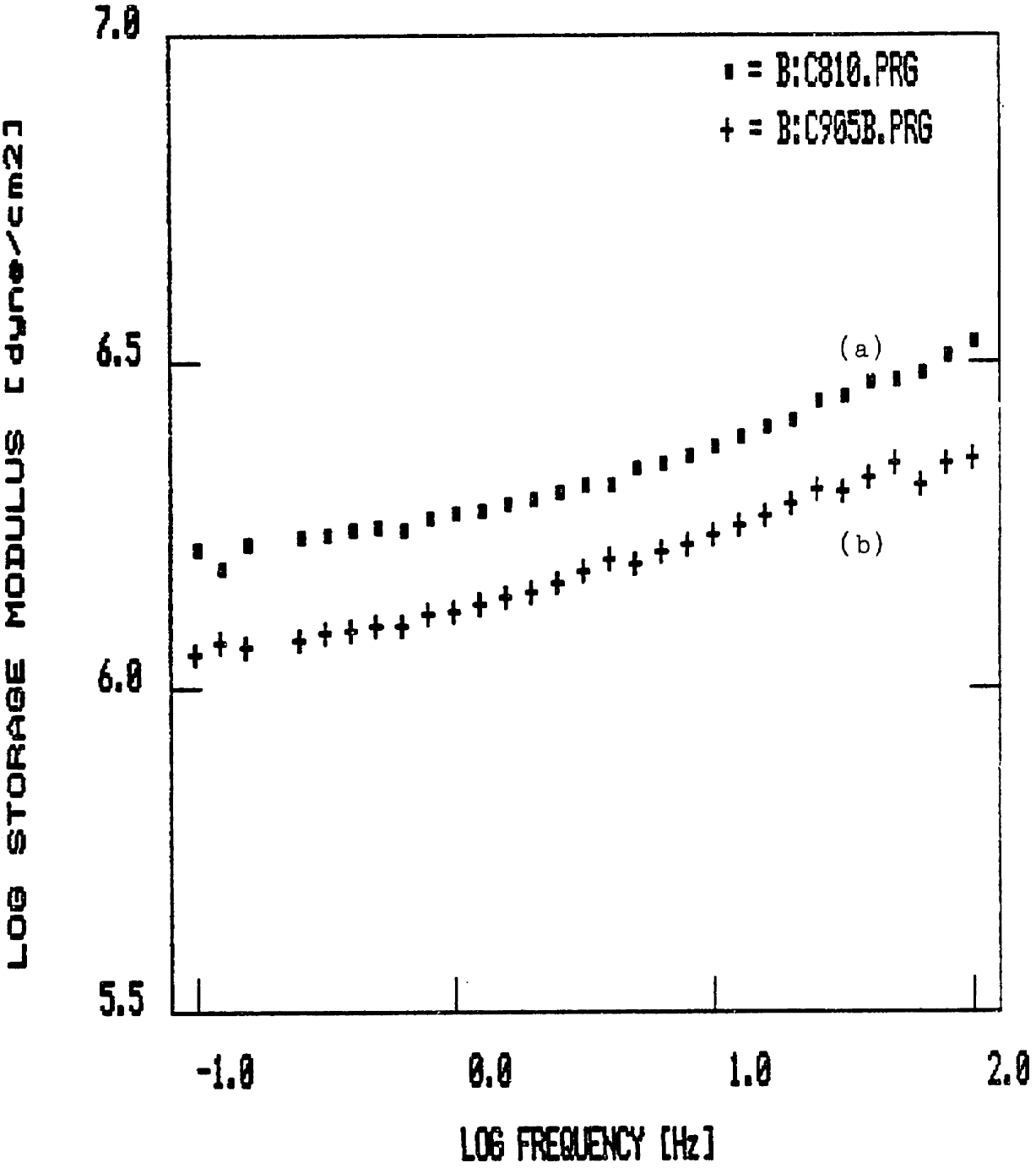


Figure 36. Log storage modulus vs. log frequency of the composite compliant coatings in test-I.
(a)$M_d$=5,970 200phr, (b)$M_d$=5,970 300phr.

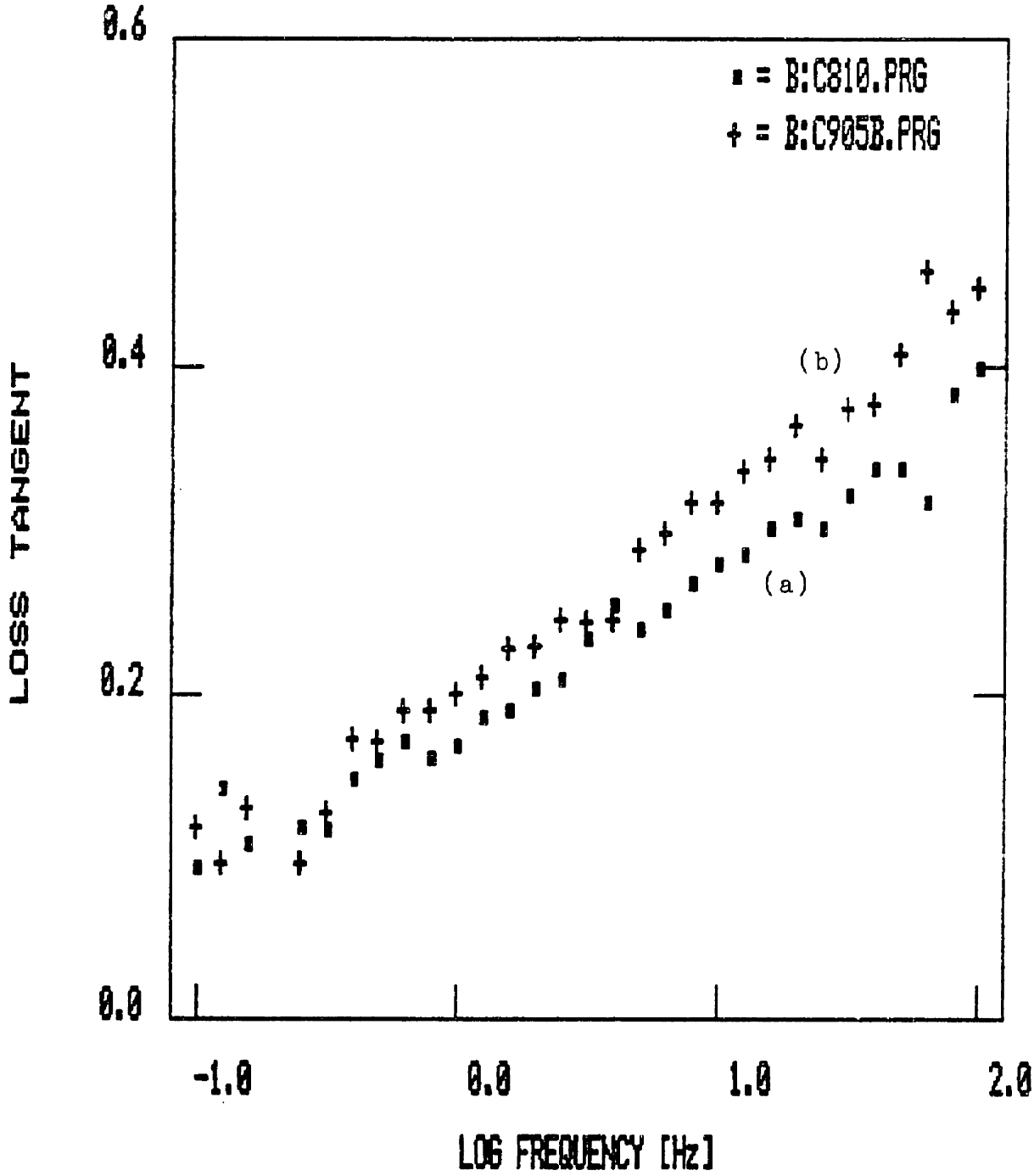


Figure 37. Loss tangent vs. log frequency of the composite compiant coatings in test-I.
(a)$M_d$=5,970 200phr, (b)$M_d$=5,970 300phr.

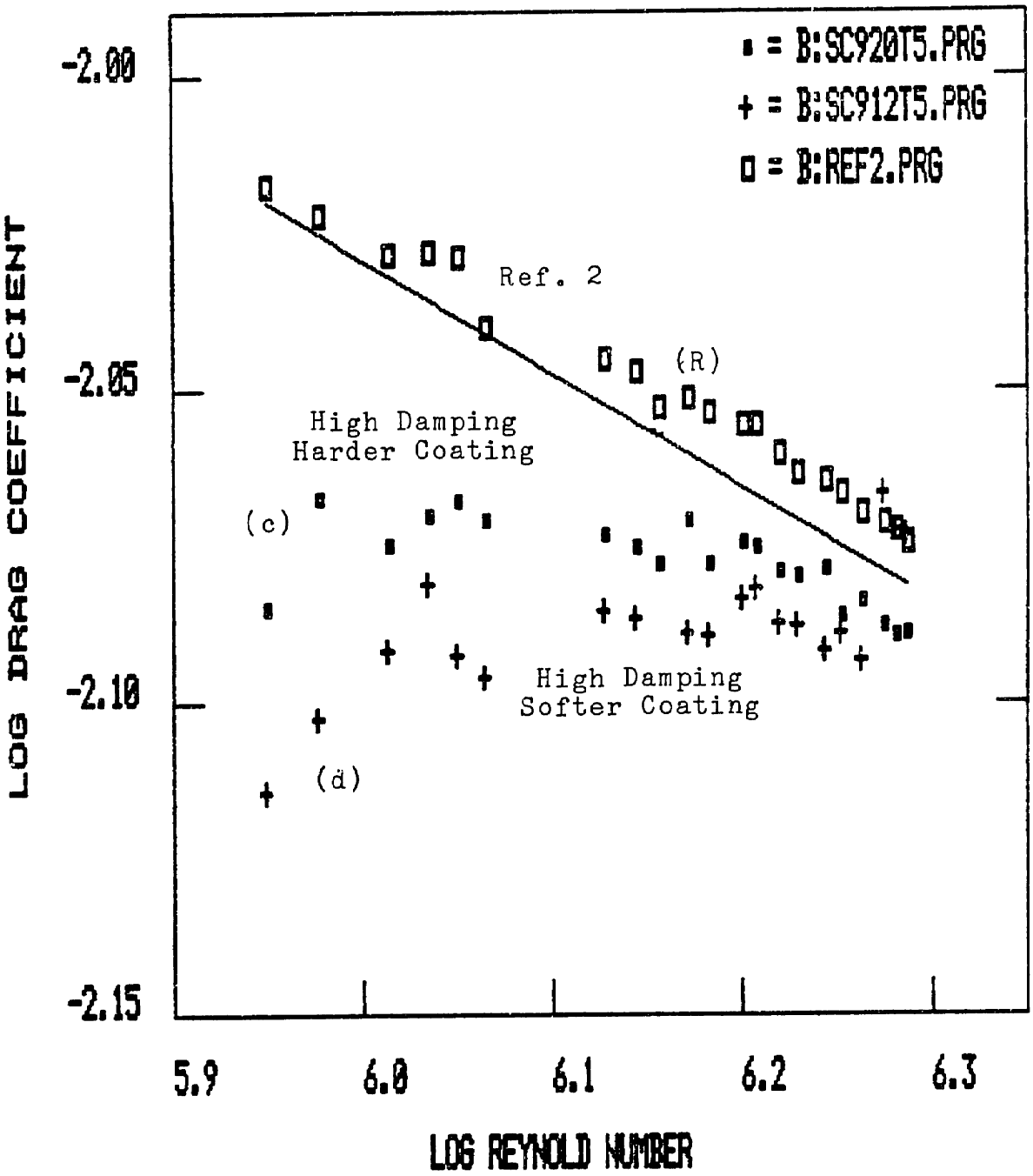


Figure 38. Log Reynolds number vs. log drag coefficient of the composite compilant coatings in test-II.
(c)$M_d$=17,250 203phr (d)$M_d$=17,250 300phr.

show high losses at relatively low frequency (lower than few hundred Hz). The dilution ratios employed in this test were 203 phr for the coating (c) and 300 phr for coating (d). In both coatings the SiH-ratio was 0.8/0.2.

The results of drag measurements of the coating (c) and (d) are illustrated in the Figure 38 and 39. Both of the coatings show significantly lower drag coefficients than the reference at the low Reynolds numbers. And the drag coefficients of the coatings approached to those of the reference as the Reynolds number increased. However, both of the coatings showed still equal or lower drag coefficients at the highest test speed (Reynolds number of $1.94 \times 10^6$). If the performance of two coatings are compared each other, the coating (c) reveals higher drag coefficients than the coating (d). The coating (c) showed maximum around 14% drag reduction at Reynolds number of $8.92 \times 10^5$, and the drag reduction ratio dropped down to 3% at Reynolds number of $1.94 \times 10^6$. The coating (d) shows better performance through the entire Reynolds number tested except the last three points. The maximum drag reduction of the coating (d) was more than 20% at Reynolds number of $8.92 \times 10^5$. The trend of drag reduction ratios of the coating (d) monotonically decreased with increasing Reynolds number, which is similar to that of coating (c).

The dynamic properties of the coatings (c) and (d) are

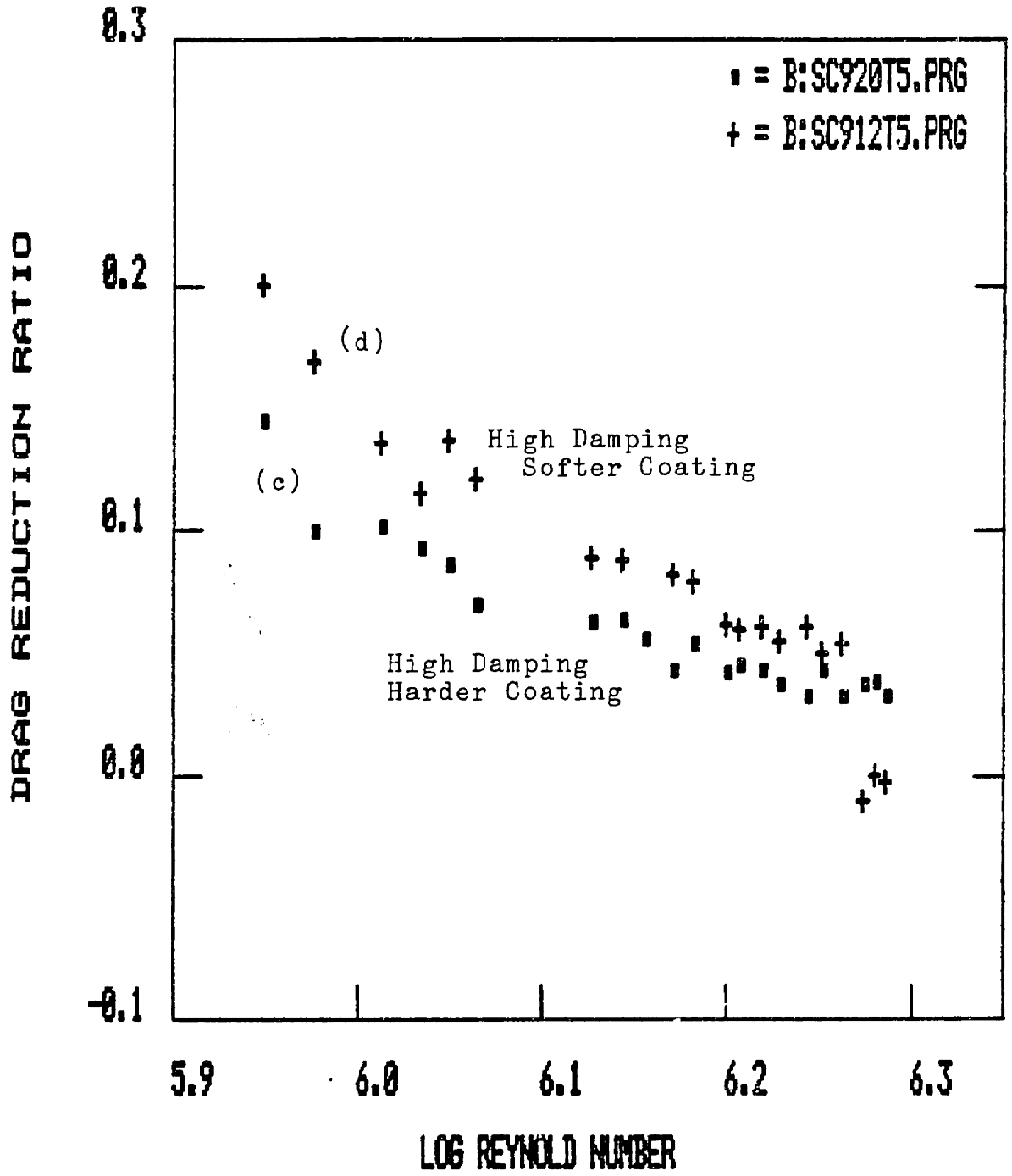


Figure 39. Log Reynolds number vs. drag reduction ratio of the composite coatings in test-II.
(c)$M_d$=17,250 203phr (d)$M_d$=17,250 300phr.

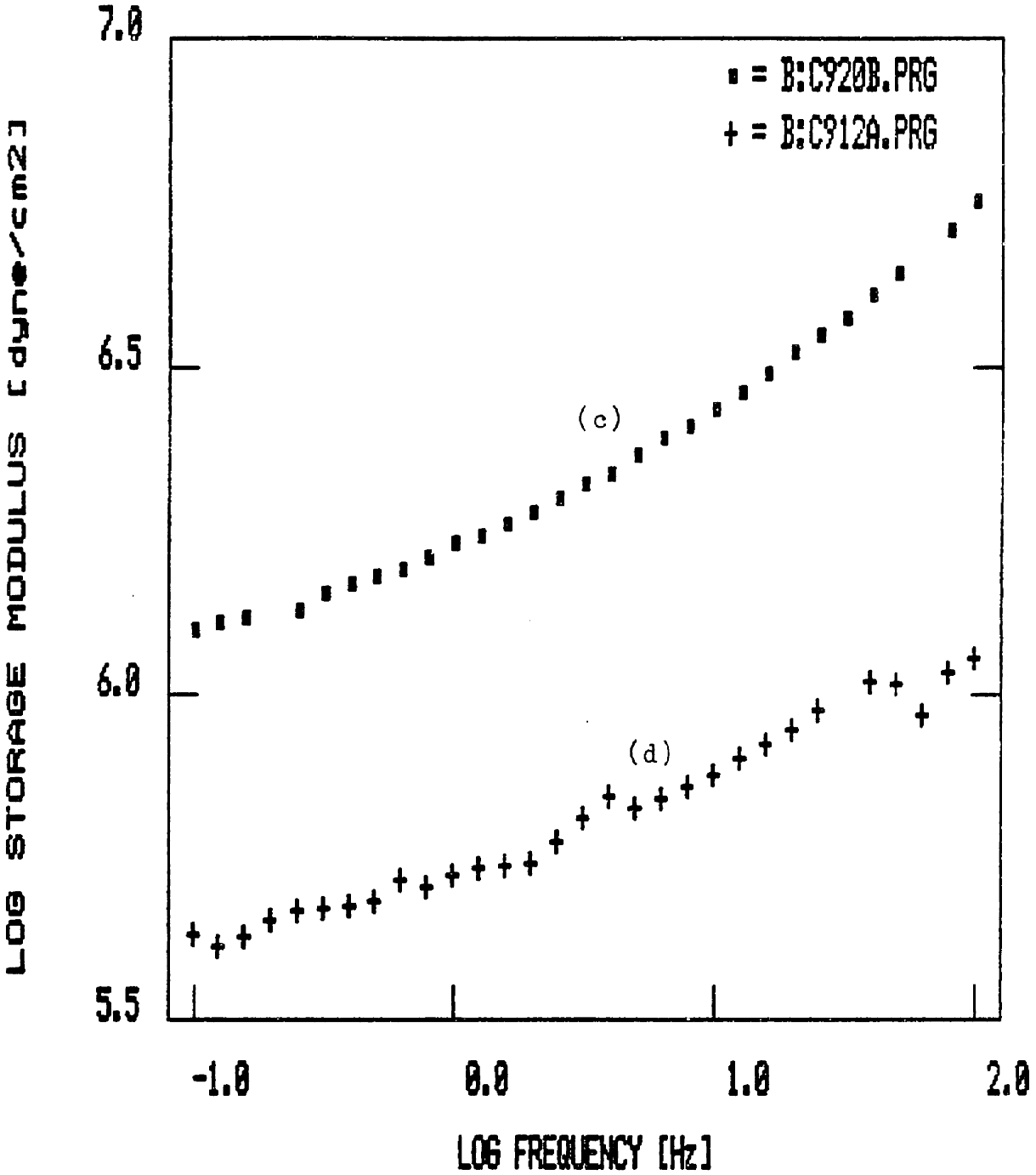


Figure 40. Log storage modulus vs. log frequency of the composite compliant coatings in test-II.
(c)$M_d$=17,250 20phr (d)$M_d$=17,250 30phr.

compared in Figures 40 and 41. The storage moduli of the coating (c) are increased from 1.29 x $10^6$ to 5.77 x $10^6$ dyne/$Cm^2$ in the frequency range of 0.1 to 100 Hz, which are about 1.4 - 1.9 times higher modulus than almost identical loss tangents in this frequency range (tan $\delta$ = 1.12 - 0.7). In this Test-II, the softer coating (coating (d)) shows better performance than the harder one (coating (c)). This result is completely opposite to the result of Test-I in which the harder coating shows drag reduction and the softer one shows equal or increase in drag. This phenomenon is not clearly understood at this moment. However, there is significant difference in their material properties between the coatings in the Test-I and Test-II, ie., the coatings in the Test-I showed lower damping and those in Test-II revealed very high damping factor.

In Test-III and IV in the Table VIII the damping effect on the skin-friction was analysed with relatively hard (a) and soft (c) coatings. Firstly, the behaviors of the coatings (a) and (c) are compared to study the effect of damping factor on the skin-friction drag (Test-III). The dilution ratio of the network in the coating (a) is 200 phr with the diluent of $M_d$ = 5,970 and that in the coating (c) is 203 phr with the diluent of $M_d$ = 17,250. And the SiH-ratios of the coatings (a) and (c) are 0.7/0.3 and 0.8/0.2, respectively.

As shown in Figures 42 and 43, the drag coefficients of coating (a) are slightly lower than those of reference disc (R)

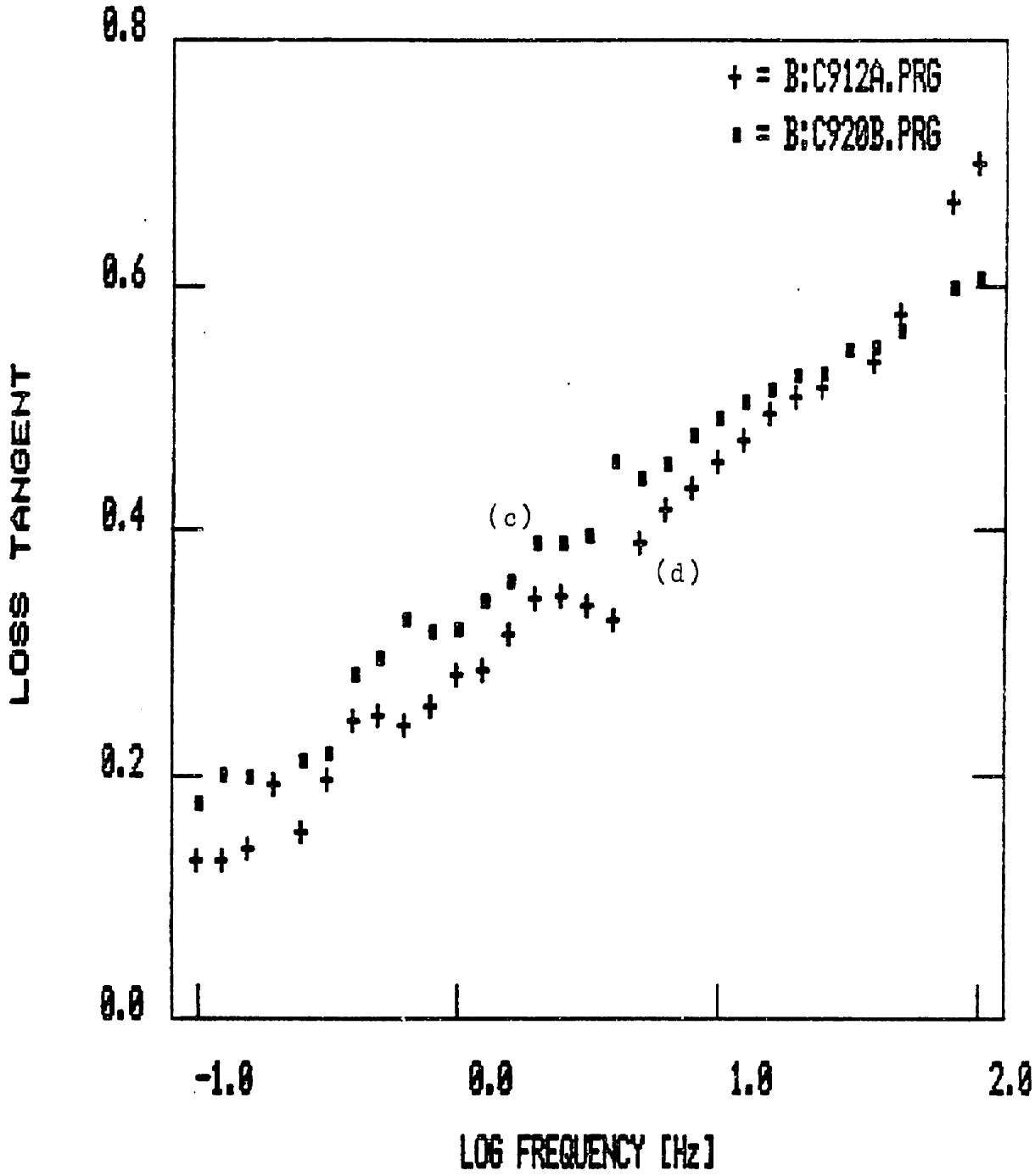


Figure 41. Loss tangent vs. log frequency of the composite compiant coatings in test-II.
(c)$M_d$=17,250 20Ø3phr (d)$M_d$=17,250 300Øphr.

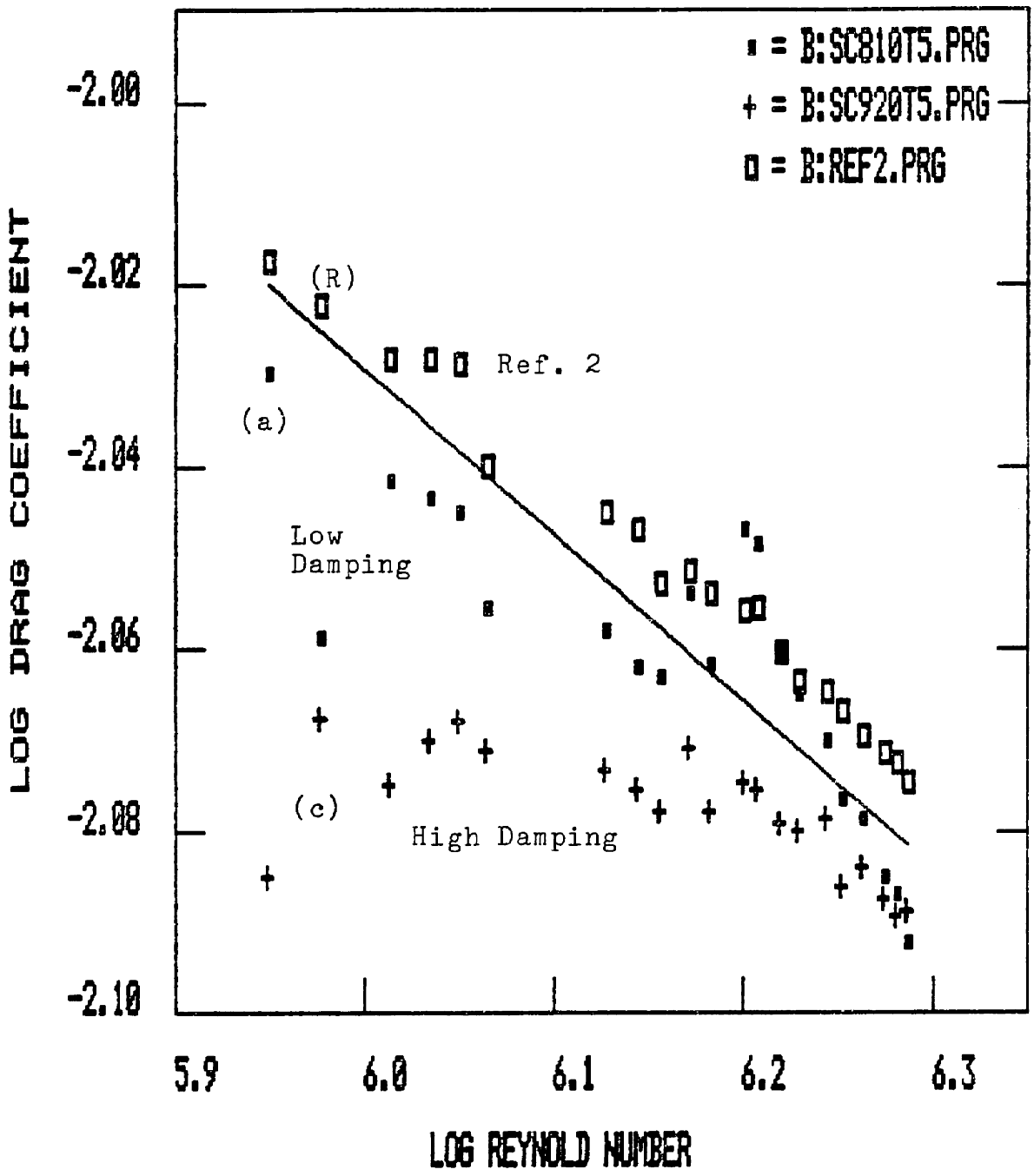


Figure 42. Log Reynolds number vs. log drag coefficient of the composite compilant coatings in test-III. (a)$M_d$=5,970 200phr, (c)$M_d$=17,250 203phr.

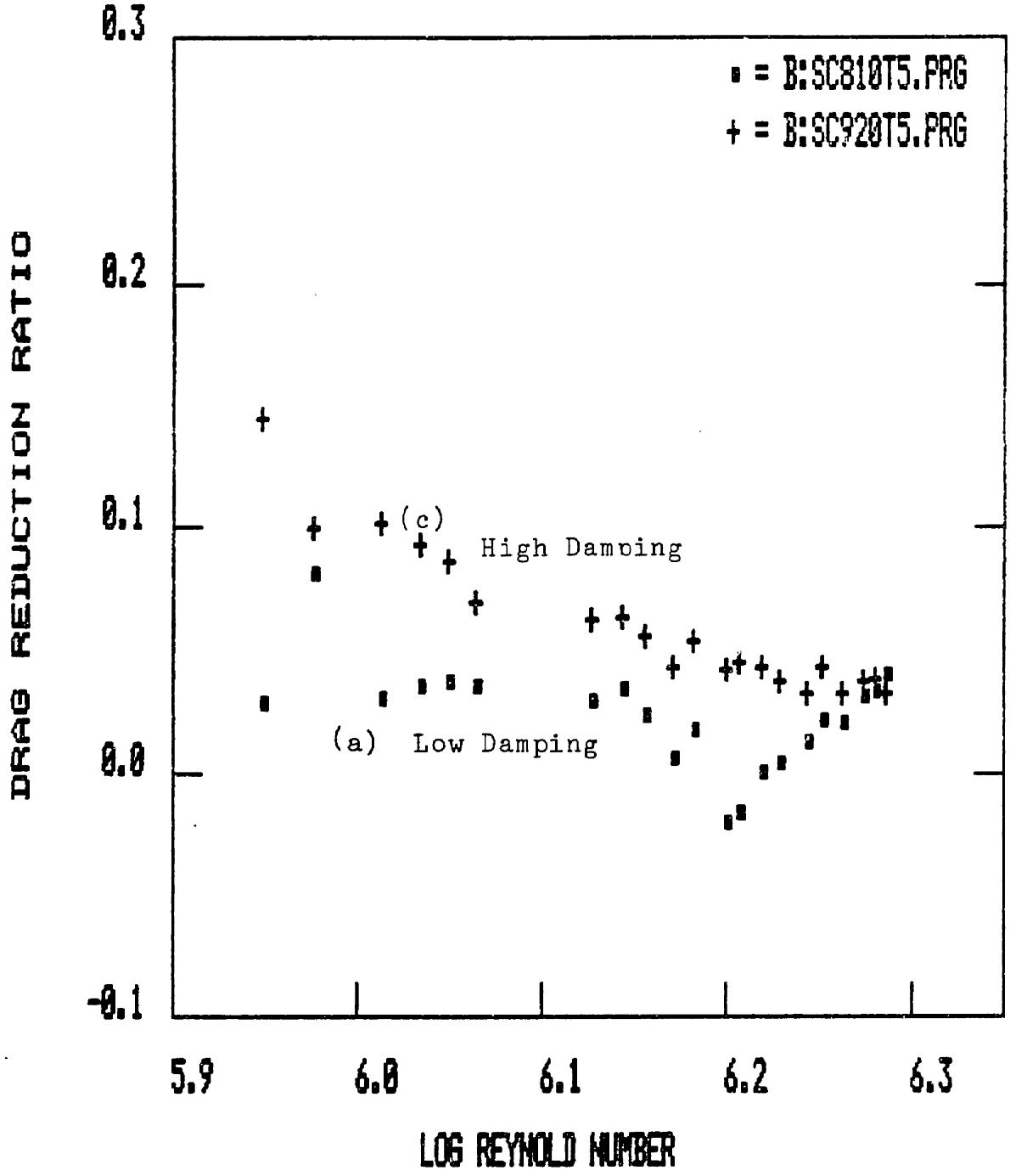


Figure 43. Log Reynolds number vs. drag reduction ratio of the composite coatings in test-III.
(a)$M_d$=5,970 200phr, (c)$M_d$=17,250 203phr.

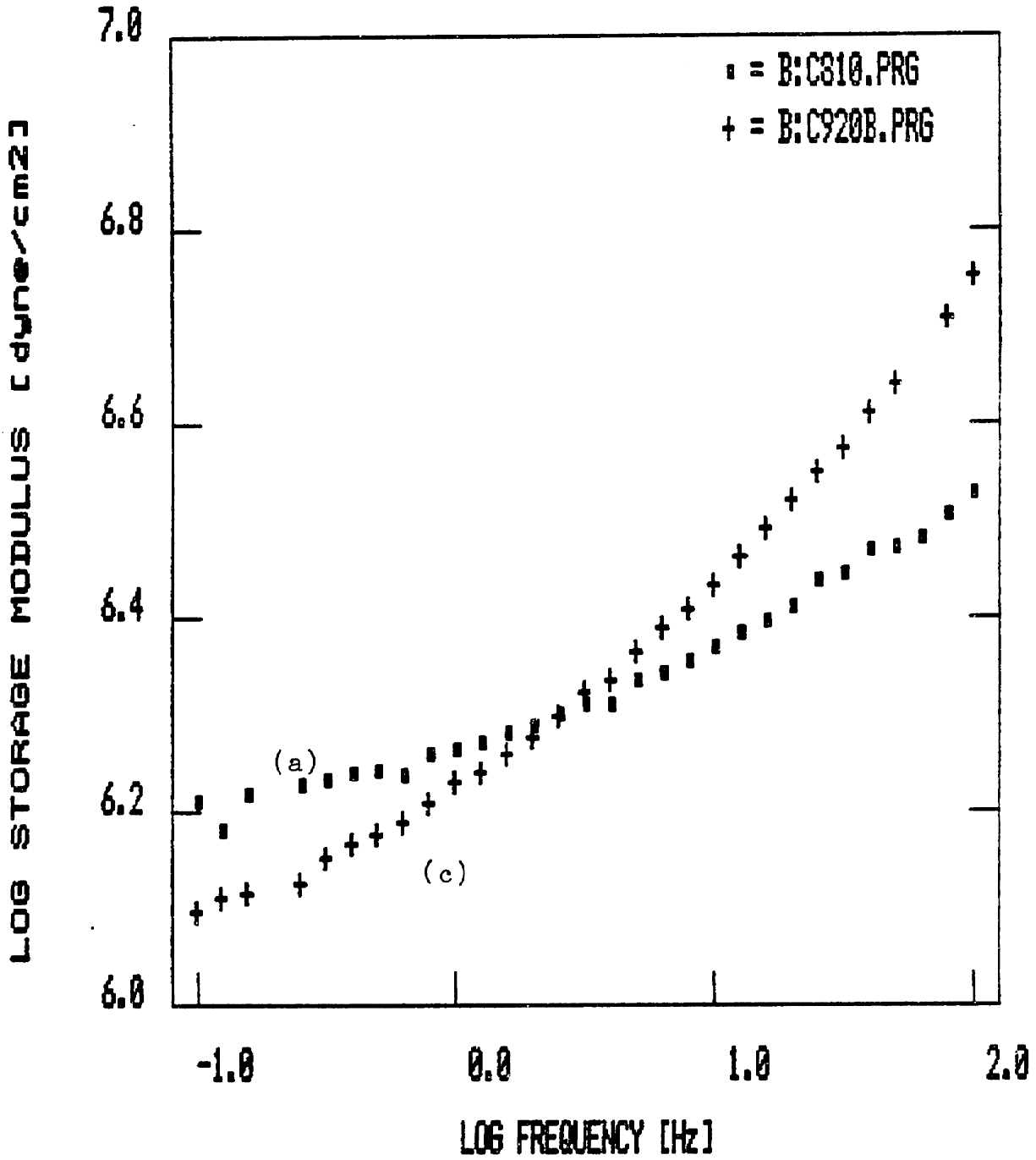


Figure 44. Log storage modulus vs. log frequency of the composite compliant coatings in test-III.
(a)$M_d$=5,970 200phr, (c)$M_d$=17,250 203phr.

(around 3 - 5% drag reduction) in the test Reynolds numbers. The plots (c) of Figure 43 reveal about 14% lower drag coefficient of the reference disc (R) as the Reynolds number increases. The coating (c) shows higher drag reduction than the coating (a) in the whole Reynolds numbers tested. Figure 44 illustrates the log storage moduli of the coatings (a) and (c) in the log frequency domain. The coating (c) with high molecular weight diluent ($M_d$ = 17,250 ) showes lower storage moduli at low frequency regime (0.1 - 2.5 Hz) than the coating (a) with low molecular weight diluent ($M_d$ = 5,970). However, at the higher frequency region (2.5 - 100 Hz) the storage moduli of the coating (c) are higher than those of the coating (a). On the other hand, the loss tangents of the coating (c) are much higher than those of coating (a) in the whole frequency range (0.1 - 100 Hz)[Figure 45]. Thus, the compliant coating with the higher damping factor shows more drag reduction than that of the lower damping factor in this test condition.

In the Test-IV in the Table VIII the effect of damping factor on skin-friction was reexamined with the coatings of low moduli (high dilution ratio of 300 phr), whereas, in the Test-III the coatings of relatively higher modulus (low dilution ratio of 200 phr) were examined. The compliant coating (b) and (d) were prepared with almost identical components: $\alpha$ , $\omega$-divinyl PDMS (Mn = 26,400), tetrafunctional junction chain extender and diluents loaded 300 phr. The only

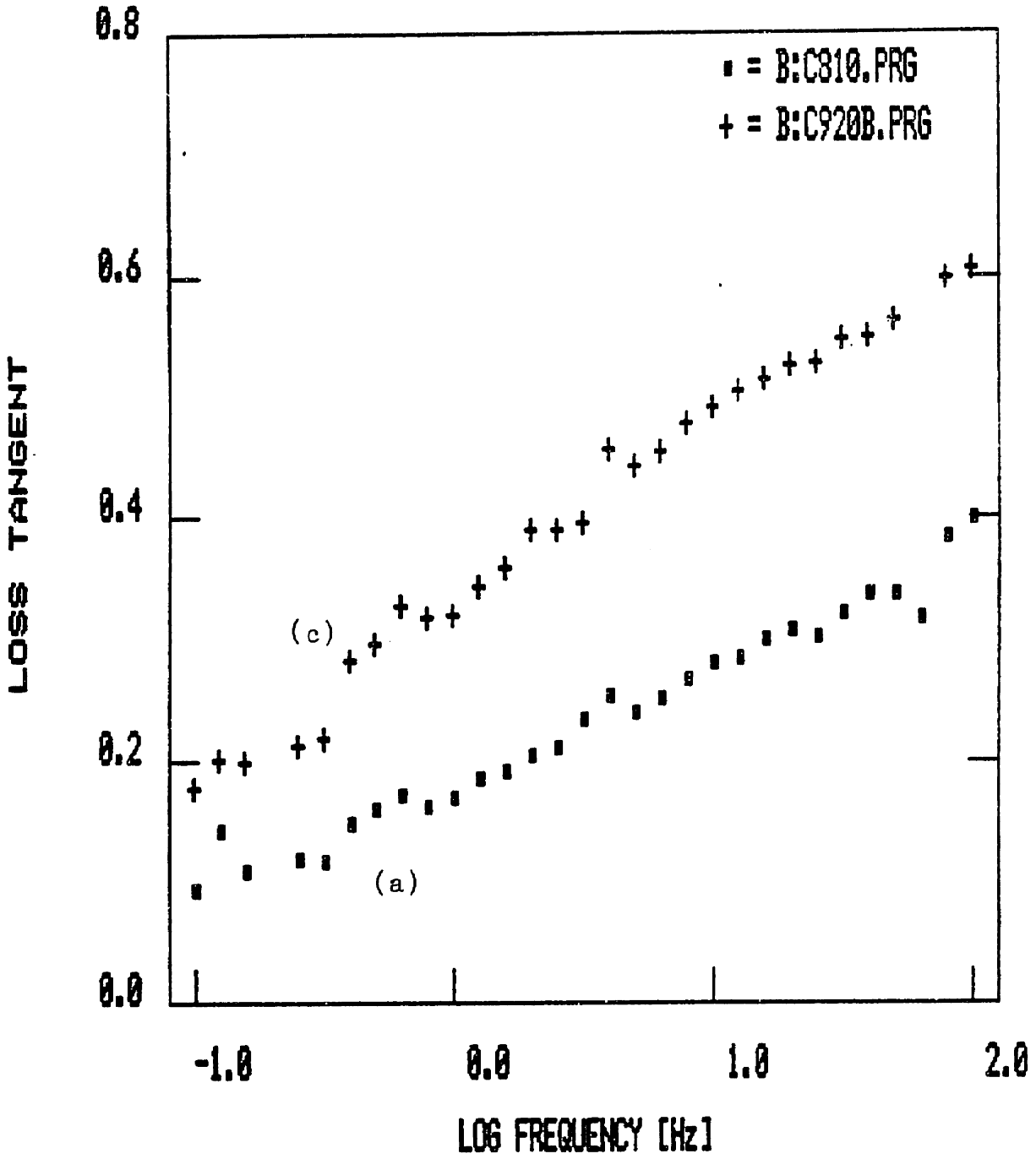


Figure 45. Loss tangent vs. log frequency of the composite compiant coatings in test-III.
(a)$M_d$=5,970 200phr, (c)$M_d$=17,250 203phr.

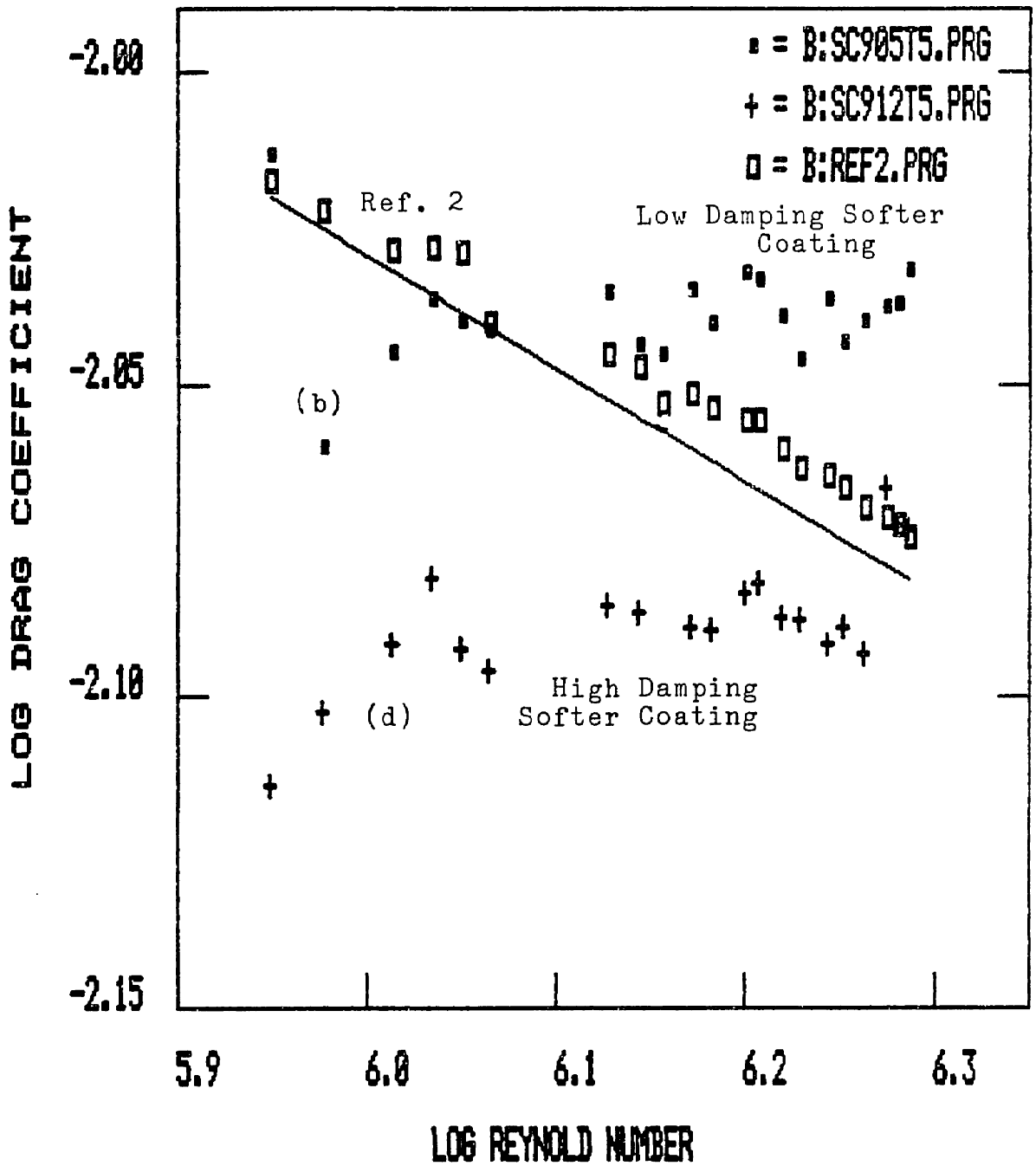


Figure 46. Log Reynolds number vs. log drag coefficient of the composite compilant coatings in test-IV. (b)$M_d$=5,970 300phr, (d)$M_d$=17.250 300phr

difference of the coatings is the molecular weight of the diluent loaded. In the coating (b) lower molecular weight diluent ($M_d$ = 5,970) was loaded, while higher molecular weight diluent ($M_d$ = 17,250) was used in the coating (d). Again, Figures 46 and 47 show log drag coefficients and the drag reduction ratios of the coating (b) and (d) in the log Reynolds number scale, respectively. There are distinct difference between the coating (b) and (d). The coating (d) shows a significant drag reduction upto 21% and relatively high drag reduction through the Reynolds number tested. On the other hand, the coating (b) shows some drag reduction in the low Reynolds number regime, however, at high Reynolds number regime a drag increase (upto 10%) was observed.

The coatings (b) and (d) show significant differences in both storage moduli and loss tangent. As shown in Figure 48, the storage moduli of the coating (b) with diluent of $M_d$ = 5,970 are from 1.12 x $10^6$ to 2.24 x $10^6$ dyne/$Cm^2$ at the frequency range of 0.1 to 100 Hz, which are 2 - 2.6 times higher than those of the coating (d). The damping factors (loss tangent) of the coating (b) are changed from 0.12 to 0.45 at the frequency range of 0.1 to 100 Hz, whereas those of the coating (d) reveal from 0.13 to 0.7 in the same frequency range (refer to Figure 49).

Considering the drag reduction via compliant coating with the dynamic properties of the coatings, the low modulus

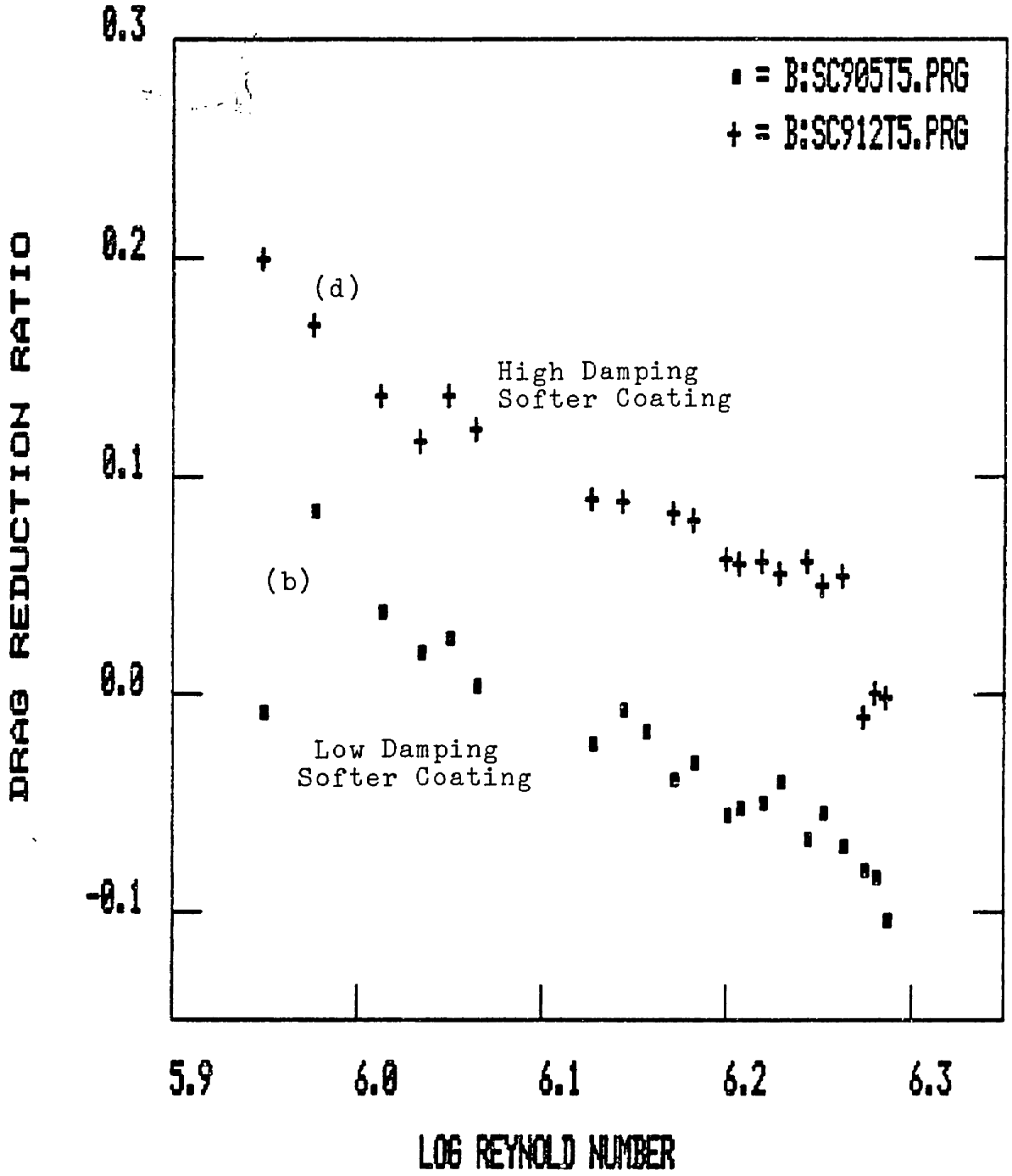


Figure 47. Log Reynolds number vs. drag reduction ratio of the composite coatings in test-IV.
(b)$M_d$=5,970 300phr, (d)$M_d$=17.250 300phr

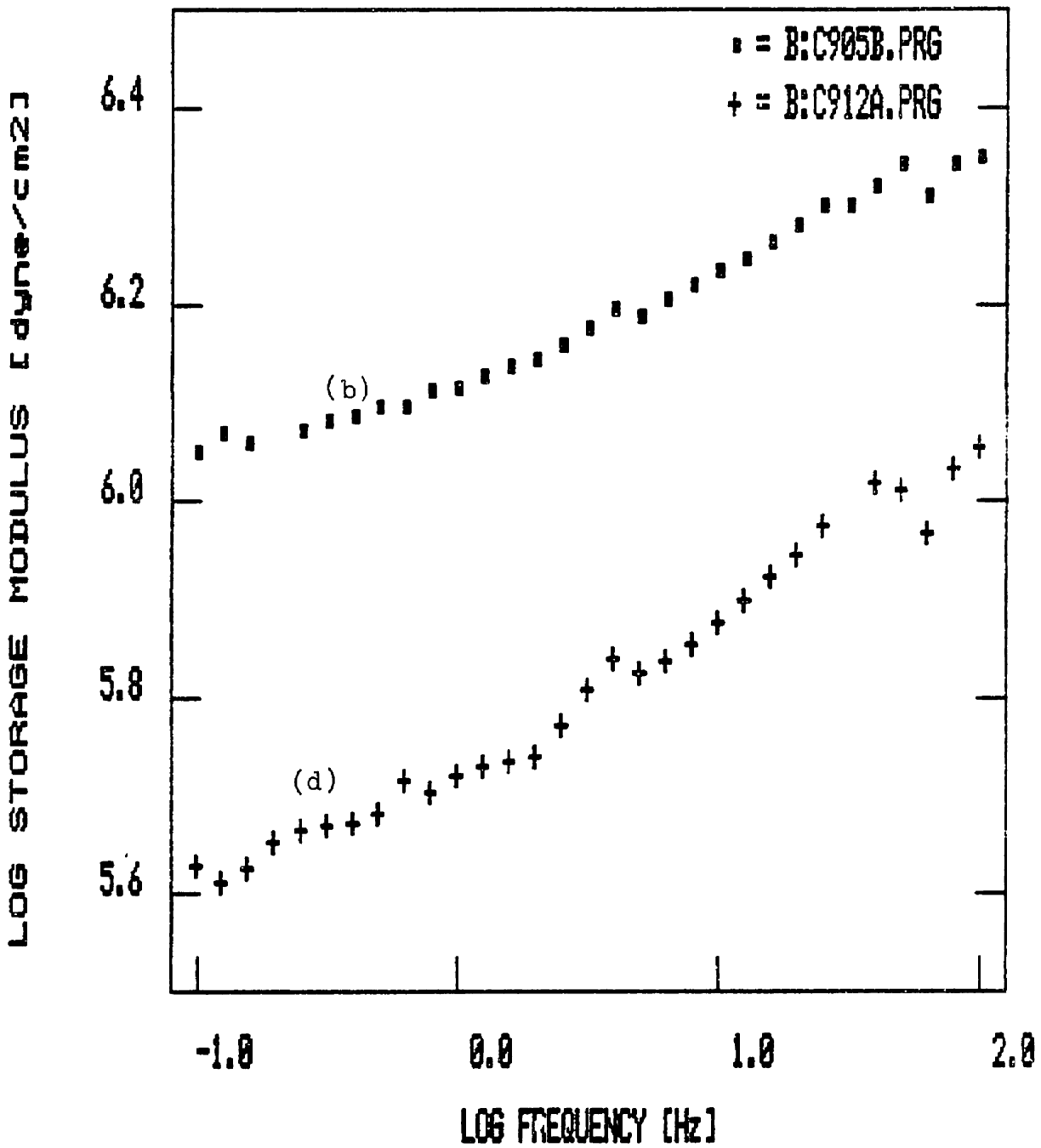


Figure 48. Log storage modulus vs. log frequency of the composite compliant coatings in test-IV.
(b)$M_d$=5,970 300phr, (d)$M_d$=17.250 300phr

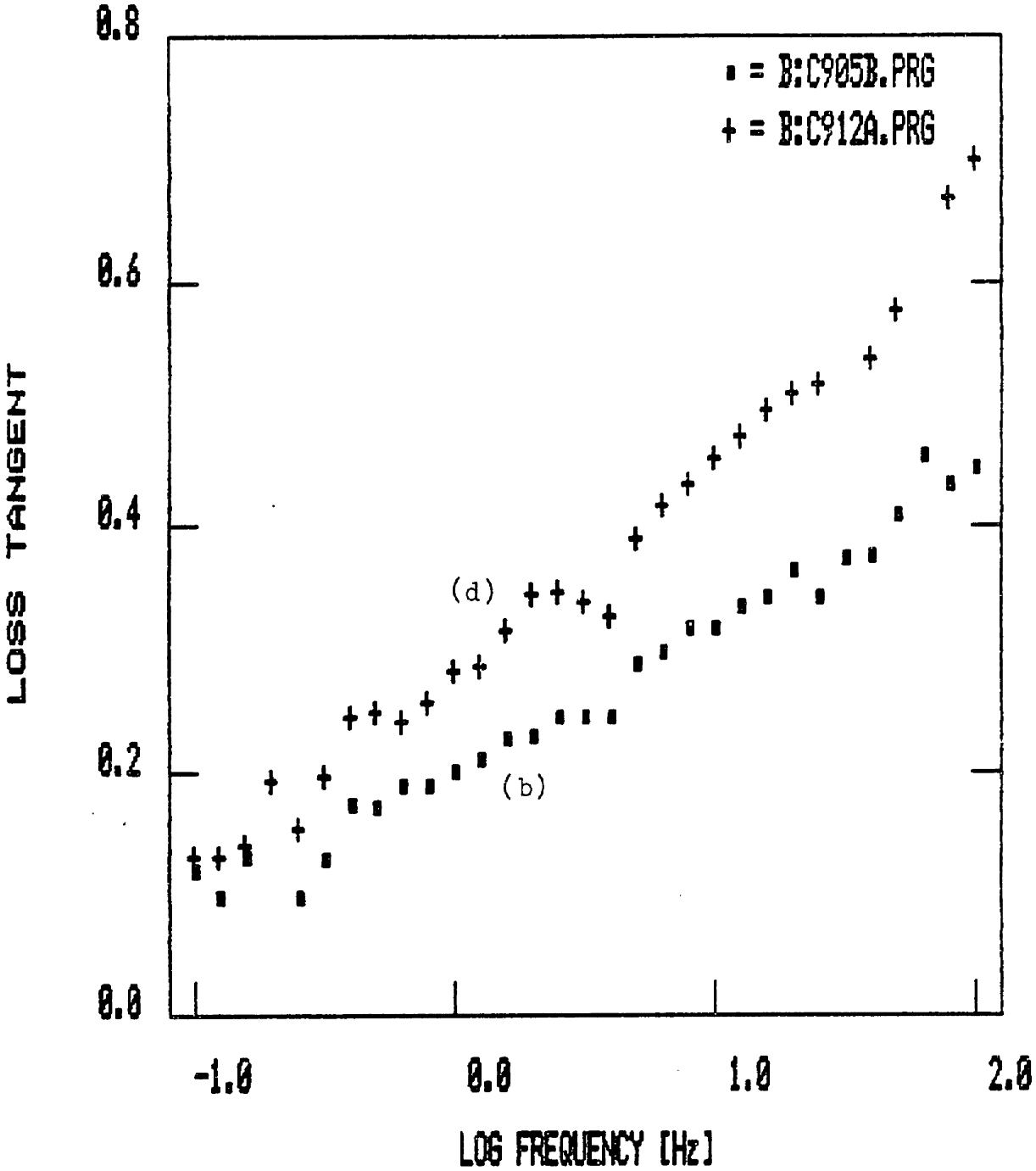


Figure 49. Loss tangent vs. log frequency of the composite compiant coatings in test-IV.
(b)$M_d$=5,970 300phr, (d)$M_d$=17.250 300phr

(softer) and high damping coating reduces the skin-friction drag significantly, whereas the higher modulus (stiffer) and lower damping coating did not. Recalling the results of the Test-I in the Table VIII, the stiffer and low damping coating (coating (a)) resulted in better performance than the coating of softer and low damping factor (coating (b)).

Suppose if the reason for the high drag reduction with the coating (d) which is soft and high damping lies on the softness of the coating, it is contradictory to the result of the Test-I in which soft coating shows poorer performance than hard one. Thus, the other material property damping factor of the compliant coating is much important factor for the favorable interaction between the turbulent fluctuations and compliant wall.

For most of coatings the largest drag reductions are observed at the lowest Reynolds number ($R_e$ = 8.92 x $10^5$). And as the Reynolds number increases, the drag reduction ratio of the coatings decreases gradually. The reason may be due to the surface divergences of the coating at the high Reynolds number, which are suppressed by using the top film at the low Reynolds numbers. By the careful observation of the coating surface with the strobe light, the static divergence of the coating covered with film was detected at the high speed. The static divergence of the coating looked very different from that of the bare coating where the top film was not placed. The bare

coating revealed very high amplitude wave height. As the rotating speed increases, the waves near the tip of the disc tend to vibrate very wildly, while the waves inside of the disc stand rather stationary. For the further increase of the rotating speed, the wild waves near the tip tend to move toward to the inside wave. On the other hand, the onset of the static divergence for the composite coating with the teflon film occurred at high Reynolds numbers corresponding to > 800 rpm, as compared to only 250 rpm for the composite coating without film. And the wild surface divergence which occurred near the tip of the coating without the film was not observed upto maximum rotating speed 1,500 rpm in the case of film covered coating.

Finally, there is a question left whether or not the velvet piles play an important role for our coating to reduce the skin-friction drag in the turbulent boundary layer. The answer is unknown at this point. To examine this question a controlled coating was fabricated and rotated in the chamber to measure skin-friction drag. The coating was made of only the dilute network (without velvet) whose compositions are exactly the same as those in the compliant coating (d) which was discussed above and showed maximum 21% drag reduction. When it was rotated in the chamber, the compliant edge bulged out due to the centrifugal force, and the coating was broken at very low rotating speed. Because the surface bulged out the

geometry of the compliant coating was no longer identical to that of reference disc. Therefore, the role of the velvet pile in controlling response of the composite coating is indeterminable because a valid test cannot be made without the use of the velvet to anchor the elastomeric network.

## Conclusions

For the purpose of varying the storage modulus and loss tangent of the network widely, chain extension of primary chain molecule and extensive dilution were useful. The molecular weight of the diluent is major variable controlling the loss factor. Low molecular weight diluent did not contribute to the increase of low frequency damping. The storage modulus of the network (compliance of the network) was governed both by diluent content and molar ratio of extender to junction molecules at constant [SiH]/[Si-Vinyl] = 1.2.

The composite compliant coatings reduced the skin-friction drag on the rotating disc upto 21% at the Reynolds number of $8.92 \times 10^5$. The coatings were fabricated out of four major components: (1) a thin stiff film as the top layer, (2) a low modulus high loss silicone elastomer, as a thin layer and as embedded on (3) the rayon fabric, and (4) a support screen. The stiffness of the top film influenced the performance of the coating profoundly: teflon film 0.005 inch thick led to the best results in the Reynolds number range of $8.92 \times 10^5$ to $1.94 \times 10^6$. The roles of top film to reduce skin-friction are postulated as follows:

(1) top film stabilizes the compliant surface from forming static divergence which increase skin-friction drastically,

(2) the high modulus film may be resonant to the turbulent fluctuations at high frequency which helps the coating to reduce the skin-friction in the turbulent boundary layer. (According to the Ash et al's hypothesis).[38]

The material properties of the compliant coatings are qualitatively correlated to the behavior of the coating in the turbulent boundary layer.

(1) The damping factor (loss tangent) of the coating is strongly related to the performance of the coating: In the present study a high damping coating reduced skin-friction more than a low damping coating.

(2) A low limit of the compliance of the coating exists. Beyond the limit the coating increases the skin-friction due to forming static divergence on the coating.

(3) Within the limit of the compliance a softer coating gives higher drag reduction than a stiff coating.

(4) The role of the velvet fabric employed in the present study is inconclusive whether it helps coatings reduce the skin-friction or not.

(5) The mechanism of the drag reduction via our composite compliant coating is still open to question;[95]

(i) whether the transition of laminar to turbulent is delayed to the higher Reynolds number, or

(ii) the lengthening of the transition zone before fully turbulent boundary layer has occurred, or

(iii) the turbulent bursting has been suppressed due to

the favorable interaction between the compliant wall and the turbulent flow, or

(iv) possible geometrical change of the coating surface would occur during rotation which provide a favorable effect on the boundary layer.

On the rotating disc the Reynolds number increases continuously with the radius of the disc from center to the tip of the disc. ($Re = r^2 \omega / \upsilon$, $0 \leq r \leq R$). Normally, the transition of laminar to turbulent boundary layer occurs at the Reynolds number of $2.5 \times 10^5 - 3.0 \times 10^5$ in the free space rotating disc. Thus, there exist three distinct boundary layers on a rotating disc, when the disc is rotated at high speed. Therefore, any of the mechanisms stated above would be possible to explain the phenomenon observed in the present study.

# APPENDIX A

Table A-1 Survey of Current Experimental Works(APPENDIX A)

| Investigator | Year | Experimentals: Compliant Material Used | Experimentals: Mech. Properties Compliant | Experimentals: Coating Shape | Results | Ref. |
|---|---|---|---|---|---|---|
| M.O.Kramer | 1957 | Ø.Ø6" thick natural rubb, diaphragm (commercial) | materials elastic modulus 133 psi (static) | Anisotropic (mounted on wire mesh) | Max. 140% inc. of transition Reynolds no. | 2 |
| M.O.Kramer | 1960 | 1) Ø.Ø2" thick natural rubb, diaphragm (commercial) 2) Ø.Ø4 xØ.Ø4 natural rubb. stubs 3) 3ØØ ctsk silicone oil | Not well defined | Anisotropic Stubbed coating | Max. 59% of drag reductio at Re=15x$10^6$ | 3 |
| M.O.Kramer | 1962 | 1) Ø.Ø3"thick natural rubb. diaphragm 2) multitude of ribs 3) 75ØØ ctsk silicone oil | Not well defined | Anisotropic ribbed coating designed to avoid small wavelength motion on surface | Max. 45% of drag reduct. at Re=14x$10^6$ | 4 |

Table A-1. Survey of Current Experimental Works(APPENDIX A)

| Investigator | Year | Experimentals: Compliant Material Used | Experimentals: Mech. Properties Compliant | Experimentals: Coating Shape | Results | Ref. |
|---|---|---|---|---|---|---|
| A.Dinkelacker | 1966 | 1) Ø.5mm natural rubb. 2) polyure-thane foam backing | Not mentioned | Anisotropic pipe | No signif. drag reduction | 46 |
| S. Taneda & H. Honji | 1967 | Commercial porous synth. rubber | Pressure vs. deformation curve | Porous | No drag reduction (ca. = drag on rigid plate) | 45 |
| F.W. Boggs, H.R. Frey & E.R. Hahn | 1961 | 1) natural rubber 2) 1000 ctsk PEO water solution 3) deep reservoir | $10.5x10^6$ dyne/ $Cm^2$ of Young's modulus | Isotropic | No drag reduc. | 44 |
| G.E.Klinzing, R.J.Kubcvcik & J.F.Marno | 1969 | Polyurethane foam, damper | Tensile st. 19 psi elongation 285% | Form material on the | 1. Signif. drag reduction in laminar boundary layer(max.20%) 2. Trans. of laminar-to-turb. turb. flow delay | 42 |

Table A-1. Survey of Current Experimental Works(APPENDIX A)

| Investigator | Year | Experimentals: Compliant Material Used | Experimentals: Mech. Properties Compliant | Experimentals: Coating Shape | Results | Ref. |
|---|---|---|---|---|---|---|
| E.M. Uram | 1966 | Similar to Kramer's coating | Not mentioned | Anisotropic | No drag reduc. | 24 |
| D.H. Fisher & E.F. Blick | 1966 | 1) commercial plastic skin (PVC) 2) viscous damping fluid | Not reported | Isotropic (air flow environment) | 1) max. 57% reduc. of rel. turbulence stress inc. as viscosity of damping fluid inc. | 11 |
| W.R. Looney & E.F.Blick | 1966 | 1) 0.0035" or 0.0025" thick PVC(stretched) 2) damping fluids (air, water, PEO, water solution) | Young modulus = 1400 psi ($9.6 \times 10^7$ dyne/$cm^2$ | Isotropic (air flow environment) | 1) 40-50% drag reduction in turbulent boundary layer 2) Young's modulus of compliant coating is important for drag reduction | 12 |
| E.F. Blick & R.R. Waltors | 1968 | 1) PVC film (0.0035-0.0025" thick) 2) Air,water, water solution of PEO(50-8000 | Young's modulus= 1400 psi) | Isotropic (In air) | 1) thinner coat- provided lower skin friction 2) compliant coatings lower turb.intensity | 13 |

Table A-1. Survey of Current Experimental Works(APPENDIX A)

| Investigator | Year | Experimentals: Compliant Material Used | Mech. Properties Compliant | Coating Shape | Results | Ref. |
|---|---|---|---|---|---|---|
| | | ctsk) in 5/16" thick-reservoir as damping fluid. | | | (proport. to skin friction) | |
| H.H. Chu & E.F. Blick | 1969 | 1) Ø.ØØ25" thick PVC film 2) 1" thick pores per inch(27 ppi) & 5/32" thick 4Ø ppi polyurethane foam as substrate 3) water as a damping fluid | Not reported | Anisotropic (in air flow) | 1) Max. 38% drag reduc. with compliant coating of 4Ø ppi substrate & water as damping fluid 2) smaller form substrate showed lower drag reduc. (28%) | 14 |

Table A-1. Survey of Current Experimental Wcrks(APPENDIX A)

| Investigator | Year | Experimentals: Compliant Material Used | Experimentals: Mech. Properties Compliant | Experimentals: Coating Shape | Results | Ref. |
|---|---|---|---|---|---|---|
| P.B.S. Lissaman & G.L.Harris | 1969 | 1) PVC film (0.0035" & 0.006" thick) 2) water & water solution of PEO of 10,000 cp. as damping | Young's modulus 3000-6000 psi | Isotropic (in air flow) | 1) 10% drag reduc. with compliant coatings 2) small effect on turbulent boundary layer due to major profiles bet. rigid & compliant wall | 30 |
| S. Kawamata, T. Kato, Y. Matsumura & T. Sato | 1971 | 1)natural rubber film (0.15-0.3 mm) Neoprene | Not reported | Isotropic | 1) 50-70% drag reduc. on compliant surface in laminar boundary layer 2) viscosity ofd damping fluid affected drag red. | 74 |

Table A-1. Survey of Current Experimental Works

| Investigator | Year | Experimentals: Compliant Material Used | Experimentals: Mech. Properties Compliant | Experimentals: Coating Shape | Results | Ref. |
|---|---|---|---|---|---|---|
| | | | | | 3) lower damping material resulted high drag reduc. 4) transition of laminar-to-turbulent was delayed on compliant wall | |
| R. Mattout & B.Cottenclan | 1972 | Mylar skin with Al rod | Not reported | Active wall | Max. 10% drag reduction | 75 |
| R.J.Hansen & D.L.Hurston | 1974 | PVC plastisol (PVC + di-2-ethyl-hexyl phthalate) | Shear storage modulus ($1\bar{0}^1 - 10^2$ rad/sec) 5,250-124,000 dyne/$Cm^2$) | Isotropic (rotating | 1) A large wave structure in compliant surface was essentially stationary rel to rotating speed | 5 |

Table A-1. Survey of Current Experimental Works

| Investigator | Year | Experimentals: Compliant Material Used | Experimentals: Mech. Properties Compliant | Experimentals: Coating Shape | Results | Ref. |
|---|---|---|---|---|---|---|
| | | | | | 2) beyond the critical condition where structure appeared the skin friction drag was inc. (depend on modulus of coating material | |
| R.N. Brown | 1975 | Air filled closed cell Neoprene (1/4" thick) | Shear storage modulus; 12.1 psi Shear loss modulus; 137 psi(calculated values) | Anisotropic | 1) There was a critical speed suddenly inc. for compliant coating 2) drag inc. may be due to surface roughness | |

Table A-1. Survey of Current Experimental Works

| Investigator | Year | Experimentals: Compliant Material Used | Mech. Properties Compliant | Coating Shape | Results | Ref. |
|---|---|---|---|---|---|---|
| A.P. Teslo & V.Y.Filipchuk | 1975 | Polyethylene pipe (160 μm) water,air as damping fluid | Not reported | Isotropic (pipe) | 1) 25% drag red. for $Re=(2-5)10^4$ in water flow 2) drag inc. for the same Reynolds no. in air flow 3) 10% drag inc. for $Re=10^5$ in water flow | 16 |
| M.C.Fischer, L.M.Weinstein, D.M.Bushnell, & R.L.Ash | 1975 | 1) PVC 0.01 thick membrane<br>0.0025 Cm thick mylar membrane | static Young's modulus(dyne/$Cm^2$) ⟶ $5.17x10^{10}$ | Anisotropic (in air flow)<br>or Isotropic | 1) Max. 61% skin-friction<br>drag reduc. on mylar/PVC plastisol surface was observed | 1 |

Table A-1. Survey of Current Experimental Works

| Investigator | Year | Experimentals: Compliant Material Used | Mech. Properties Compliant | Coating Shape | Results | Ref. |
|---|---|---|---|---|---|---|
| | | RTV silicone | E(RTV)=6.89X10$^6$ | | 2) dynamic | |
| rubber | dyne/Cm | 2) 100 ppi polyurethane foam | E(PU)=5.52X10$^5$ dyne/Cm | | modulus, damping of coating material was important factor for achieving drag reduc. | |
| | | PVC plastisol | E(PVC)=6.21X10$^4$ dyne/Cm | | | |
| K.W.McAlistor | 1974 | 1) thin PVC membranes (0.002" or 0.004") 2) water,air, water solution of PEO (10,000 cp) 3) dry or flooded open cell polyurethane foam (45 ppi & 70 ppi) | Not reported | Isotropic or Anisotropic (wind tunnel test) (duplicated Blick's coating) | Drags for compliant surface equal to or slightly higher than that obtained for the rigid surface | 31 |

Table A-1. Survey of Current Experimental Works

| Investigator | Year | Experimentals: Compliant Material Used | Experimentals: Mech. Properties Compliant | Experimentals: Coating Shape | Results | Ref. |
|---|---|---|---|---|---|---|
| J.N.Hefner & L.M.Weinstein | 1976 | 1) PVC sheets 2) Polyurethane foam 3) air, water, water solution of PEO. Duplicated. Ref. 24,26 | Not reported | Anisotropic (wind tunnel test) | 1) No drag reduction was observed 2) small standing waves were appeared on compliant surface at certain flow velocity | 32 |
| L.M.Weinstein, M.C.Fischer, & R.L.Ash | 1975 | 1) Ø.ØØ25 Cm thick Mylar Silicone rubber film 2) Ø.64 Cm thick polyurethane foam | Not reported | Anisotropic (wind tunnel test) | 1) 20% reduc. of boundary layer thickness for compliant surface (Mylar surface) 2) No effect on boundary thickness for silicone rubber coated compliant surface | 43 |

Table A-1. Survey of Current Experimental Works

| Investigator | Year | Experimentals: Compliant Material Used | Mech. Properties Compliant | Coating Shape | Results | Ref. |
|---|---|---|---|---|---|---|
| L.M. Ash, L.M.Weinstein, D.M.Bushnell, & R.Balasubramaian | 1975 | 1) Mylar membrane 2) PVC plastisol polyurethane foam | Not reported | Anisotropic (wind tunnel test) | 1) Surface motion of compliant wall was studied and suggested short wave length motion was required to achieve high drag reduction 2) previous works were reviewed | 38 |
| K.O. Kramer | 1977 | 1) Elastic paint (ep) (top: 1 mil) 2) latex rubb. (center: 0.014") 3) Rubber (bottom:0.04") 4) Butyrate film (bf) (Top: 2 mil) | $E_{bp}$ =2x10$^5$ psi $E_{ep}$ =1x10$^5$ psi | Isotropic (laminate) | 1) 28-29% reduc. 2) top layer film affects results greatly | 40 |

Table A-1. Survey of Current Experimental Works

| Investigator | Year | Experimentals: Compliant Material Used | Experimentals: Mech. Properties Compliant | Experimentals: Coating Shape | Results | Ref. |
|---|---|---|---|---|---|---|
| J.M. McMichael, P.S.Klebanoff, & N.E.Mease | 1980 | 1) Mylar membrane (0.025mm thick) 2) 4.76mm thick open-celled polyurethane foam | Not reported | Anisotropic | 1) Low amplitude - large wavelength motion predominant 2) No signif. change from rigid surface skin-reduction coefficient was observed | 33 |
| R.J. Hansen, D.L. Hunston C.C. Ni & M.M.Reischman | 1980 | PVC plastisol | Shear modulus $3.28 \times 10^{3}$ dyne/$Cm^{2}$ | Isotropic | 1) Large amplitude and large wavelength motions on compliant coating was produced 2) Essentially standing wave was observed | 76 |

Table A-1. Survey of Current Experimental Works(APPENDIX A)

| Investigator | Year | Experimentals: Compliant Material Used | Experimentals: Mech. Properties Compliant | Experimentals: Coating Shape | Results | Ref. |
|---|---|---|---|---|---|---|
| R.J. Hansen, D.L. Hunston C.C. Ni & M.M.Reischman | 1980 | PVC plastisol | Shear modulus 5,200-124,000 dyne/$Cm^2$ | Isotropic | 1) Large scale surface waves 2) Increase of drag was observed beyond critical velocity of flow which was caused by the spanwise wave structure on compliant surface | 6 |
| M.V.Kanarskiy & A.P.Teslo | 1980 | 1) Natural rubber(600 μm) Polyethylene film(1 μm ) 2) Open-cell polyurethane foam (0.75mm depth) | Not reported | Anisotropic (air flow) | 1) Max. 60% reduction of mean level of pressure fluctuations. (Polyurethane foam covered with polyethylene) | 18 |

Table A-1. Survey of Current Experimental Works

| Investigator | Year | Experimentals: Compliant Material Used | Experimentals: Mech. Properties Compliant | Experimentals: Coating Shape | Results | Ref. |
|---|---|---|---|---|---|---|
| S.C.Dickinson J.L. Power, & J.J.Eynck | 1984 | 1) Natural rubber(0.0015" thick) 2) Neoprene (0.04" thick) 3) closed cell (cc) → neoprene foam (0.25" thick) | Not reported G=6.1-19.2 psi | Multilayer homogeneous | Same drag or higher drag force | 25 |
| L.P. Kozlov, V.I.Korobov & V.V.Babenko | 1983 | Polyurethane foam | Well studied Wide range of frequency | Anisotropic | 1) Signif. reduc. (max. ca. 50%) 2) Higher damping of the foam, higher reduction | 19 |

# APPENDIX B

Determination of Crosslinking Density(APPENDIX B)

Miller and Macosko[56] derived equations describing the structure of networks formed by the end-linking of $A\phi_0$ (junction precursor of functionality $\phi_0$ ) with $B_2$ (network chain precursor). The fundamental parameter in their relation is the probability that looking "out" from an A group on a junction leads to a finite chain, $P(F_A^{out})$. For the $A\phi_0 + B_2$ system,

$$\frac{\varepsilon^2}{R} P(F^{out})^{\phi_0 - 1} - P(F_A^{out}) - \frac{\varepsilon^2}{R} + 1 = 0 \qquad (1)$$

where, $\phi_0$ is the functionality of the junction precursor, $\varepsilon$ is the extent of reaction of vinyl groups (or other end groups of chain molecule) and R is the molar ratio of $Si-H/Si-CH=CH_2$ group used in the network formation. The probability that looking "out" from the terminal vinyl group leads to a finite chain, $P(F_B^{out})$, is related to $P(F_A^{out})$ for $A\phi_0 + B_2$ network by,

$$P(F_B^{out}) = 1 - R[1-P(F_A^{out})]^2/\varepsilon \qquad (2)$$

The sol fraction, $W_s$, is related to these quantities as follows:

$$W_s = W_{A_{\phi_0}}[P(F_A^{out})]^{\phi_0} + W_{B2}[P(F_B^{out})]^2 \qquad (3)$$

where, $W_{A_{\phi_0}}$ and $W_{B2}$ are the weight fractions of $A_{\phi_0}$ and $B_2$ respectively in the initial mixture. Equations (1) through (3)

enable one to calculate $\varepsilon$ , $P(F_A^{out})$ and $P(F_B^{out})$ from sol fraction, $W_s$. From these values crosslinking density is estimated.

$$\upsilon/V = [A_{\phi_0}]_0 \sum_{i=3}^{\phi_0} i\, P(X_i)/2 \qquad (4)$$

$$P(X_i) = \binom{\phi_0}{i} [1-P(F_A^{out})]^i [P(F_B^{out})]^{\phi_0 - i} \qquad (5)$$

where, $[A_{\phi_0}]_0$ is the initial concentration of junction precursor, $P(X_i)$ is the probability that an $A\phi_0$ group chosen at random is a junction of functionality, i and $\binom{\phi_0}{i}$ is the notation for the number of combinations of $\phi_0$ things taken i at a time.

## BIBLIOGRAPHY


1. M. C. Fischer, L. M. Weinstein, D. M. Bushnell and R. L. Ash, AIAA Paper No. 75-833 (AIAA 8th Fluid and Plasma Dynamics Conf.), 1975.

2. M. O. Kramer, J. Aero. Sci. 24, 459, 1957.

3. M. O. Kramer, ASNE J., 25, Feb. 1960.

4. M. O. Kramer, Naval Engineers J., 74, 341, 1962.

5. R. J. Hansen and D. L. Huston, J. Sound and Vibr., 34, 297, 1974.

6. R. J. Hansen, D. L. Hunston, C. C. Ni, M. M. Reischman and J. W. Hoyt, Viscous Drag Reduction Prog. in Aero. & Astro, 72, 1980.

7. M. O. Kramer, Memorandum RM-3018-PR, The RAND Corp., Satnta Monica, CA, Aug. 1962.

8. D. M. Bushnell, J. N. Hefner and R. L. Ash, The Phys. Fluids, 20, No. 10, Pt. II, 1977, S31.

9. D. Gyorgyfalvy, J. Aircraft, 4, NO. 3, 1967, 186.

10. M. T. Landahl, Fluid Mech., 13, 609, 1962.

11. D. H. Fisher and E. F. Blick, J. Aircraft 3, (2), 163, 1966.

12. W. R. Looney and E. F. Blick, J. Spacecraft, 3, (10), 1562, 1966.

13. E. F. Blick and R. R. Walters, J. Aircraft, 5, (1), 11, 1968.

14. H. H. Chu and E. F. Blick, J. Spacecraft, 6, (6), 763, 1969.

15. E. F. Blick, R. R. Walters, R. Smith and H. Chu, AIAA Paper No. 69-165, 1969.

16. R. N. Brown, Turbulence in liquid, Proc. of the 4th Biennial Symposium on Turb. in Liq., 21, 1975.

17. A. P. Teslo and V. Y. Filipchuk, NASA Tech. Translation NASA TT F-16, 555, 1975.

18. M. V. Kanarsiy and A. P. Teslo, Fluid Mechanics-Soviet Research, 9, (5), 1980.

19. L. P. Kozlov, V. I. Korobov and V. V. Babenko, Reports of the Ukarainian Academy of Sce., Series A-Physical, Mathematical and Tech. Sci., 45, 1983.

20. Y. C. Fung, "Foundations of Solid Mechanics", Englewood Cliffs, N.J., 1965.

21. S. A. Orszag, NASA Report, NASA-CR-2911, 1979.

22. S. A. Orszag, NASA Report, NASA-CR-3071, 1979.

23. R. L. Ash, NASA Report, NASA-CR-2387, 1974.

24. E. M. Uram, Letter Report No. 1127, Davidson Laboratory, Hoboken, NJ, Feb. 1966.

25. S. C. Dickinson, J. L. Power and J. J. Eynck, David W. Taylor Naval Ship Research and Devel. Center Report, DTNSRDC-84/060, Aug. 1984.

26. T. B. Benjamin, J. Fluid Mech., 9, 513, 1960.

27. D. Gyorgyfalvy, J. Aircraft, 4, (3), 186, 1967.

28. R. E. Kaplan, MIT Aeroelasticity and structure Research Laboratory Report No. 116-1, 1964.

29. H. B. Karplus, Ill. Inst. Tech. Research Inst., Report No. IITRI 1205-4, 1963.

30. P. B. S. Lissaman and G. L. Harris, AIAA Paper No. 69-164, 1969.

31. K. W. McAlister and T. M. Wynn, NASA TM X-3119, 1974.

32. J. N. Hefner and L. M. Weinstein, J. Spacecraft, 13, (8), Engineering Note, 502, 1976.

33. J. M. McMichael, P. S. Klebanoff and N. E. Mease, "Symposium on Viscous Drag Reduction", Prog. in Astro & Aero., 72, 410, 1980.

34. M. C. Fischer, L. M. Weinstein, D. M. Bushnell and R. L. Ash, AIAA Paper No. 75-833, 1975.

35. J. E. Ffowcs Williams, Bolt-Beranek and Newman Inc., Report No. 1138, 1964.

36. G. Zimmermann, Phys. Fluids, 20, (10), Pt II, S214, 1977.

37. N. A. Jaffe, T. T. Okamura and A. M. O. Smith, AIAA J., 8, 301, 1970.

38. R. L. Ash, D. M. Bushnell, L. M. Weinstein and R. Balasubramanian, presented at 4th Biennial Symposium on Turbulence in Liquies, Univ. Missouri Rolla, 220, 1975.

39. R. Grosskreutz, University Sci. J., 1, 65, 1975, Univ. Dar es Salaam .

40. K. O. Kramer, Naval Engineers J., 189, (5), 41, 1977.

41. R. L. Smith and E. F. Blick, J. of Hydronautics, 3, (2), 100, 1969.

42. G. E. Klinzing, R. J. Kubovcik and J. F. Marno, I & EC Proc. Desn. and Devpt., 8, (1), 112, 1969.

43. L. M. Weinstein, M. C. Fischer and R. L. Ash, AIAA J., 13, (7), 956, 1975

44. F. W. Boggs, H. R. Frey and E. R. Hahn, U. S. Rubber Co. Rpt., Wayne, N.J., Contract NOW-60-0227-C, 1961.

45. S. Taneda and H. Honji, Report of Research Institute of Applied Mechanics, 15, (49), 1, 1967.

46. A. Dinkelacker, J. Sound Vib., 4, (2), 187, 1966.

47. A. P. Teslo, et al., Joint Publications Research Service, Arlington, VA JPRS-60785, 1973.

48. H. Schlichting, "Boundary Layer Thory", 7th ed., McGrow-Hill Inc., New York, 1979.

49. L. A. Dorfman, "Hydrodynamic Resistance and The Heat Loss of Rotating Solids", Olive and Boyd LTD., Edinburgh, UK, chpt. 4 and 6, 1963.

50. D. Seyferth, "J. Organometallic Chem. Lib. Series Vol. 3", chpt. 13, Elsevier, New York, 1976-1981.

51. W. Noll, "Chemistry and Technology of Silicones", Academic Press, New York, 1968.

52. P. J. Flory and J. Rehner, Jr., J. Chem. Phys., 512, 1943.

53. K. O. Meyer, Ph.D Thesis at MIT (Dept. of Chem. Engeering), April, 1980.

54. P. J. Flory, "Principles of Polymer Chemistry", Cornell University Press, Ithaca, N.Y., 1953.

55. P. J. Flory, J. Chem. Phys., 66, 5720, 1977.

56. H. M. James and E. Guth, J. Polym., Sci., 4, 153, 1949.

57. L. M. Dossin and W. W. Graessley, Macromolecules, 12, 123, 1979.

58. N. R. Langley, Macromolecules, 1, 348, 1968.

59. H. C. Kan and J. D. Ferry, Macromolecules, 11, 1049, 1978.

60. W. W. Grassley, Advances in Polym. Sci., 16, 1, 1974.

61. J. D. Ferry, "Viscoelastic Properties of Polymers", 3rd ed., John Wiley & Sons Inc., New York, chpt. 10, 1980.

62. M. Mooney, J. Appl. Phys., 19, 434, 1948.

63. R. S. Rivlin, Phil. Trans. Royal Soc. London, Ser. A, 241, 379, 1948.

64. R. S. Rivlin, Phil. Trans. Royal Soc. London, A242, 173, 1949.

65. M. A. Llorente and J. E. Mark, J. Chem. Phys., 71, 682, 1979.

66. J. E. Mark and M. S. Llorente, J. Am. Chem. Coc., 102, 632, 1980.

67. J. E. Mark and J. L. Sullivan, J. Chem. Phys., 66, 100, 1977.

68. D. R. Miller and C. W. Macosko, Macromolecules, 9, 206, 1976.

69. A. L. Andrady, M. S. Llorente and J. E. Mark, J. Chem. Phys., 72, 000, 1980.

70. K. O. Meyers, M. Bye, and E. W. Merrill, Macromolecules, 13, 1045, 1980

71. J. D. Ferry, "Viscoelastic Properties of Polyers ", 3rd ed., chpt. 1, John Wiley & Sons, Inc., New York, 1980.

72. N. W. Tschoegl, "The Theory of Linear Viscoelastic Behavior", Academic press, 1980.

73. S. Kawamata, T. Kato, Y. Matsumura and T. Sato, Theoretical & Applied Mechanics, 21, ed. Japan Nat. Comm. for Theor

& Appl. Mech., 507, 1971.

74. S. Mattout and B. Collenceau, Societe Bertin and Cie, Note Technique No. 71-C1-09, 1972.

75. R. J. Hansen, D. L. Hunston, C. C. Ni and M. M. Reischman, J. Sound and vib., 68, (3), 317, 1980.

76. J. D. Ferry, "Viscoelastic Properties of Polymers", 3rd., Chapt 2, John Wiley & Sons, Inc., N.Y., 1980.

77. O. Kramer and J. D. Ferry in Sci and Techn. Rubber, edited by F. R. Eirich, Academic Press, N.Y., Chapt 5, 1978.

78. N. R. Langley and J. D. Ferry, Macromolecule, 1, (4), 353, 1968.

79. J. D. Ferry, R. F. Landel and M. L. Williams, J. Appl. phys., 26, 359, 1955.

80. M. Mooney, J. Polym. Sci., 34, 599, 1959.

81. R. H. Valentine, J. D. Ferry, T. Homma and K. Ninomiya, J. Polym. Sci., pt A-2, 6, 479, 1968.

82. E. Mackawa, R. G. Mancke, and J. D. Ferry, J. Phys. Chem., 69, 2811, 1965.

83. O. Kramer, R. Greco, R. A. Neira and J. D. Ferry, J. Polym. Sci., Polym. Phys ed., 12, 2361, 1974.

84. O. Kramer, R. Greco and J. D. Ferry, J. Polym. Sci., Polym. Phys. ed., 13, 1675, 1975.

85. W. M. Prest, Jr., Polym. J., 4, 163, 1973.

86. A. Y. Malkin, O. Y. Sabsai, L. P. Lukyanova, K. A. Chochua and V. P. Azovtsev, Vysokomol. Soyed. A18, (9), 2035, 1976.

87. A. J. Barlow, G. Harrisen and J. Lamb., Proc. Roy. Soc. (London), A282, 1964.

88. D. L. Hunston, C. J. Knauss, M. B. Palmer and R. R. Mgers, Trans. Soc. Rheo., 16, (1), 45, 1972.

89. D. J. Plazek, W. Dannhauser and J. D. Ferry, J. Colloid Sci., 16, 101, 1961.

90. M. Mooney, J. Polym. Sci., 34, 599, 1959.

91. J. D. Ferry, "Viscoelastic Properties of Polymers", chapt 13, 3rd ed., John Wiley & Son, N.Y., 1980.

92. W. Lynch, "Handbook of Silicone Rubber Fabrication", chapt 7, Van Nortrand Reinhold Co., N.Y., 1978.

93. E. W. Merrill, Private Communication with Bushnell in the annual "ONR Meeting in 1984".

94. C. B. Kaufman and D. O. Cowan in "Inorganic Synthesis", E. G. Rochow, Ed., McGraw-Hill, N.Y., 6, 214, 1969.

95. The author is indebted to Dr. John Razzano of the General Electric Corporation, Silicone Divisiion for providing the , -divinyl PDMS of various molecular weights (1-518-237-3330).

96. J. D. Ferry, "Viscoelastic Properties of Polymers", 3rd ed., chapt. 17-E, John Wiley & Sons, Inc., 1980.

97. R. West, J. Amer. Chem. Soc., 76, 6015, 1954.

98. C. W. Macosko and W. M. Davis, Rheol. Acta, 13, 814, 1974.

99. C. W. Macosko and F. C. Weissert, ASTM STP553, 127, 1974.

100. E. J. Roschke, J. Sound and Vibration, 46,(4), 591, 1976.

101. Electro-Craft Corp., USA, "DC Motors speed controls servo systems", An engineering handbook, chapt 2, Pergamon Press, N.Y., 1977.